Association Euratom - Risø National Laboratory annual progress report 2005

Bindslev, H.; Singh, Bachu Narain

Publication date:
2006

Document Version
Publisher's PDF, also known as Version of record

RISØ

Risø-R-1579(EN)

Association Euratom - Risø National Laboratory Annual Progress Report 2005

Risø National Laboratory
Roskilde
Denmark
November 2006

Author: Edited by H. Bindslev and B.N. Singh
Title: Association Euratom - Risø National Laboratory Annual Progress Report 2005
Department: Optics and Plasma Research Department

Risø-R-1579(EN)
November 2006

Abstract:

The programme of the Research Unit of the Fusion Association Euratom - Risø National Laboratory covers work in fusion plasma physics and in fusion technology. The fusion plasma physics research focuses on turbulence and transport, and its interaction with the plasma equilibrium and particles. The effort includes both first principles based modelling, and experimental observations of turbulence and of fast ion dynamics by collective Thomson scattering. The activities in technology cover investigations of radiation damage of fusion reactor materials. These activities contribute to the Next Step, the Long-term and the Underlying Fusion Technology programme. A summary is presented of the results obtained in the Research Unit during 2005.

ISSN 0106-2840
ISSN 1901-3922
ISSN 1396-3449
ISBN 87-550-3557-4
ISBN 87-550-3558-2 (internet)

Pages: 70
Figures: 45
References: 28

Risø National Laboratory
Information Service Department
P.O.Box 49
DK-4000 Roskilde
Denmark
Telephone +45 46774004
bibl@risoe.dk
Fax +45 46774013
www.risoe.dk

Contents

Preface

In 2005 seven parties, EU, Japan, Russia, China, USA, Korea and India, agree jointly to build and exploit ITER, and to place ITER in Cadarache in France. ITER is a major experimental facility for the development of fusion as an energy source. It is expected that ITER will be ready for scientific exploitation in 2016. The mission of ITER is to demonstrate that nuclear fusion can be exploited as an energy source. ITER represents an unprecedented international cooperation in the field of science and technology. It also represents a valuable opportunity for cooperation between public research organisations and private industry. Risø participates in the internationally coordinated activities to develop fusion and sees itself as having a key role in facilitating the participation of Danish industries in the international fusion programme.

The principle being pursued with ITER is the fusion of hydrogen isotopes to form helium. To make the fusion process run at a significant rate the hydrogen gas must be heated to high temperatures where it ionises and turns into a plasma. The plasma must be confined to achieve suitable densities and sustain the high temperature. ITER will use a magnetic field for the confinement. While fusion holds the promise of providing a sustainable source of energy, which is environmentally sound, it also presents considerable scientific and engineering challenges. Key issues in the final steps towards realising fusion energy production include:

Improving the plasma energy confinement, that is the ratio between the energy of the plasma and the heating power required to sustain the plasma energy. Improving energy confinement implies reducing energy transport out of the plasma, which principally is due to turbulence. So what we really need to do is to understand and control turbulence.

Channelling the energy of fast ions, produced in fusion reactions, into heating the bulk plasma without driving turbulence and without premature exit of the fast ions from the plasma. This requires understanding and control of the dynamics of the fast ions in interaction with other particles and with waves.

Development of materials, which maintain required mechanical properties under high and sustained neutron fluxes. Neutrons, produced in the fusion reactions, are not confined by the magnetic field. They pass through the first wall of the chamber surrounding the plasma, slowing down on impact with atoms in the wall, thereby giving rise to dislocations in the wall material, which affect the properties of the material.

Risø contributes to fusion research in all these areas: 1) codes, modelling turbulence and transport, are continually improved, and benchmarked against experiments. Of particular note this year has been Risø's modelling of bursts of plasma ejected from the plasma edge. These simulations have found quantitative agreement with experimental observations. 2) Central to understanding the dynamics of fast ions is are temporally and spatially resolved measurements of the fast ion velocity distributions in the plasma. Risø, in collaboration with MIT (USA) and EURATOM partners, is exploiting and developing millimetre wave based collective Thomson scattering (CTS) diagnostics at the TEXTOR and ASDEX upgrade tokamaks in FZ-Jülich and the Max-Planck Institute for plasma physics in Garching (near Munich). Significant effort also goes into developing a fast ion CTS diagnostic for ITER. 3) In the field of irradiated materials Risø investigates the properties of copper alloys relevant to ITER, and of iron alloys, which will be an essential component of a commercial fusion power plant.

1 Summary of Research Unit activities

The activities in the Research Unit cover two main areas:

Fusion Plasma Physics, which includes:

- *Theoretical and numerical turbulence studies*. Turbulence and the associated anomalous transport is investigated using first principles based models and solving these by means of numerical codes in full toroidal geometry. These models are continuously being developed and benchmarked against experimental data and codes at other associations. The dynamics of bursts of fluctuations leading to profile relaxation have been studied in models for flux-driven interchange mode turbulence, where the back reaction of the turbulence on the equilibrium flows and profiles are accounted for.
- *Fast Ion Collective Thomson Scattering.* Risø has taken the lead in the development and exploitation of fast ion collective Thomson scattering diagnostics for TEXTOR, ASDEX Upgrade (AUG) and ITER. These projects are carried out in close collaborations with MIT, and with the TEC† and AUG teams.

Fusion Technology, which includes:

- Experimental and theoretical investigations of the effects of irradiation on the microstructural evolution and on the physical and mechanical properties of metals and alloys relevant to the Next Step, the Long Term and Underlying Fusion Technology Programme.

The **global indicators** for the Research Unit in 2005 are:

Professional staff:	13.6	man-years
Support staff:	7.9	man-years
Total expenditure - incl. mobility:	3.13	MioEuro
Total Euratom support:	0.80	MioEuro

† TEC: the Trilateral Euregio Cluster, a collaboration of FOM Institute for Plasma Physics, Holland; ERM/KMS, Belgium and Forschungszentrum Jülich, Germany.

2 Plasma Physics and Technology

2.1 Introduction

H. Bindslev
henrik.bindslev@risoe.dk

A plasma is a dense collection of free ions and electrons. The transitions from solids to fluids to gases are associated with increases in internal energy, the breaking of bonds and changes of physical properties. The same is true of the transition from a gas to a plasma; in fact the plasma is rightfully described as the fourth state of matter, its physics differing as much from that of gases as that of solids does. Just as solid state physics is involved in a broad range of applications, so it should be no surprise that plasmas have a wide range of applications, that their physics and chemistries are rich, and that the methods of generation and diagnosis are wide and complex.

Our activities in high temperature plasmas, aimed at developing fusion energy, are coordinated with the European EURATOM fusion programme through an agreement of association on equal footing with other fusion laboratories in Europe. Our EURATOM association facilitates extensive collaboration with other fusion research laboratories in Europe, crucial in the ongoing build-up of competencies at Risø, and gives us access to placing our experimental equipment on large fusion facilities at the Max-Planck Institute for Plasma Physics in Garching and at the Research Centre Jülich, both in Germany. Our association with EURATOM also provides the basis for our participation in the exploitation of the European fusion research centre, JET, located in England. With its organisation of national programmes as EURATOM associations, the European fusion programme is a successful example of a large *European Research Area.* Our activities in high temperature plasma research and the development of fusion energy are introduced in subsection 2.1.1, and described in further detail in subsection 2.2 discussing turbulence and transport in fusion plasmas, and in subsection **2.3** discussing our use of millimetre waves for investigating the dynamics of fast ions in fusion plasmas.

2.1.1 Fusion plasma physics

H. Bindslev
henrik.bindslev@risoe.dk
www.risoe.dk/euratom

Producing significant amounts of fusion energy requires a plasma with a temperature of 100 to 200 million degrees and densities of 1 to 2 times 10^{20} particles per cubic metre, corresponding to a pressure of 1 to 5 atmosphere. Unlike gases, plasmas can be confined and compressed by magnetic fields. At the required temperatures the plasma must be lifted off material walls to prevent the plasma from rapid cooling. This is done by suspending the plasma in a toroidally shaped magnetic field that also acts to balance the plasma pressure. The required temperature and densities have been achieved in the joint European fusion experiment, JET. The production of net energy adds the requirement that the energy in the plasma be confined at least on the order of six seconds. The confinement time is the characteristic time for cooling off if heating was switched off or, equivalently, the ratio of plasma energy to required heating power to sustain that energy content. Achieved confinement times are on the order of one second. Higher density could compensate shorter confinement time and visa versa, so a simplified statement of the target is that the product of temperature, density and confinement time should be six

atmosphere × seconds and is currently one atmosphere × seconds. Progress towards the goal principally involves improving the confinement time or, equivalently, reducing the energy transport in the plasma. The energy transport in fusion grade plasmas is principally due to turbulence, one of our main research activities reported in subsection 2.2. Significant progress towards the goal is expected with the next step fusion experiment, ITER. In ITER significant fusion rates are expected and with that the fast ion populations in the plasma will increase dramatically compared with present machines. The fast ions may then influence the plasma significantly. As a consequence, the dynamics of fast ions and their interaction with the rest of the plasma is one of the central physics issues to be studied in ITER. It is in fact also one of our main research topics in fusion as reported in subsection **2.3**.

The fields of turbulence, transport and fast ions are closely knit. With steep gradients in plasma equilibrium parameters and with populations of energetic ions far from thermal equilibrium, fusion plasmas have considerable free energy. This energy drives turbulence, which in turn acts back on the equilibrium profiles and on the dynamics of the fast ions. The turbulence naturally gives rise to enhanced transport, but also sets up zonal flows that tear the turbulent structures apart and result in edge transport barriers; most likely at the root of the poorly understood, but experimentally reliably achieved, high confinement mode (H-mode). This non-linear interplay between turbulence and equilibrium also supports transient events reminiscent of edge localised modes (ELMs) where energy and particles are ejected from the plasma edge in intermittent bursts.

This set of topics is the focus of our fusion plasma physics research: With first-principles based codes we seek to model the interplay between plasma turbulence, transport and equilibrium. This modelling is tested against experimental data in collaboration with other fusion plasma physics institutes. To elucidate the physics of fast ions and their interplay with turbulence, waves and transient events, we are engaged in the diagnosis of confined fast ions by collective Thomson scattering (CTS) at the TEXTOR tokamak at the Research Centre Jülich and at the ASDEX upgrade tokamak in the Max-Planck Institute for Plasma Physics in Garching, both in Germany.

2.2 Turbulence and transport in fusion plasmas

O. E. Garcia, V. Naulin, A. H. Nielsen and J. Juul Rasmussen
volker.naulin@risoe.dk; jens.juul.rasmussen@risoe.dk

The transport of heat and particles across the confining magnetic field of fusion plasmas is one of the most important and interesting, but also most difficult areas of contemporary fusion research. It is well established that the “anomalous” transport component mediated by low frequency turbulence is far larger than the classical and neo-classical collisional transport, at least in the edge region. It is thus of utmost importance to achieve a detailed understanding of anomalous transport and the underlying turbulence for the design of an economical viable fusion reactor based on magnetic confinement schemes. In spite of a dramatic progress in experiment, theory and computations during recent years the quantitative understanding is still very sparse and any predictive capacity is at best rudimentary. Even very fundamental phenomena such as transitions from low confinement regime (L-mode) to high confinement regime (H-mode), the profile resilience and the particle pinch, that are routinely observed and classified experimentally, have no generally accepted explanations.

The activities within plasma turbulence and transport are mainly focussed on topics related to edge and scrape-off-layer (SOL) regimes of toroidal plasmas. It is generally

acknowledged that the conditions near the edge of the plasma are dictating the global performance, which seems natural since all transport has to go through the edge region. Theoretical and numerical investigations of first principle models form the majority of the work performed. We emphasize benchmarking of results and performance both with other codes and increasingly with experimental observations.

Our activities are strongly integrated into the EURATOM fusion program, and we have active collaborations with several EURATOM laboratories on theoretical issues as well as on direct comparisons of our results with experimental observations. We have a strong standing within the EFDA-JET program, with V. Naulin as deputy task force leader of Task-Force Transport. We are actively participating in the Integrated Tokamak Modelling (ITM) Task Force on the validation and benchmarking of codes. Several of our numerical codes are in use at different European laboratories, where they are used for specific purposes, ranging from experimental comparisons to education of students. Particular mention should be made of the collaboration with the TCV group at CRPP, EPFL in Lausanne, which has resulted in the first ever quantitative comparison and agreement between experimental data and numerical results from a first-principle based numerical modelling of the dynamics and turbulence in the SOL (see Sec. 2.2.3). Similar detailed comparisons are underway for JET (see Sec. 2.2.4) and other devices.

The work carried out through 2005 comprises the following items:

- Investigations of the turbulence and transport at the edge and SOL of toroidal plasmas by applying the two dimensional, electrostatic edge-SOL turbulence code, ESEL (Sec. 2.2.1). It is well established that the turbulence and transport in the edge and SOL of toroidal plasmas are strongly intermittent and involve outbreaks of hot plasma. These structures, often referred to as “blobs”, are formed near the last closed flux surface (LCFS) and propagate far into the SOL. The convective transport mediated by the blob-like structures prevails in virtually all confinement states, including edge-localized modes. They have a profound influence on the pressure profiles in the SOL, the ensuing parallel flows, and the power deposition on plasma facing components. The ESEL code describes the perpendicular dynamics and transport events in the SOL together with a self consistent development of the SOL profiles at the outboard midplane. The profiles of density, electron temperature, and vorticity are evolved together with the fluctuations, without making a scale separation-ansatz, i.e., allowing relative fluctuation levels of order unity and profile variations by many orders of magnitude. The general features of the ESEL code and the results particularly on the statistical properties of the fluctuations are presented in Sec. 2.2.1. While we in Sec. 2.2.2 provide a discussion of realistic parameters for the dissipations and parallel losses in the SOL to be employed in the ESEL code. Section 2.2.3 contains the description of the successful quantitative comparison between the experimental results from TCV (EPFL, Lausanne) and the ESEL code. The initial efforts in performing quantitative comparisons with JET results are presented in the following section (2.2.4), where we show fine agreement with the profiles of density, temperature and effective diffusivities in the SOL.
- The basic dynamics of plasma blobs, or generally field aligned structures, in the SOL is well described in terms of nonlinear interchange motions; see Sec. 2.2.5. It is shown that the blobs are accompanied by dipolar vorticity and electrostatic potential fields. They propagate radially through the SOL at a velocity of approximately one tenths of the ion sound speed.

- To investigate the influence of finite ion temperature and finite ion Lamor radius on the dynamics in the edge/SOL we are developing a gyro-fluid code for the two dimensional interchange dynamics as a generalization of the ESEL code (see Secs. 2.2.6). Initial investigations have demonstrated significant changes in the details of the propagation of individual blobs.

- Transport of impurities in the edge and SOL are investigated numerically using the ESEL-code in Sec. 2.2.7. The impurity density is assumed to be low, and impurities are described as particles that are passively advected by the turbulent E×B-velocity. The impurities are rapidly mixed in the SOL region and even particles released far into the SOL are rapidly transported inside the LCFS.

- To contribute to the development of 1D transport models we have considered a model based on the concept of turbulence spreading in Sec. 2.2.8. This model is found to allow for the description of pinch effects, profile resilience, fast cold pulse propagation and heat wave propagation. The model will be integrated into the JET suite of transport models.

- We have "exported" our codes to several laboratories within EURATOM, where they have been adapted and employed for specific purposes. In Sec 2.2.9 we describe the modelling of the TORPEX device (EPFL, Lausanne), while Sec. 2.2.10 deals with the modelling of drift wave dynamics in a high-density helicon device (IPP, Greifswald). Our basic Hasegawa-Wakatani code is now in use at several laboratories for producing "synthetic" turbulence data for testing various diagnostic methods. As an example, Sec. 2.2.11 describes the testing of a super-resolution method for improving data measured at low resolution.

- Finally, in sec. 2.2.12 we describe the collaboration with the Experimental Plasma Physics Group at the University of Innsbruck on the evaluation of fluctuation data measured with probes in the edge region and SOL of Tokamaks. Specifically this comprises recent results from ISTTOK (Lisbon, Portugal) and ASDEX Upgrade (IPP, Garching).

2.2.1 Intermittency and convective transport at the boundary of magnetically confined plasmas

O. E. Garcia, V. Naulin, A. H. Nielsen and J. Juul Rasmussen
odd.erik.garcia@risoe.dk

An electrostatic drift-ordered fluid model for turbulence in the edge and scrape-off layer (SOL) of plasmas confined by a strong toroidal magnetic field has been derived. The model describes the nonlinear evolution of electron density, temperature and fluid vorticity in a local slab domain at the outer midplane without any scale separation assumption. The non-uniform magnetic field drives interchange motions which maintain a turbulent state in the plasma boundary region.[1-5]

The model employs a simplified treatment of the parallel transport of mass, heat, and momentum in the region of magnetic field lines intersecting material walls. Numerical simulations are shown to result in intermittent transport caused by radial motion of localized blob-like structures which are erupted from the plasma edge region into the SOL.[2-6] Associated with these plasma filaments are dipolar structures of the vorticity and electrostatic potential. Analysis of single-point recordings reveals asymmetric conditional waveforms with a steep front and a trailing wake. This is shown in Figure 1(a) for probe positions P_i ranging from the plasma edge (P_1) to the far SOL (P_7).

The statistical distributions of the particle density and electron temperature are strongly skewed and flattened, revealing an abundance of positive bursts in the time series. The change of the particle density distribution function from Gaussian in the edge region to strongly skewed and flattened in the SOL is demonstrated in Fig 1(b). The distribution develops an exponential tail towards large fluctuation amplitudes. These results are in excellent agreement with similar analysis made on data from experimental probe measurements.[5]

Coarse graining and spectral analysis of the probe signals further indicate the presence of long-range correlations in the particle density fluctuations,[4] as has also been found from analysis of experimental data in several experimental. Finally, conditional statistics of the radial particle flux demonstrates the intermittency of the turbulent plasma transport and the quasi-periodic apparency of blob structures due to bursting in the global turbulence level. These results are presented in Figure 2, showing for example that 50% of the total turbulent transport is due to conditional flux events with amplitudes larger than 2.5 times the standard deviation.[4]

This work clearly indicates that plasma fluctuations and cross-field transport in the tokamak SOL are results of turbulence originating in the region of closed field lines and spreading intermittently to the region of open field lines due to radial motion of blob-like structures. This provides an explanation for the large fluctuation levels and broad particle density profiles commonly observed in the far SOL at large average particle densities.[5]

1. J. P. Graves, J. Horacek, R. A. Pitts, and K. I. Hopcraft, Plasma Phys. Control. Fusion **47**, L1 (2005).
2. O. E. Garcia, V. Naulin, A. H. Nielsen, and J. Juul Rasmussen, Phys. Rev. Lett. **92**, 165003 (2004).
3. O. E. Garcia, V. Naulin, A. H. Nielsen, and J. Juul Rasmussen, Phys. Plasmas **12**, 062309 (2005).
4. O. E. Garcia, V. Naulin, A. H. Nielsen, and J. Juul Rasmussen, Phys. Scripta **T122**, 89 (2006).
5. O. E. Garcia, J. Horacek, R. A. Pitts, A. H. Nielsen, W. Fundamenski, J. P. Graves, V. Naulin, J. Juul Rasmussen, Plasma Phys. Control. Fusion **48**, L1 (2006).
6. O. E. Garcia, N. H. Bian, V. Naulin, A. H. Nielsen, and J. Juul Rasmussen, Phys. Plasmas **12**, 090701 (2005).

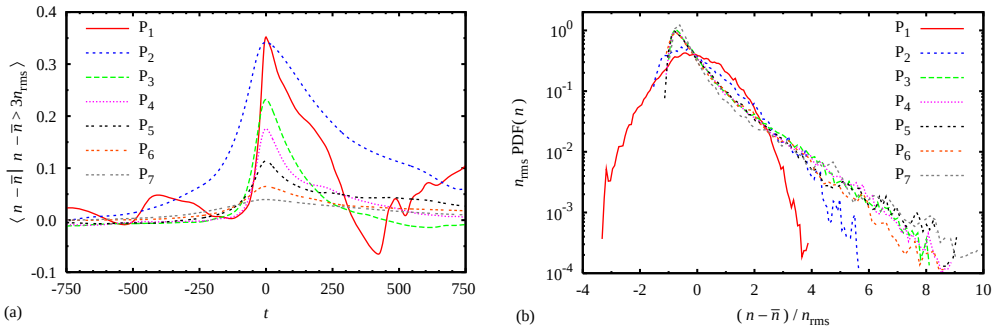

Figure 1. The conditionally averaged particle density signal (a) and the probability distribution function (b) derived from single-point measurements across the plasma edge region.

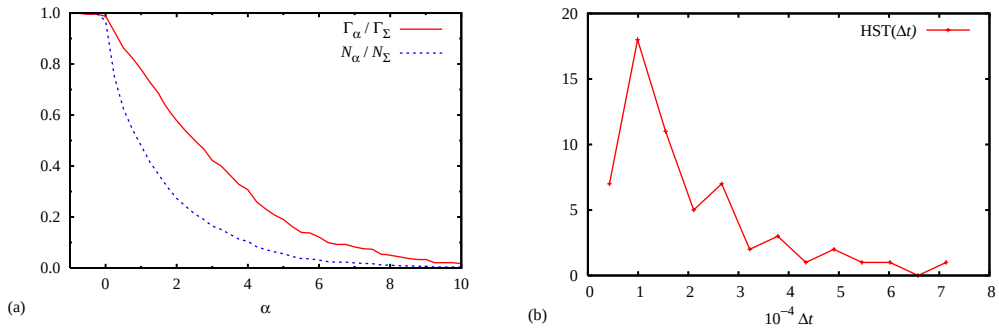

Figure 2. (a) Accumulated conditional radial turbulent particle flux Γ_α normalized by the total flux Γ_Σ as a function of the amplitude condition $\alpha\Gamma_{rms}$. The flux is averaged over the poloidal direction and the radial position corresponds to that of probe P_3. Also shown is the associated relative count number N_α for conditional flux events with respect to the maximum possible number N_Σ of conditional sub-records. (b) Histogram of the waiting time Δt for flux events larger than 4 times the flux standard deviation.

2.2.2 Neoclassical dissipation and parallel losses in interchange driven scrape-off layer turbulence

W. Fundamenski (UKAEA Fusion Association, Culham Science Centre, Abingdon,UK), O. E. Garcia, V. Naulin, A. H. Nielsen, J. Juul Rasmussen, R. A. Pitts, J. Horacek* and J. P. Graves* (*CRPP, EPFL, CH-1015 Lausanne, Switzerland)*
odd.erik.garcia@risoe.dk

It has recently become clear that collective plasma dynamics governed by interchange motions in the plane perpendicular to the magnetic field successfully describes the many experimental observations of intermittent turbulence and transport in the scrape-off layer of magnetically confined plasmas.[1] However, collisional dissipation and parallel transport significantly influences the collective dynamics and must be taken into account in a complete description of particle and heat transport in the plasma boundary region.[2]

Motivated by the successful comparison between interchange turbulence simulations and probe measurements, first principles expression have been derived for the parameters governing collisional diffusion and parallel losses of mass, momentum and energy in the tokamak scrape-off layer. These transport coefficients are based on neoclassical perpendicular transport (Pfirsch-Schlüter diffusion) and classical parallel transport (sub-sonic advection and Spitzer-Härm diffusion). General dimensionless fluid groups are obtained, and various collisionality regimes are discussed.[2]

When numerical values derived from these expressions are used to compute dissipation and parallel damping coefficients for an electrostatic interchange turbulence model, simulations correctly reproduce the radial profiles of particle density and electron temperature measured in Ohmic and L-mode regimes on the TCV and JET tokamaks.[1,2] Moreover, the dynamical evolution of the pressure profile is used to infer the transport driven parallel flows towards the divertor targets and is found to be in good agreement with experimental measurements.[1] An example of the parallel Mach flow profile derived from the turbulence simulations is presented in Figure 3. Such transport driven parallel flows is routinely observed in confinement experiments.

1. O. E. Garcia, J. Horacek, R. A. Pitts, A. H. Nielsen, W. Fundamenski, J. P. Graves, V. Naulin, J. J. Rasmussen, Plasma Phys. Control. Fusion **48**, L1 (2006).

2. W. Fundamenski, O. E. Garcia, V. Naulin, R. A. Pitts, A. H. Nielsen, J. Juul Rasmussen, J. Horacek, J. P. Graves, and JET EFDA Contributors, "Neoclassical dissipation and parallel losses in interchange driven scrape-off layer turbulence", submitted to Nuclear Fusion.

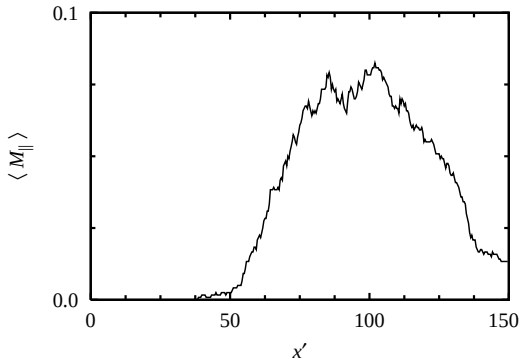

Figure 3. Radial variation of the average parallel Mach number estimated from interchange turbulence simulations of the outer midplane region. The radial position x'=50 corresponds to the last closed magnetic flux surface.

2.2.3 Interchange turbulence in the TCV scrape-off layer

O. E. Garcia, V. Naulin, A. H. Nielsen, J. Juul Rasmussen, R. A. Pitts, J. Horacek*, J. P. Graves* (*CRPP, EPFL, CH-1015 Lausanne, Switzerland) and W. Fundamenski (UKAEA Fusion Association, Culham Science Centre, Abingdon ,UK)*
odd.erik.garcia@risoe.dk

Probe measurements of electrostatic plasma fluctuations in the scrape-off layer (SOL) of the TCV tokamak[1] are compared with results from two-dimensional interchange turbulence simulations which employ a simple description of open and closed field line regions, resulting in the first ever quantitative agreement between experimental data and a first-principles based physics description of the turbulent fields in the tokamak SOL.[2]

Here we consider a typical diverted, ohmically heated and high density deuterium TCV plasma and show that the same fluctuation statistics seem to be quantitatively obeyed by the output time series of a numerical simulation. The model is adapted to the experimental situation as closely as possible within the constraints of the physics and geometry currently included in the numerical model. In particular, all model parameters are theory based and evaluated using experimentally measured quantities.

As a consequence of profile relaxations, the edge layer intermittently erupt blob-like structures into the SOL which may subsequently transport far into the wall shadow. One such structure is seen Figure 4, showing the mushroom-like shape of the blob front to the left which is associated with a dipolar vorticity field shown to the right. Fast radial motion of such blob structures leads to large relative fluctuation levels and contributes significantly to the local time-averaged plasma density profile throughout the SOL. Interchange motions thus appear as a strong candidate mechanism for the explanation of the broad radial plasma profiles, leading to strong main chamber recycling, commonly observed in the SOL of current tokamak experiments.[1,2]

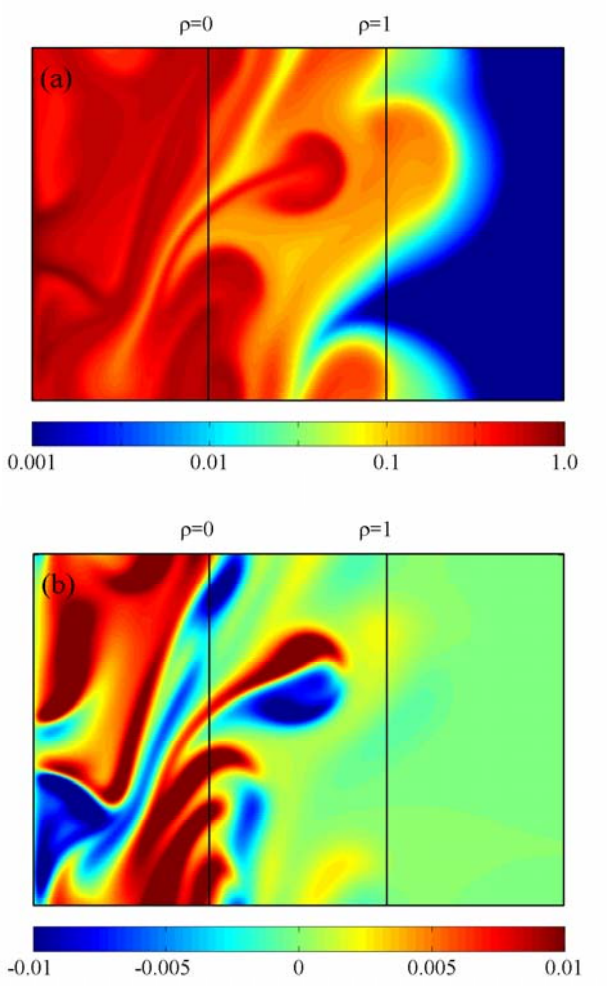

Figure 4. Contour plot of the particle density (a) and electric drift velocity (b) in the drift plane perpendicular to the magnetic field, showing a blob-like structure in the scrape-off layer associated with a dipolar vorticity field. The left (ρ=0) and right (ρ=1) vertical lines indicate the last closed magnetic flux surface and the wall radius, respectively.

As an example of the excellent agreement between experimental probe measurements and turbulence simulations, Figure 5 presents the radial variation of the time-averaged profile, the relative fluctuation level, and the skewness (S) and flatness (F) moments of the particle density fluctuations. Note that the two latter moments vanish for a Gaussian probability distribution function. Similarly good agreement has been found for the statistical distribution of the radial turbulent particle flux. Also the radial variation of the particle density autocorrelation time and the conditionally averaged waveform are found to compare favourably, showing that the simulations match both the typical shape of bursty events and the temporal correlations.[2]

This work provides great confidence that SOL turbulence is largely governed by interchange motions, and opens the door towards eventual predictive capability for SOL transport levels.

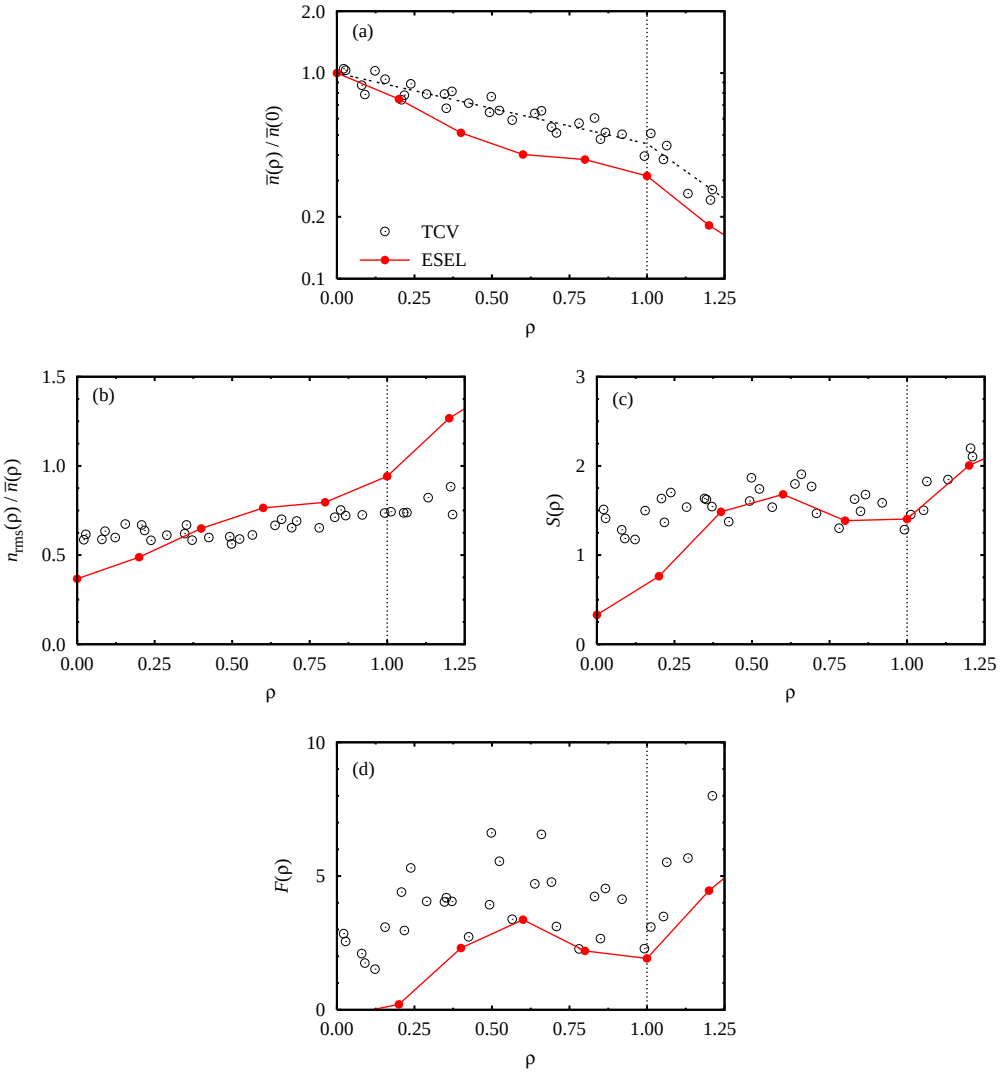

Figure 5. Radial variation of (a) average profile, (b) relative fluctuation level, (c) skewness, and (d) flatness moments of the particle density, revealing excellent agreement between experiments on the TCV tokamak and interchange turbulence simulations (ESEL).

1. J. P. Graves, J. Horacek, R. A. Pitts, and K. I. Hopcraft, Plasma Phys. Control. Fusion **47**, L1 (2005).
2. O. E. Garcia, J. Horacek, R. A. Pitts, A. H. Nielsen, W. Fundamenski, J. P. Graves, V. Naulin, J. Juul Rasmussen, Plasma Phys. Control. Fusion **48**, L1 (2006).

2.2.4 2D interchange turbulence simulations for JET relevant parameters

E. Garcia, V. Naulin, A. H. Nielsen, J. Juul Rasmussen, R. A. Pitts, J. Horacek* (*CRPP, W. Fundamenski (UKAEA Fusion Association, Culham Science Centre, Abingdon, OX14 3DB, UK), O. EPFL, CH-1015 Lausanne, Switzerland), B. Gonçalves (Associação EURATOM-IST, 1049-001 Lisbon, Portugal), C. Hidalgo (Associacion EURATOM-CIEMAT,Av. Complutense 22, 82040 Madrid, Spain) M. Hron (Association EURATOM-IPP.CR, Prague, Czech Republic) and JET-EFDA contributors*
anders.h.nielsen@risoe.dk

The two-dimensional, electrostatic, edge-SOL turbulence code ESEL[1] simulates the perpendicular dynamics of transport events in the SOL together with a self consistent development of the SOL profiles at the outboard midplane. Profiles of density n, electron temperature T_e, and vorticity are evolved together with the fluctuations, without making a scale separation-ansatz, i.e., allowing relative fluctuation levels of order unity and

profile variations by many orders of magnitude. Parallel losses in the SOL are described by the classical sub-sonic advection and Spitzer-Härm diffusion, and are dependent on local values of n and T_e, while perpendicular collisional dissipation is approximated by Pfirsch-Schlüter neoclassical diffusivities. The input parameters of the code are: the density and electron temperature at the separatrix, magnetic field strength B_0, major radius R_0, and the parallel connection length to the divertor targets $L_{\|} \sim \pi R_0 q_{95}$ where q_{95} is the q value at 95% of poloidal flux.

ESEL simulations were performed with input parameters corresponding to typical JET ohmic discharges[2]:

$n_0 = 10^{19}$ m^{-3}, $T_{e,0} = 45$ eV, $T_{i,0} = 80$ eV,

$R_0 = 3$ m, $B_0 = 2.0$ T, $q_{95} = 2.7$.

The resulting density and temperature profiles, shown in Figures 6(A) and 6(B), indicate a stronger decay of the profiles close to the separatrix than further outwards. Steeper temperature profiles reflect the slower loss of particles to the divertor compared to electron energy. Figure 6(C) depicts the radial profiles of the turbulent perpendicular energy fluxes, split up into convective, conductive and fluctuating parts;

$$\left\langle nTv_r \right\rangle = \left\langle (n_0 + \tilde{n})(T_0 + \tilde{T})v_r \right\rangle = T_0 \left\langle \tilde{n}v_r \right\rangle + n_0 \left\langle \tilde{T}v_r \right\rangle + \left\langle \tilde{n}\tilde{T}v_r \right\rangle .$$

In Figure 6(D) the corresponding collisional energy flux profiles are presented. The former are found to exceed the latter by two orders of magnitude. The radial turbulent particle flux profile is broader when compared to the turbulent heat flux profile, reflecting the faster parallel loss of electron energy. The effective particle and thermal diffusivity at the outer midplane, including the effects of both collisional and turbulent perpendicular transport are shown in Figure 6(E) and the effective convective velocities are shown in Figure 6(F). The diffusivities increase from the separatrix to a peak value at some 20 mm into the SOL, in qualitative agreement with experimental observation[3]. The ESEL simulations for JET further predict parallel Mach numbers M ~ 0.2 in agreement with Mach probe measurements.

On the basis of the reasonable agreement between simulation and experiment, we conclude that the SOL radial transport in JET ohmic plasmas is dominated by electrostatic interchange turbulence.

1. O. E. Garcia, J. Horacek, R. A. Pitts, A. H. Nielsen, W. Fundamenski, J. P. Graves, V. Naulin, J. J. Rasmussen, Plasma Phys. Control. Fusion **48**, L1 (2006).
2. W. Fundamenski, O. E. Garcia, V. Naulin, R. A. Pitts, A. H. Nielsen, J. Juul Rasmussen, J. Horacek, J. P. Graves, and JET EFDA Contributors, “Neoclassical dissipation and parallel losses in interchange driven scrape-off layer turbulence”, submitted to Nuclear Fusion.
3. K. Erents et al. Plasma Phys. Controlled Fusion **46** (2004) 1757.

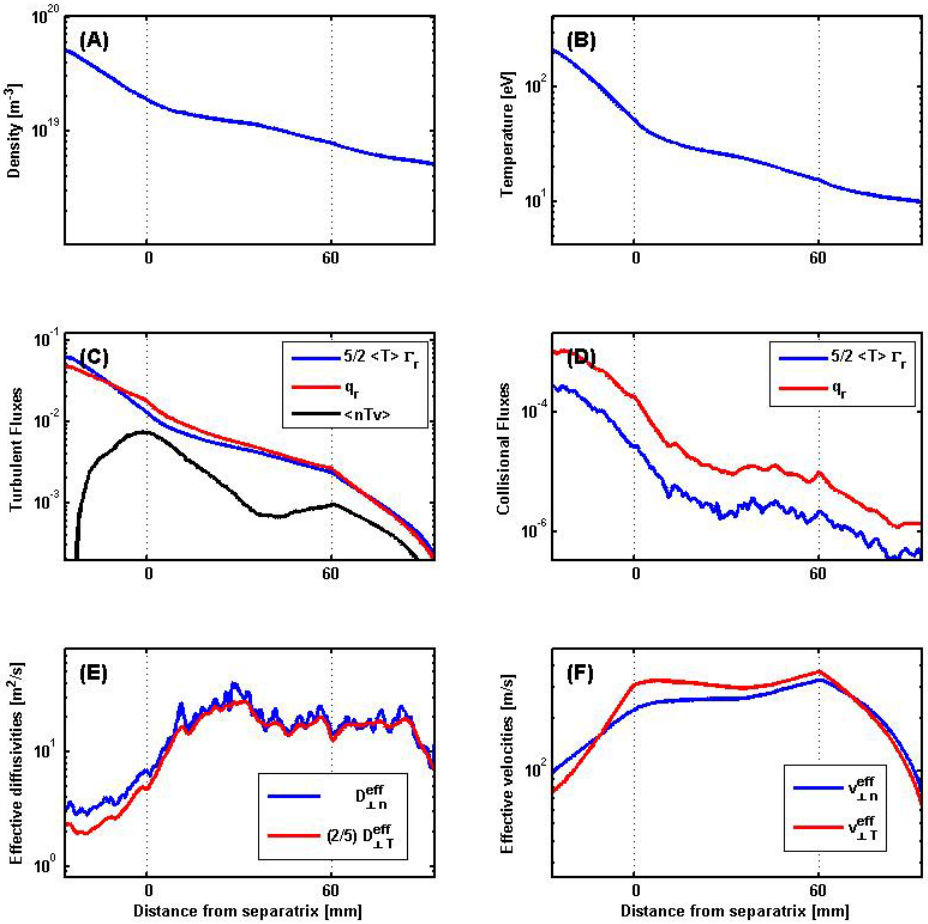

Figure 6. Density (A) and temperature (B) profiles from simulations. Turbulent (C) and collisional convective, conductive and fluctuating energy fluxes (D), effective diffusivities (E) and effective convective velocities (F).

2.2.5 Radial interchange motions of filamentary structures in fluids and magnetized plasmas

O. E. Garcia, V. Naulin, A. H. Nielsen, J. Juul Rasmussen, and N. H. Bian (School of Physics and Astronomy, UMIST, Manchester, M60 1QD, UK)
odd.erik.garcia@risoe.dk

Experimental measurements demonstrate that radial convection of localized plasma filaments dominates the cross-field transport of particles and heat through the scrape-off layer of magnetically confined plasmas. This results in significant plasma-wall interactions with potentially severe consequences for the next generation fusion experiments. A theory has recently been developed that successfully describes the physical mechanism underlying radial motion of isolated filamentary structures, which appears as blobs in the plane perpendicular to the magnetic field.[1,2]

A two-field interchange model has been studied by means of numerical simulations on a biperiodic domain perpendicular to the magnetic field. The simulations were initialized with a stationary blob-like structure on top of a uniform background plasma. It has been shown that such plasma filaments develop dipolar vorticity and electrostatic potential fields, resulting in rapid radial acceleration and formation of a steep front and a trailing wake, similar to experimental measurements. Figure 7 shows, from left to right, the plasma density, electric drift vorticity, and electric potential at one instance of time during the radial blob motion.

While the dynamical evolution strongly depends on the amount of collisional diffusion and viscosity, the structure travels a radial distance many times its initial size in all parameter regimes in the absence of parallel losses. For small collisional dissipation the structure is unstable to fragmentation by secondary instabilities, resulting in complex waveforms from single-point recordings even for an isolated structure. The plasma filament eventually decelerates due to dispersion by the convective flows. In the ideal limit, there is an inertial scaling of the maximum filament velocity, given by the acoustic speed times the square root of the structure size relative to the length scale of the magnetic field.[2]

For the relevant parameter regimes, the results are found to compare favorably with experimental probe measurements and fast camera imaging in the scrape-off layer of tokamak plasmas.[2]

1. N. H. Bian, S. Benkadda, J.-V. Paulsen, and O.E. Garcia, Phys. Plasmas **10**, 671 (2003).
2. O. E. Garcia, N. H. Bian, V. Naulin, A. H. Nielsen, and J. Juul Rasmussen, Phys. Plasmas **12**, 090701 (2005).

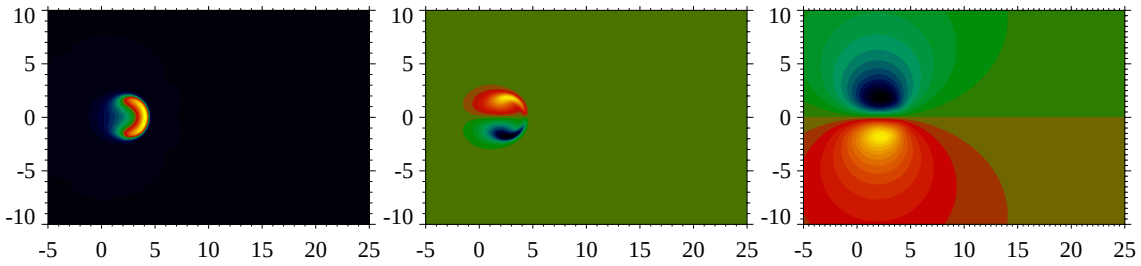

Figure 7. From left to right is shown the plasma density, electric drift vorticity, and electrostatic potential in the plane perpendicular to the magnetic field at one instance during radial blob motion.

2.2.6 A gyro-fluid model for turbulence and transport in the edge region of a toroidal plasma

J. Madsen, J. Staerk, V. Naulin, J. Juul Rasmussen, A. Kendl (Institute for Theoretical Physics, University of Innsbruck, A-6020 Innsbruck, Austria), O.E. Garcia and A. H. Nielsen
jens.juul.rasmussen@risoe.dk

It is well established that the turbulence and transport in the edge and scrape-off-layer (SOL) of toroidally magnetized plasmas is strongly intermittent and involves outbreaks of hot plasma. These structures, often referred to as “blobs”, are formed near the last closed flux surface (LCFS) and propagate far into the SOL. The convective transport mediated by the blob-like structures prevails in virtually all confinement states, including edge-localized modes. They have a profound influence on the pressure profiles in the SOL, the ensuing parallel flows, and the power deposition on plasma facing components. The basic blob dynamics is well described in terms of nonlinear interchange motions[1,2] in the limit of cold ions (see Secs. 2.2.1 and 2.2.5).

In experiments in large devices it is, however, observed that the ion temperature in the SOL is comparable to or even higher than the electron temperature due to the rapid loss of hot electrons. Thus, it appears important to investigate the influence of finite ion temperature on the dynamics in the edge and SOL.

We have initiated the development of a gyro-fluid model for the turbulent dynamics in the edge and SOL. The model describes the evolution of the electron and ion densities and temperatures coupled through the polarization equation[3]. It governs two-dimensional interchange dynamics at the outer midplane of a toroidally magnetized plasma and contains the global evolution of the full profiles. It is as such a generalization of the Risø ESEL-code[2] (Sec. 2.2.1).

Initially, we have applied the model to investigate the influence of finite ion temperature and finite Lamor radius effects on the propagation properties of isolated blob structures for various electron to ion temperature ratios. The basic features of the blob propagation are not altered by finite ion temperatures, but the detailed behaviour may be significantly changes, in cases of high temperature ratios preventing nonlinear fragmentation and thus enhancing the radial advection properties of such filamentary structures, which may result in detrimental power deposition on plasma facing components.

1. O.E. Garcia, V. Naulin, A. H. Nielsen, and J. Juul Rasmussen, Phys. Plasmas **12**, 062309 (2005).
2. O.E. Garcia, N. H. Bian, V. Naulin, A. H. Nielsen, and J. Juul Rasmussen, Phys. Plasmas **12,** 090701 (2005).
3. D. Strintzi and B. Scott, Phys. Plasmas (2004) **11,** 5452.

2.2.7 Turbulent transport and mixing of impurities in the edge of a toroidal plasma

J. Gavnholt, S. Boudaud, O.E. Garcia, V. Naulin, A.H. Nielsen and J. Juul Rasmussen
jens.juul.rasmussen@risoe.dk

The transport of impurities in the edge plasma region is of increasing concern in fusion research experiments. The impurities are mainly generated at the first wall and plasma facing components, but are subsequently transported into the edge region and often all the way to the plasma centre. The transport is found to be strongly anomalous and turbulence is certainly playing a decisive role.

The transport in the edge and scrape-off-layer (SOL) of toroidal plasmas is found to be strongly intermittent and involves large outbreaks of hot plasma (Sec. 2.2.1). These bursts have a significant effect on the profiles of density and temperature and will strongly influence the mixing and transport of impurities. We have investigated the transport of impurities in the edge and SOL numerically using the ESEL-model[1] governing the interchange dynamics at the outboard mid-plane of a toroidal device.

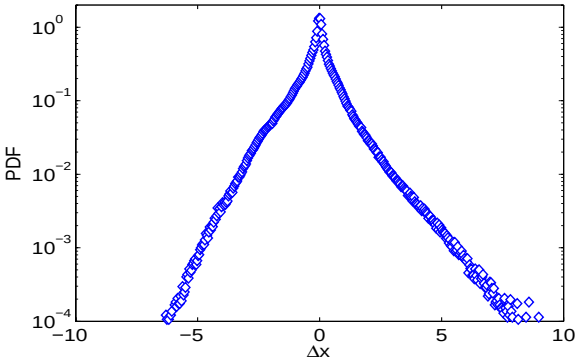

Figure 8. The PDF of the radial displacement, Δx, measured over Δt = 50 for all particles.

The dynamics of the impurities in the turbulent flow is investigated by employing a test particle approach[2]. The impurity density is assumed to be low and the impurities are ionised, thus they are described as particles that are passively advected by the turbulent ExB-velocity. We observe that the impurity transport cannot be described by a simple diffusion process; it is strongly anomalous with step-length probability distributions (PDF) having fat non-Gaussian tails that decays approximately exponentially as shown in Figure 8. However, the impurities are rapidly mixed in the SOL region and the impurity density attains an "equilibrium" profile ranging well into the edge of the plasma inside the LCFS. The "mixing" time is found to be weakly influenced by the initial position of the impurities, and is only few times the characteristic period of the bursts. Thus, even particles released far into the SOL are rapidly transported inside the LCFS, see Figure 9.

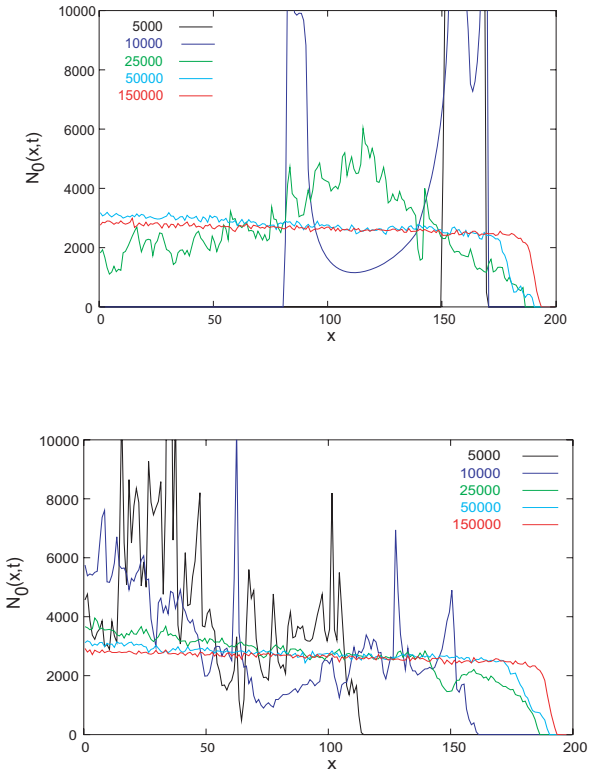

Figure 9. Evolution of the impurity density, N_0, averaged over the poloidal-direction. Impurities are released in a narrow band around x = 160 (left panel) and x = 40 (right panel). The last closed flux surface is located at x = 50.

1. O.E. Garcia, V. Naulin, A.H Nielsen and J. Juul Rasmussen, Phys. Rev. Lett. 92, 165003 (2004); Phys. Plasmas 12, 062309 (2005); Phys. Scripta T122, 89 (2006).

2. V. Naulin, Phys. Rev. E 71, 015402, (2005); M. Priego, , O.E. Garcia,., V. Naulin, , and J. Juul Rasmussen, Phys. Plasmas 12, 062312(2005) V. Naulin, O.E. Garcia, M., Priego, and J. Juul Rasmussen, Physica Scripta T 122, 129-134 (2006).

2.2.8 Turbulence spreading, anomalous transport, and pinch effect

V. Naulin, A. H. Nielsen and J. Juul Rasmussen
volker.naulin@risoe.dk

Traditional transport models are based on local assumptions balancing an instability growth rate with the turbulent flux, resulting in the paradigmatic mixing length approach.

Alternatives are based on look-up tables or similar heuristic approaches. All these models, which only accounts for the local properties of the plasma, fail if more complex transport phenomena are to be described, such as up gradient transport or fast pulse propagation. As a remedy for that approach we suggest a simple alternative based on the transport of the turbulence away from the place of its origin. A paradigmatic model[1] describing transport and turbulence spreading as coupled processes is proposed, trying to unify the approaches of penetrative overshoot and overshoot. Direction of the transport is, opposed to earlier models which took nonlocal effects into account, dependent on the local phase relationship between velocities and transported quantities. As a natural consequence asymmetric radial spreading of the turbulence, up-gradient transport in regions where the turbulence is damped, and front propagation are observed. The model accounts for the interaction between the microscale of the turbulence and the meso-, respectively, system scale on which profile modifications occur. Comparison with direct numerical simulations of two-dimensional interchange turbulence shows qualitatively good agreement with the proposed transport model. Key transport features are reproduced even in the presence of coherent blob-like structures. Features of cold pulse dynamics and heat wave propagation are investigated for JET pulses.

1. V. Naulin, A.H. Nielsen, and J. Juul Rasmussen, Phys. Plasmas 12, 122306 (2005).

2.2.9 Simulations of plasma dynamics in the TORPEX device

*V. Naulin, S. Mueller,[*] and A. Fasoli[*] (*CRPP, EPFL, CH-1015 Lausanne, Switzerland)*
volker.naulin@risoe.dk

TORPEX[1] is a toroidal plasma experiment without confinement properties. The purely external magnetic field is composed of a toroidal component overlaid with a variable vertical magnetic field. Plasma production is by RF-Heating. The geometry of the device allows simulating for cold plasma (ion temperature negligible) the competing effects of parallel losses and perpendicular turbulent transport. Dimensions of the device are small enough for the plasma to be simulated with state of the art computers, while the long parallel correlation length allows resolving the toroidal angle with only one drift plane in the most extreme case. A numerical code utilizing this principle is under development and will help to implement and verify sheath boundary conditions for fluid codes in general.

1. S. H. Müller, A. Fasoli, B. Labit, M. McGrath, M. Podesta, and F. M. Poli, Phys. Rev. Lett. 93, 165003, (2004).

2.2.10 Drift waves in a high-density cylindrical helicon discharge

Christiane Schroeder, Olaf Grulke*, Thomas Klinger*, Thomas Windisch* (*IPP Greifswald, Germany), Volker Naulin*
volker.naulin@risoe.dk

A low-frequency instability is investigated in a helicon plasma, which is characterized by comparably high plasma-beta and high collision frequencies. Single movable Langmuir probes and a poloidal probe array are used for studies of spatiotemporal dynamics and for characterization of the background plasma parameters. All experimentally observed

features of the instability are found to be consistent with drift waves. A linear nonlocal numerical model for drift modes, based on the two-fluid description of a plasma, is used for comparison between the experimental observations and theory. Comparing numerical and experimental frequencies, it is found that the experimentally observed frequencies are consistent with drift waves. The numerical results show that the high electron collision frequencies provide the strongest destabilization mechanism in the helicon plasma.[1]

Three dimensional simulations of the whole experiments are under way.

1. C. Schröder, O. Grulke, T. Klinger and V. Naulin, Phys. Plasmas **12**, 042103 (2005).

2.2.11 A super-resolution method for spatio-temporal plasma diagnostics

I. Teliban[*]*, D. Block*[*]*, A. Piel*[*] *(Institut für Experimentelle und Angewande Physik, Universitat Kiel, 24340 Kiel, German) and V. Naulin*
volker.naulin@risoe.dk

To study turbulence, high spatial and temporal resolution is required. In experiments, plasma diagnostics are characterized by low spatial and high temporal resolution. An adapted super-resolution algorithm is proposed to improve the spatial resolution by using temporal information[1]. The performance of the super-resolution algorithm is compared with simple interpolation techniques. The performance of the algorithm is benchmarked by means of synthetic data.

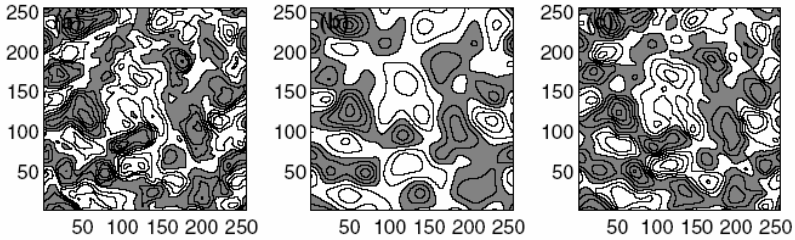

Figure 10: (a) Full resolution image of turbulent fluctuation obtained from a Hasegawa–Wakatani drift wave model. The grey and white regions represent negative and positive fluctuation amplitudes. The plot is normalized to its maximum. The contour lines are equidistant with a separation of 0.2. (b) Result of simple interpolation applied to a downsampled plot (a). Contour levels and normalization are identical with plot (a). (c) Result of super-resolution applied to the same downsampled data as used for (b). Normalization and contour levels are again identical with plot (a).

It was shown that simple interpolation of typical experimental data does not yield reliable results for turbulence investigations. Amplitude, trajectory and shape are found to be subject to severe errors even for structures, which are much larger than the spatial Nyquist limit. A detailed comparison with super-resolved data revealed that amplitude, trajectory and shape are significantly improved by the application of our super-resolution algorithm. These important physical quantities are found to be reproduced qualitatively and quantitatively, even for structures smaller than the spatial Nyquist limit. Further, improvement in spatial resolution has been demonstrated. Especially, the application of the super-resolution algorithm to turbulence data obtained from a Hasegawa–Wakatani drift wave model showed that the algorithm is able to deal with typical turbulence data and significantly improve the results. Hence the proposed super-resolution is found to be suitable for plasma turbulence investigation. This method promises better diagnostics of the transport processes in plasma turbulence and especially the investigation of large

scale coherent structures, their dynamics and the lifetime will benefit from super-resolution.

1. I. Teliban, D. Block, A. Piel, and V. Naulin, Plasma Phys. Contr. Fusion, 48, 419 (2006).

2.2.12 Probe measurements of fluctuations in the edge and scrape-off layer of toroidal devices

P.C. Balan, R.W. Schrittwieser*, C. Ionita* (*Institute for Ion Physics, University of Innsbruck, Austria), V. Naulin and J. Juul Rasmussen*
jens.juul.rasmussen@risoe.dk

The Experimental Plasma Physics Group at the University of Innsbruck is performing fluctuation measurements in the edge region and Scrape-off-Layer (SOL) at various European Tokamaks. The purpose of these measurements is to characterise the turbulent fluctuations and in particular to investigate the turbulent driven particle flux and the Reynolds Stress, which governs the momentum transport. The measurements are carried out with arrays of cold as well as emissive probes. The aim of the collaboration with the Innsbruck group is to contribute to the evaluation of the probe measurements and perform comparisons with results from simulations of plasma turbulence.

The investigations have comprised measurements at ISTTOK in Portugal and ASDEX Upgrade at IPP Garching.

In the ISTTOK measurements a probe array consisting of three emissive and one cylindrical probe was applied. The probe array was able to record the density, the poloidal and radial electric field, and their fluctuations, simultaneously. The statistical properties of the poloidal electric field and of the turbulent particle flux, measured with cold and emissive probes, were compared. Both the root mean square of the poloidal electric field and the fluctuation-induced particle flux were found to be significantly larger when measured with the emissive probes, indicating that temperature fluctuations are important for determining the particle flux. A clear reduction of the turbulent particle flux and an improvement of the plasma confinement were observed during negative edge biasing with an emissive electrode.

For the measurements in ASDEX Upgrade a fast reciprocating probe shaft was used on the mid-plane manipulator. The probe head was mounted with five pins. Three pins measure the floating potential and its fluctuations and the remaining two pins are biased to ion saturation and swept, respectively. During a discharge typically a few reciprocations into the plasma were performed. The probe configuration allowed the calculation of the radial fluctuation-induced particle flux simultaneously with the Reynolds stress. Initial evaluations indicate that the Reynolds stress and the fluctuations-induced particle flux show increased bursting behaviour during ELMs, revealing part of the ELM fine structure.

2.3 Millimetre waves used for diagnosing fast ions in fusion plasmas

H. Bindslev, S.B. Korsholm (also at MIT Plasma Science and Fusion Center, Massachusetts, USA), F. Meo, P.K. Michelsen, S. Michelsen, S.K. Nielsen and E.L. Tsakadze
henrik.bindslev@risoe.dk
www.risoe.dk/euratom/cts

Millimetre waves, corresponding to frequencies in the 100 GHz range, permit probing and imaging on the centimetre scale and transmission of signals with bandwidths in excess of 10 GHz. Coherent sources are now available from the micro- to Megawatt range, CW. These technologies, widely used in fusion research, and in many cases specifically developed for fusion research, are now being considered for a broader range of commercial applications, including new GigaBit wireless Internet highways and wide area networks which avoid expensive trenching of optical fibres.

In the world of fusion, the millimetre waves are used extensively both as a diagnostic tool and as an actuator for manipulating the plasma locally as well as globally. Central to achieving these objectives is the fact that millimetre waves, like laser light, can be projected in narrow focused beams and, unlike laser light, the millimetre waves can interact strongly with the plasma.

At Risø we develop and exploit millimetre wave diagnostics for measuring the velocity distribution of the most energetic ions in fusion plasmas. The measurements are resolved in space on the centimetre scale and in time on the millisecond scale.

The most energetic (or fast) ions are the result of fusion reactions and auxiliary heating. Their interaction with the bulk plasma is the main mechanism by which the fusion plasmas reach and sustain the high temperatures of 100-200 million degrees Kelvin required for fusion. The considerable energy associated with the fast ions can also drive turbulence in the plasma, and degrade the confinement of the plasma and of the fast ions themselves. Understanding and controlling the dynamics of fast ions are central tasks in the development of fusion energy, and one of the main research topics for the next large fusion facility, ITER. It is a task we seek to contribute to by developing and exploiting the unique diagnostic capability of millimetre wave based collective Thomson scattering (CTS).

The group has developed fast ion CTS diagnostics for the TEXTOR and ASDEX Upgrade tokamaks, which are located at the Research Centre Jülich and at the Max-Planck Institute for Plasma Physics in Garching, both in Germany. These projects are conducted in collaboration with MIT, the Max-Planck Institute for Plasma Physics in Garching and the TEC[1] consortium.

The upgraded CTS system for TEXTOR was brought into operation in 2005 and first results obtained. Details of this work are given in subsections 2.3.1 to 2.3.4. The ASDEX Upgrade CTS receiver system was ready in 2004. In 2005 further tests and commissioning was carried out, details of which are given in subsection 2.3.5. Commissioning of the full system and first results are awaiting operation of the new dual frequency gyrotron.

A study by Risø, of the feasibility of measuring the fast ion phase space distribution in ITER by CTS was completed in 2003. The study revealed that a CTS system based on a 60 GHz probe has the highest diagnostic potential, and is the only CTS system expected to be capable of meeting all the ITER fast ion measurement requirements with existing

or near term technology. Since then a detailed design has been under development. The focus in 2005 has been on detailed engineering design of invessel components. Especially, the antenna system on the high field side presents a challenge due to the limited space between and behind blanket modules. Results of this work are described in subsection 2.3.6.

1. TEC: the Trilateral Euregio Cluster, comprising Association EURATOM-Forschungszentrum Jülich GmbH, Institut für Plasmaphysik, Jülich, Germany; Association EURATOM-FOM, Institute for Plasma Physics, Rijnhuizen, The Netherlands; and Association EURATOM-ERM/KMS, Belgium.

2.3.1 First results from the upgraded fast ion collective Thomson scattering diagnostic at TEXTOR

S. K. Nielsen, H. Bindslev, S.B. Korsholm (also at MIT), F. Leipold, F. Meo, E. L. Tsakadze, S. Michelsen, P. Michelsen and P. Woskov (MIT)
stefan.kragh.nielsen@risoe.dk

During 2005, the first results were obtained from the upgraded collective Thomson scattering (CTS) system at TEXTOR (Institut für Plasmaphysik, Jülich, Germany). The upgraded parts of the system (2004) include new receiver electronics, a quasi optical transmission line and a universal polarizer. Furthermore, the plasma facing mirror is movable which eases the task of finding and confirming the presence of beam overlap between the receiver and the probe beam. Also a new data acquisition system has been installed allowing synchronized sampling of all 42 frequency channels with a sampling frequency of 100 ksamples/s at 24 bit resolution. The probe consists of a 110 GHz gyrotron operated by the FOM team from the Netherlands. Further details on the upgraded CTS system at TEXTOR can be found in the annual report of 2003 section 2.2.4 and that of 2004 section 2.3.2.

2.3.2 Fast ion data

S. K. Nielsen, H. Bindslev, S.B. Korsholm (also at MIT), F. Meo, E. L. Tsakadze, P. Woskov(MIT)
stefan.kragh.nielsen@risoe.dk

The main commissioning of the CTS system at TEXTOR was carried out in February 2005. The commissioning included obtaining beam overlap between the receiver and the probe (gyrotron) and this was achieved in a number of geometries. In order to distinguish the scattered signal from the background plasma noise the probe beam is modulated 2 ms on and 2 ms off. A time trace of the signal sampled in one of the CTS channels is shown in figure 11.

Several physics programs/campaigns have been conducted on TEXTOR using the CTS fast ion diagnostic. Amongst others, measurements of the anisotropy in the velocity distribution of beam ions and slowing down of the beam ions have been measured during 2005. An example of the development of the 1D fast ions distribution function resolved along the direction 45 degrees to the magnetic field during the turn off of the co-current neutral beam injector at TEXTOR is shown in figure 12. Also a program/campaign studying the fast ion redistribution during sawtooth oscillations has been initiated at the end of 2005. Furthermore, an investigation of a possible interference between Ion Cyclotron Resonance Heating (ICRH) system and the gyrotron has been started.

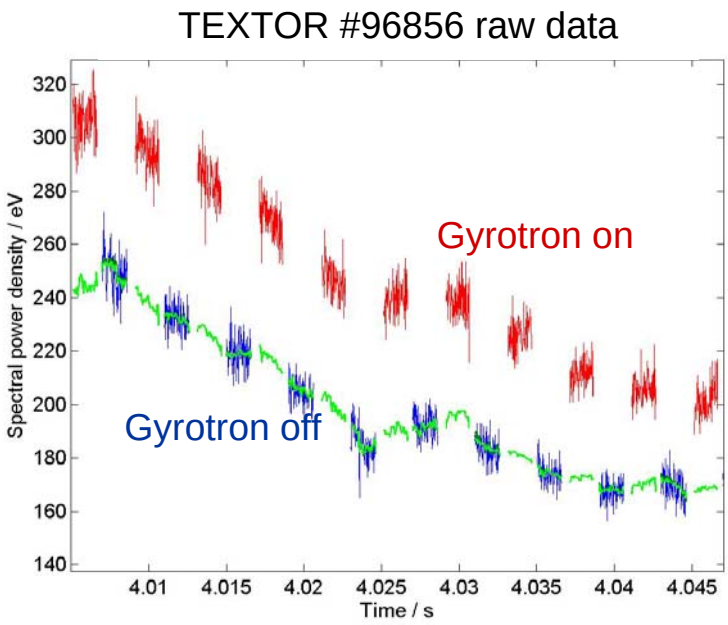

Figure 11: Example of raw data during overlap. The green line is the fitted background signal.

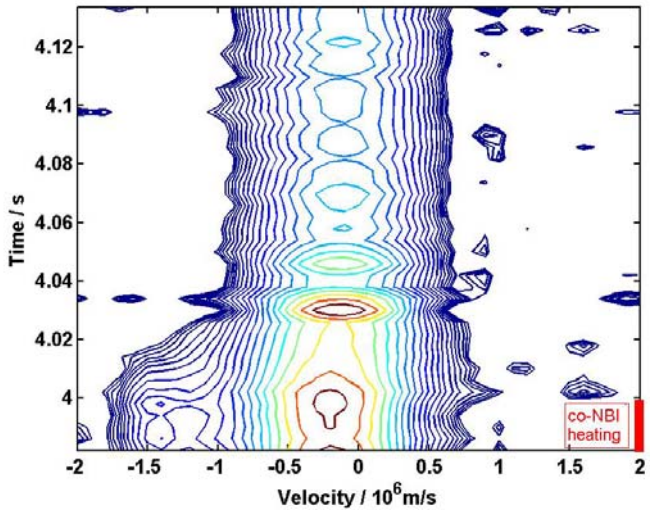

Figure 12: Evolution of the 1D fast ion distribution function projected 45 degrees to the magnetic field during the turn-off of the co-current NBI. The fast ions in the bottom left corner can been seen to thermalise within 40 ms.

2.3.3 Tuning of the 110 GHz FOM gyrotron at TEXTOR

S .K. Nielsen, S .B. Korsholm(also at MIT), F. Meo, P. Woskov(MIT), F. Leipold
stefan.kragh.nielsen@risoe.dk

It is of high importance that the probe used for fast ion collective Thomson scattering is spectrally clean. The power of the scattered radiation is several orders of magnitude lower than the probing radiation. Hence any spectrally impure signal emitted from the gyrotron would corrupt the CTS measurements. The FOM 110 GHz gyrotron has four control parameters, namely the electron beam acceleration voltage, the cathode voltage, the magnet current and the filament voltage. Changing these values affect both the output frequency of the main mode and the power output. More importantly, when doing scattering experiments, these parameters also influence the amount of spurious modes

emitted from the gyrotron. During 2005, a great effort has been made to investigate the parameter range of the gyrotron giving spectrally clean output with all power in a single mode. Figure 13a shows an example of a spectrally impure gyrotron output, while figure 13b shows a result of gyrotron tuning. Two spectrally pure gyrotron settings were found: one setting at 100.11 GHz with an estimated power of 50 kW and another setting at 109.97 GHz with an output power estimated to be 180 kW.

Also the frequency drift of the gyrotron was measured during a 50% duty cycle (2 ms on/2 ms off) for 400 ms. This drift is shown in figure 14 and is due to thermal heating of the gyrotron cavity.

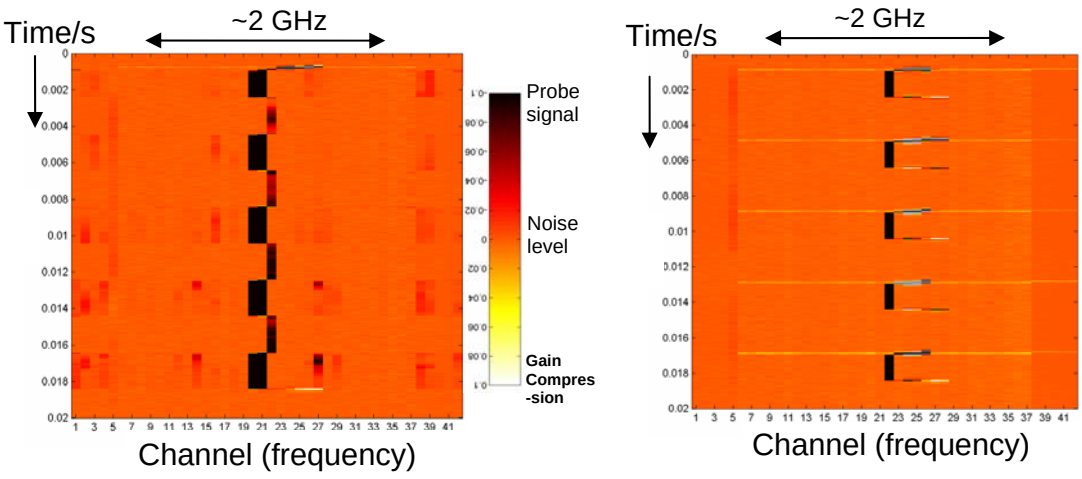

(a) (b)

Figure 13a: example of spectrally impure gyrotron mode. During the on time of the gyrotron (wide black line) several spurious modes are present. Figure 13b: example of spectrally pure gyrotron mode after tuning. During the on time of the gyrotron the responds is only seen in one channel. In the ramp up and ramp down phase some higher frequency modes may be seen.

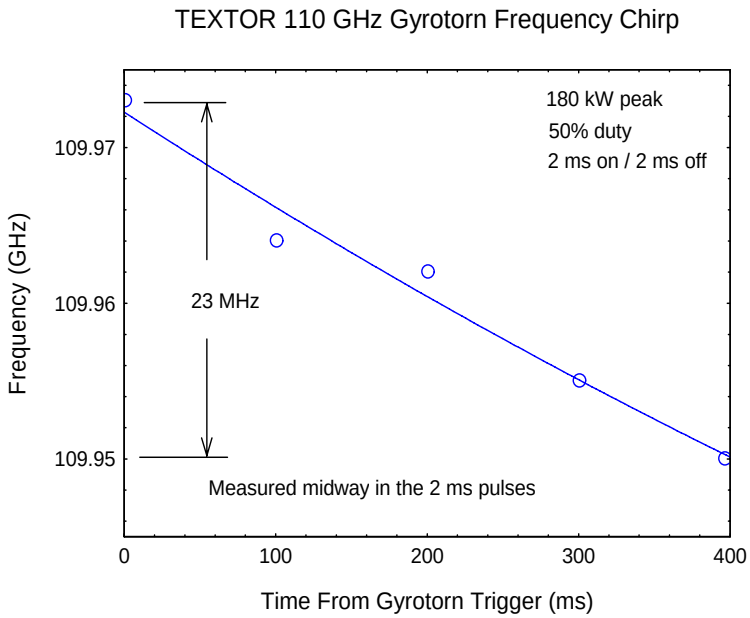

Figure 14: measurements of the Gyrotron frequency drift due to thermal heating of the gyroton cavity.

2.3.4 Alignment of the in-vessel components of the TEXTOR mm-wave CTS transmission line

E. L. Tsakadze, S. B. Korsholm, F.Leipold, M. Jessen, S. Nimb and J. Holm
erekle.tsakadze@risoe.dk

During the 2005 TEXTOR summer opening a new set of motors was installed 3 meters from the vacuum vessel, which via a shaft and belt transmission enables remote movement of the in-vessel mirror during a plasma shot.

Following the motor installation a re-alignment of the CTS transmission line was performed. Particular attention was paid to the alignment of the in-vessel quasi-optical mirrors relative to the corrugated circular (CC) waveguide and, thus, to the rest of the system.

The alignment was carried out by means of an alignment laser and a low power 110 GHz microwave source connected to the CTS receiver horn defining the CTS beam pattern. A mobile receiver mini-rig was constructed to measure the microwave beam pattern both inside the vessel (see figure 15) and between the machine vessel and the CTS receiver. A typical beam pattern measured by the mini-rig inside the vessel after alignment is shown in Figure 16. One may see that the shape of the beam transmitted through the CTS antenna and measured inside the machine is still very close to a Gaussian.

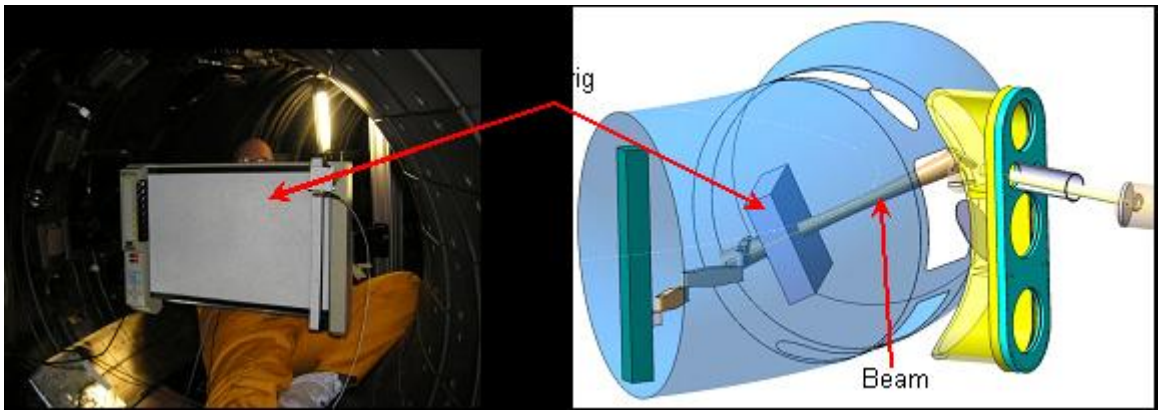

Figure 15: Installation and beam pattern measurement by the Risø-made mini-rig.

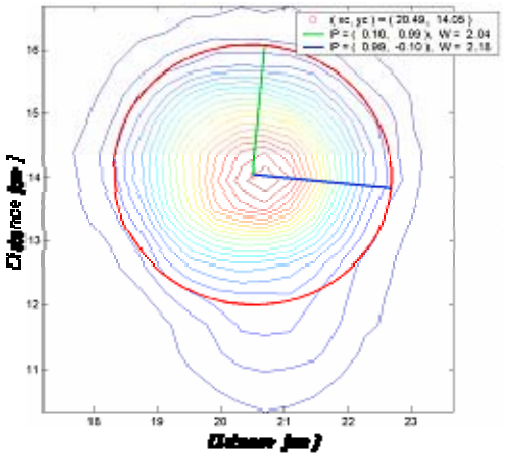

Figure 16: Measured microwave beam pattern (contour-plot) and its Gaussian fit (red ellipse) inside the machine.

Upon completing the alignment procedure a verification of the different viewing directions were performed using the alignment laser and the mini-rig. More than 300 points were mapped and imported into the code controlling the viewing direction of the moveable/first mirror.

2.3.5 Collective Thomson scattering diagnostic at ASDEX Upgrade

F. Meo, H. Bindslev, S.B. Korsholm (also at MIT Plasma Science and Fusion Center, Massachusetts, USA), P.K. Michelsen, S. Michelsen, S.K. Nielsen and E.L. Tsakadze
fernando.meo@risoe.dk

The ASDEX Upgrade (AUG) CTS diagnostic system was described in the annual report of 2004 subsection 2.4.2 and in that of 2005 in subsection 2.3.1. The new AUG dual frequency gyrotron, which will provide the probe radiation for the CTS diagnostic, was expected to be ready for testing during the spring 2005. This would have permitted the first CTS measurements in the summer of 2005. However, the AUG gyrotron infrastructure for launching power into the plasma was not ready and the decision was made to postpone these experiments till 2006. There were, however, several investigations and improvements made to the CTS receiver system in 2005.

Prior to October 2005, the measured transmission line throughput was about 70-75%. In addition, the beam pattern was not known. A 110 GHz Gunn oscillator was installed in the receiver box to radiate through the receiver horn into the transmission line towards the tokamak. A mobile receiver mini-rig was used to measure the beam pattern at different locations. Using a specially designed two way laser as a reference, the alignment of each component was done by changing the mirrors angles to match the maximum radiation to the laser reference. The most sensitive portion of the transmission line was receiver horn position and the coupling mirror to the waveguide (ref. annual report of 2004 subsection 2.4.2). The radiation was also measured at the end of the transmission line in the torus hall. The alignment was improved to about 85-90% throughput.

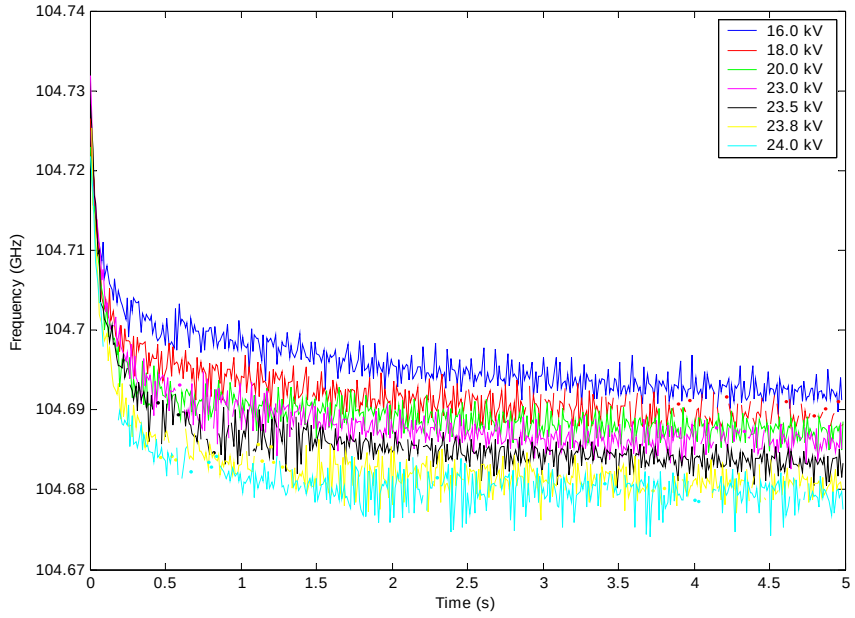

Figure 17: Measured frequency versus time of the dual frequency gyrotron, which will provide the probeing radiation for the CTS diagnostic at ASDEX Upgrade.

There was significant progress to the gyrotron commissioning by IPP with a maximum launched power of 500 kW for 5 seconds into the main load (at 105 GHz). For CTS measurements, it is important to investigate the gyrotron behavior during its operation. The first aspect is the frequency evolution caused by thermal effects of the cavity. The second is spurious modes that may exist in the spectrum.

It is important that the frequency evolution during a discharge be minimized. The experiments were done by analyzing the gyrotron signal from a pick-off wave guide installed in the vicinity of the main central high power load. Two methods of frequency measurements were done simultaneously each offering high temporal resolution and long operation times; the first was using the CTS receiver to digitize an analogue output from a free running spectrum analyzer supplied by IPP. The second method measured the frequency down converted signal using a harmonic mixer and an oscilloscope. An example of the frequency evolution as a function of power can be seen in the Figure 17. Powers ranged from 100 – 460 kW and the frequency drift was less that 100 MHz. The frequency drift increases with increasing power as expected and 90% of the drift occurred in the first 100 ms.

Discharges were also made with a 40 ms modulation period and a 50 % duty cycle. Figure 18 shows the two types of frequency evolutions: a base portion where the reference value decreases with time and a drift at every gyrotron turn on time. The gyrotron voltage rise time is 0.5 ms and hence this second type of frequency drift must still be due to thermal effects of the cavity.

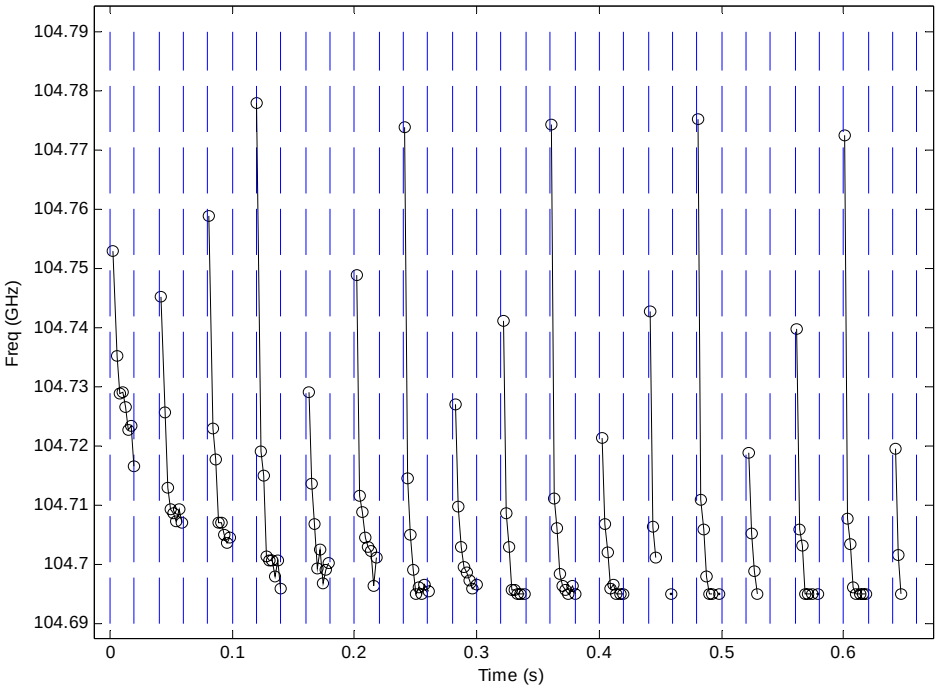

Figure 18: Measured frequency versus time of the dual frequency gyrotron, which will provide the probing radiation for the CTS diagnostic at ASDEX Upgrade. Here the power is modulated with a 40 ms modulation period and a 50 % duty cycle.

The data suggests the cooling efficiency of the new gyrotron is very high. For an off time of 20 ms, there is an 80 MHz drift in 7 ms which is not acceptable for CTS measurements. There were preliminary studies (at 140 GHz frequency) done with 5 ms off time. These studies have shown a significant improvement where the frequency drifts 25 MHz during the first 2 ms.

The frequency measurements enabled us to retune the notch filters to a more precise value and with a narrower and deeper notch. Another important gyrotron prerequisite for CTS measurements is the gyrotron mode purity. The panel separating the MOU boxes was removed to measure the spurious radiation from MOU#1 where the gyrotron is located. The figure below shows the data measured for modulated operation at 500 kW. Thus far, for the largest power of 500 kW, the spectrum was clean. A sample measurement is shown in Figure 19. Studies are still preliminary. Experiments on TEXTOR have shown that reflections back to the gyrotron are one of the main causes of spurious modes. Therefore further tests need to be done while launching into the vacuum vessel through the diamond window.

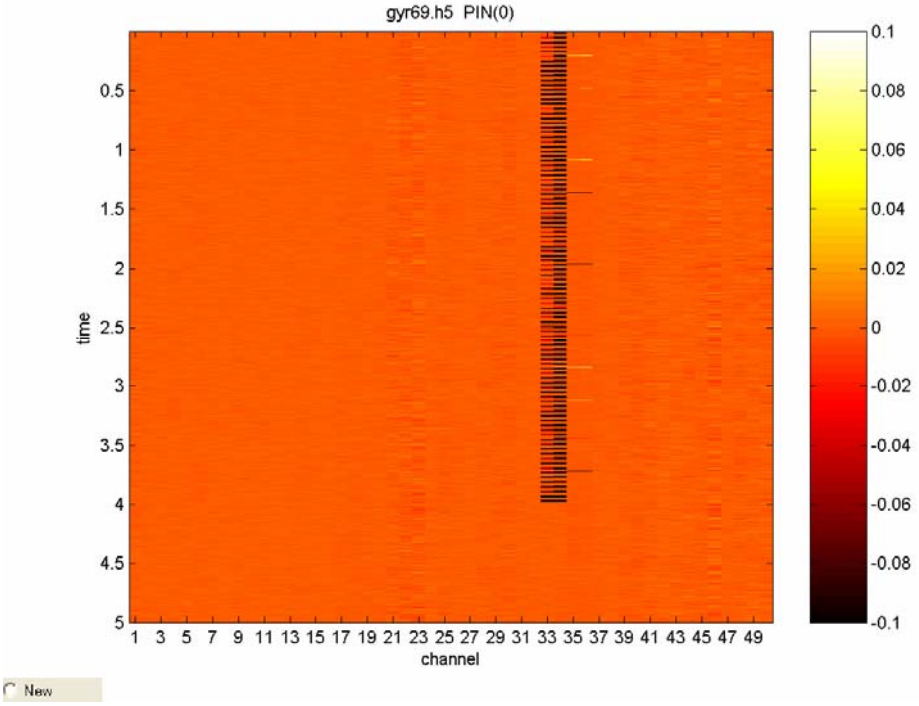

Figure 19: Spectrum of AUG gyrotron output measured with AUG CTS receiver. Spectrum is free of spurious modes.

2.3.6 Detailed integrated design of CTS for ITER

P.K. Michelsen, H. Bindslev, A.W. Larsen, F. Meo, S. Michelsen, S. Nimb, A.H. Nielsen and E.L. Tsakadze
poul.michelsen@risoe.dk

In 2003 the Risø CTS group finished a feasibility study and a conceptual design of an ITER Fast Ion Collective Thomson Scattering System. The purpose of the CTS diagnostic is to measure the distribution function of fast ions in the plasma. The feasibility study demonstrated that the only system that can fully meet the ITER measurement requirements for confined fusion alphas is a 60 GHz system. The study showed that with two powerful microwave sources at this frequency (gyrotron) and two antenna systems, one on the low field side (LFS) and one on the high field side (HFS), it should be possible to resolve the distribution function of fast ions both for perpendicular

and parallel velocities with good spatial and temporal resolution. As a continuation of this work a detailed integrated design of a Fast Ion Collective Thomson Scattering diagnostic for ITER has been developed further in 2005.

In the first part of the work an optimization of design of the HFS receiver system is considered. Overlap and scattering simulations were performed for the updated HFS-antenna system taking into account the different beam diameters calculated by Gaussian optics for a variety of ITER plasma profile. The results show that the measurement requirements are satisfied with the new mirror position imposed by the various engineering constraints.

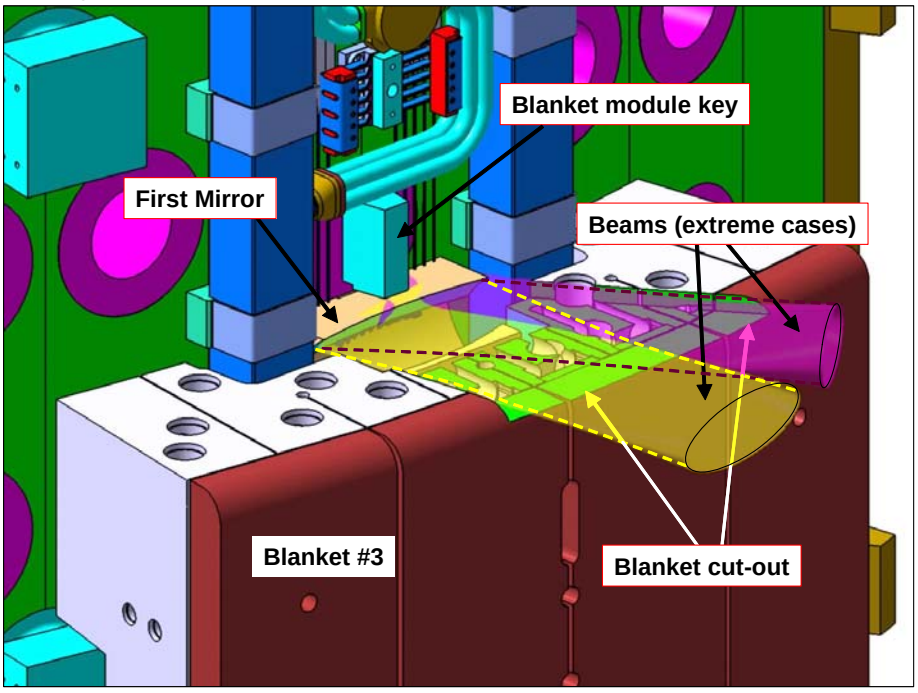

Figure 20: CATIA drawing showing the beam patterns of the high field side CTS receiver antennae, a blanket module with cuts, back vacuum vessel wall and other systems in the vicinity of the HFS CTS receiver antennae.

A detailed design of front-end components was carried out in close collaboration with the ITER IT. The antenna systems both on the high field side (HFS) and on the low field side (LFS) were considered. On the HFS the horizontal and vertical dimensions of the first mirror are limited by the space available between the cooling manifolds and the space between blanket module key and the earth-strap mounting block, respectively. However, the feasibility report has shown that the CTS can satisfy the diagnostic requirements within these constraints. The largest integration issue is the size of the vertical gap between the blankets through which the receiver is viewing the plasma. Presently the vertical gap in the ITER design is 10 mm. According to the feasibility report, the vertical gap should be no less than 30 mm in order to satisfy the measurement requirements. Figure 20 shows the high field side forward scattering (HFS-FS) receiver system without the upper blanket #4. The blanket cut-out, shown in green, is angled in one direction, where the measurements are taking place. Also shown are the two beams at the limits of the angular coverage needed for the profile (7° and 37° from radial). Because the blanket module key limits the vertical position of the first mirror, it was necessary to lower the *effective* slot, so no cut-out would be required in blanket module #4. To develop an optimum design for the HFS-FS receiver antenna, including the geometry of the slot formed by the blanket cut-away, modelling and experimentation

with a mock up was used. The mock up included flexible implementation of horns and quasioptical components behind the blanket, and a model of the blanket. Waves were propagated in reverse in the mock up, i.e. from the receiver horn, via quasi-optical mirror through the slot. Beam patterns after transmission through the slot were measured as well power trapped on the back side of the slot. These measurements were compared with model calculations based on both anisotropic Gaussian beam modelling and on 2D full wave modelling based on finite difference codes. 3D full wave modelling does not appear possible because of the size of the structures relative to the wavelength. The results show that beam transmission through a slot with a width of 300 mm and a vertical opening of 30 mm is possible with acceptable transmission.

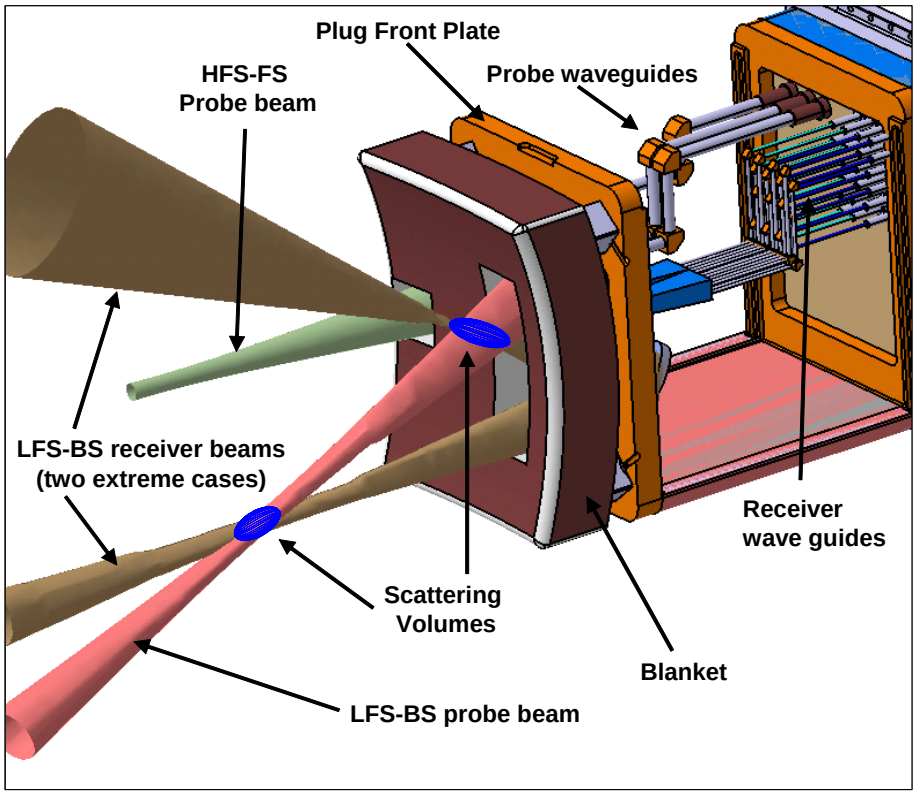

Figure 21: CATIA drawing showing the beam patterns of the low field side CTS receiver antennae, the two probe beams, port plug with apertures and waveguides.

Figure 21 shows the CTS design in port plug #12 with the 3D Gaussian beams. The two extreme low field side backward scattering (LFS-BS) receiver beams are in brown, the LFS-BS probe beam is shown in pink, and the HFS-FS probe beam in light green. The blue ellipses are the scattering volumes at both limits of the measurement.

The apertures for the LFS-BS probe and receiver have been combined from the previous design to 273 mm (H) and 1186 mm (V). The updated CTS apertures have also been lowered. This has some conflict with the aperture for the visible continuum array diagnostic. However, this diagnostic is located in the centre of the port viewing toroidally through this aperture. Hence, it is possible for both the CTS and visible continuum to share a common aperture. The shape and dimension of this shared aperture is yet to be determined. Finally, the extra horn array and transmission lines for the receiver and probe of a fuel ion ratio diagnostic have been added to the design. The latter is also based on collective Thomson scattering and can use the same probe as the LFS-BS fast ion CTS. The feasibility of such a diagnostic was investigated and found to be promising for a 60 GHz CTS but not for a 28 THz (CO_2 laser) CTS.

2.4 Publications and conference contributions

International publications

Basse, N.P.; Zoletnik, S.; Michelsen, P.K., Study of intermittent small-scale turbulence in Wendelstein 7-AS plasmas during controlled confinement transitions. Phys. Plasmas (2005) v. 12 p. 012507.1-012507.11

Basse, N.P.; Zoletnik, S.; Michelsen, P.K., Small-angle scattering theory revisited: Photocurrent and spatial localization. Phys. Scr. (2005) v. 71 p. 280-292

Basse, N.P.; Zoletnik, S.; Michelsen, P.K., Study of intermittent small-scale turbulence in Wendelstein 7-AS plasmas during controlled confinement transitions. Phys. Plasmas (2005) v. 12 p. 012507.1-012507.11

Bian, N.H.; Garcia, O.E., Structures, profile consistency, and transport scaling in electrostatic convection. Phys. Plasmas (2005) v. 12 p. 042307.1-042307.12

Chakrabarti, N.; Juul Rasmussen, J.; Michelsen, P.K., Ion temperature gradient driven mode in presence of transverse velocity shear in magnetized plasmas. Phys. Plasmas (2005) v. 12 p. 074501.1-074501.4

Donné, A.J.H.; Bock, M.F.M. de; Classen, I.G.J.; Hellermann, M.G. von; Jakubowska, K.; Jaspers, R.; Barth, C.J.; Meiden, H.J. van der; Oyevaar, T.; Pol, M.J. van de; Varshney, S.K.; Bertschinger, G.; Biel, W.; Busch, C.; Finken, K.H.; Koslowski, H.R.; Krämer-Flecken, A.; Kreter, A.; Liang, Y.; Oosterbekk, H.; Zimmermann, O.; Telesca, G.; Verdoolaege, G.; Domier, C.W.; Luhmann, N.C.; Mazzucato, E.; Munsat, T.; Park, H.; Kantor, M.; Kouprienko, D.; Alexeev, A.; Ohdachi,S.; Korsholm, S.; Woskov, P.; Bindslev, H.; Meo, F.; Michelsen, P.K.; Michelsen, S.; Nielsen, S.K.; Tsakadze, E.; Shmaenok, L., Overview of core diagnostics for TEXTOR. Fusion Sci. Technol. (2005) v. 47 p. 220-245

Egedal, J.; Bindslev, H.; Budny, R.V.; Woskov, P., Impact of beam ions on alpha-particle measurements by collective Thomson scattering in ITER. Nucl. Fusion (2005) v. 45 p. 191-200

Garcia, O.E.; Bian, N.H., Shear dispersion and turbulence decorrelation by differential rotation. Phys. Plasmas (2005) v. 12 p. 014503.1-014503.4

Garcia, O.E.; Bian, N.H.; Naulin, V.; Nielsen, A.H.; Juul Rasmussen, J., Mechanism and scaling for convection of isolated structures in nonuniformly magnetized plasmas. Phys. Plasmas (2005) v. 12 p. 090701.1-090701.4

Garcia, O.E.; Naulin, V.; Nielsen, A.H.; Juul Rasmussen, J., Turbulence and intermittent transport at the boundary of magnetized plasmas. Phys. Plasmas (2005) v. 12 p. 062309.1-062309.14

Gavnholt, J.; Juul Rasmussen, J.; Garcia, O.E.; Naulin, V.; Nielsen, A.H., Up-gradient transport in a probabilistic transport model. Phys. Plasmas (2005) v. 12 p. 084501.1-084501.4

Krolikowski, W.; McCarthy, G.; Saffman, M.; Bang, O.; Wyller, J.; Juul Rasmussen, J., Modulation instability in generalized nonlinear optical media. In: Trends in lasers and electro-optics research. Arkin, W.T. (ed.), (Nova Science Publishers, Hauppauge, NY, 2005) p. 265-284

Milovanov, A.V.; Juul Rasmussen, J., Fractional generalization of the Ginzburg–Landau equation: an unconventional approach to critical phenomena in complex media. Phys. Lett. A (2005) v. 337 p. 75-80

Naulin, V., Impurity and trace tritium transport in tokamak edge turbulence. Phys. Rev. E (2005) v. 71 p. 015402.1-015402.4

Naulin, V.; Kendl, A.; Garcia, O.E.; Nielsen, A.H.; Juul Rasmussen, J., Shear flow generation and energetics in electromagnetic turbulence. Phys. Plasmas (2005) v. 12 p. 052515.1-052515.10

Naulin, V.; Nielsen, A.H.; Juul Rasmussen, J., Turbulence spreading, anomalous transport, and pinch effect. Phys. Plasmas (2005) v. 12 p. 122306.1-122306.9

Priego, M.; Garcia, O.E.; Naulin, V.; Juul Rasmussen, J., Anomalous diffusion, clustering, and pinch of impurities in plasma edge turbulence. Phys. Plasmas (2005) v. 12 p. 062312.1-062312.11

Schröder, C.; Grulke, O.; Klinger, T.; Naulin, V., Drift waves in a high-density cylindrical helicon discharge. Phys. Plasmas (2005) v. 12 p. 042103.1-042103.6

Senchenko, S.L.; Bohr, T., Shape and stability of a viscous thread. Phys. Rev. E (2005) v. 71 p. 056301.1-056301.7

Westerhof, E.; Hoekzema, I.A.; Hogeweij, G.M.D.; Jaspers, R.J.E.; Schuller, F.C.; Barth, C.J.; Bindslev, H.; Bongers, W.A.; Donne, A.J.H.; Dumortier, P.; Grift, A.F. van der; Kalupin, D.; Koslowski, H.R.; Kramer-Flecken, A.; Kruijt, O.G.; Cardozo, N.J.L.; Meiden, H.. van der; Merkulov, A.; Messiaen, A.; Oosterbeek, J.W.; Prins, P.R.; Scholten, J.; Udintsev, V.S.; Unterberg, B.; Vervier, M.; Wassenhove, G. van, Electron cyclotron resonance heating on TEXTOR. Fusion Sci. Technol. (2005) v. 47 p. 108-118

Reports

Bindslev, H.; Singh, B.N (eds.), Association Euratom - Risø National Laboratory annual progress report 2004. Risø-R-1520(EN) (2005) 62 p. www.risoe.dk/rispubl/ofd/ris-r-1520.htm

Conference papers published in proceedings

Garcia, O.E.; Gavnholt, J.; Naulin, V.; Nielsen, A.H.; Juul Rasmussen, J., Turbulent transport and mixing of impurities in the edge plasma (poster). In: Contributed papers. 32. European Physical Society conference on plasma physics, Tarragona (ES), 27 Jun - 1 Jul 2005. (European Physical Society, Paris, 2005) (Europhysics Conference Abstracts, vol. 29C) P-1.030 (4 p.)

Horacek, J.; Garcia, O.E.; Graves, J.P.; Pitts, R.A.; Nielsen, A.H.; Naulin, V.; Juul Rasmussen, J., Plasma electrostatic turbulence in TCV tokamak edge: direct comparison of experiment with 2D simulation. In: Contributed papers. 32. European Physical Society conference on plasma physics, Tarragona (ES), 27 Jun - 1 Jul 2005. (European Physical Society, Paris, 2005) (Europhysics Conference Abstracts, vol. 29C) O-4.004 (4 p.)

Krolikowski, W.; Bang, O.; Briedis, D.; Dreischuh, A.; Neshev, D.; Nikolov, N.; Petersen, D.E.; Juul Rasmussen, J.; Wyller, J., Nonlocal solitons. In: Nonlinear optics applications. International congress on optics and optoelectronics, Warsaw (PL), 28 Aug - 2 Sep 2005. Karpierz, M.A.; Boardman, A.D.; Stegeman, G.I. (eds.), (International Society for Optical Engineering, Bellingham, 2005) (SPIE Proceedings Series, 5949) p. 75-84

Meo, F.; Bindslev, H.; Hoekzema, J.A.; Korsholm, S.B.; Leuterer, F.; Michelsen, P.K.; Michelsen, S.; Nielsen, S.K.; Tsakadze, E.L.; Westerhof, E.; Woskov, P., Progress of the CTS diagnostics on TEXTOR and ASDEX upgrade (poster). In: Contributed papers. 32. European Physical Society conference on plasma physics, Tarragona (ES), 27 Jun - 1 Jul 2005. (European Physical Society, Paris, 2005) (Europhysics Conference Abstracts, vol. 29C) P-4.080 (4 p.)

Naulin, V.; Garcia, O.E.; Nielsen, A.H.; Juul Rasmussen, J., Turbulent transport of plasma edge impurities. In: Contributed papers. 32. European Physical Society conference on plasma physics, Tarragona (ES), 27 Jun - 1 Jul 2005. (European Physical Society, Paris, 2005) (Europhysics Conference Abstracts, vol. 29C) O-5.004 (4 p.)

Naulin, V.; Juul Rasmussen, J.; Wood, M.P., Pinch effects in turbulent impurity transport. In: Theory of fusion plasmas. Proceedings. Joint Varenna-Lausanne international workshop, Varenna (IT), 30 Aug - 3 Sep 2004. Connor, J.W.; Sauter, O.; Sindoni, E. (eds.), (Società Italiana di Fisica, Bologna, 2004) p. 365-371

Nielsen, S.K.; Bindslev, H.; Egedal, J.; Hoekzema, J.A.; Korsholm, S.B.; Meo, F.; Michelsen, P.K.; Michelsen, S.; Tsakadze, E.L.; Westerhof, E.; Woskov, P., Fast ion behaviour measured from CTS (poster). In: Contributed papers. 32. European Physical Society conference on plasma physics, Tarragona (ES), 27 Jun - 1 Jul 2005. (European Physical Society, Paris, 2005) (Europhysics Conference Abstracts, vol. 29C) P-4.081 (4 p.)

Priego, M.; Garcia, O.E.; Naulin, V.; Juul Rasmussen, J., Clustering and pinch of impurities in plasma edge turbulence (poster). In: Contributed papers. 32. European Physical Society conference on plasma physics, Tarragona (ES), 27 Jun - 1 Jul 2005. (European Physical Society, Paris, 2005) (Europhysics Conference Abstracts, vol. 29C) P-1.031 (4 p.)

Ratynskaia, S.; Rypdal, K.; Milovanov, A.V.; Knapek, C.; Khrapak, S.; Juul Rasmussen, J.; Morfill, G.E., Nonlocality and memory effects in grain dynamics on a 2D dust plasma quasi-crystal. In: Contributed papers. 32. European Physical Society conference on plasma physics, Tarragona (ES), 27 Jun - 1 Jul 2005. (European Physical Society, Paris, 2005) (Europhysics Conference Abstracts, vol. 29C) O-4.013 (4 p.)

Publications for a broader readership

Bindslev, H, Stjernekraft, Weekendavisen 18.-24. november 2005, Ideer, p. 4

Jensen, V.O., Hvor står fusionsforskningen i dag?. Kvant (2005) (no.4) p. 6-13

Unpublished conference papers

Bindslev, H., Fusionsenergi. DR2 tv-udsendelse: Viden om: Fusionsenergi, 27 Sep 2005. Unpublished. Abstract available

Bindslev, H., Hvad går projektet ud på, og hvilke muligheder giver ITER de danske virksomheder?. Konference om danske erhvervsmuligheder i ITER projektet, København (DK), 21 Nov 2005. Unpublished.

Bindslev, H.; Hoekzema, F.; Korsholm, S.B.; Leuterer, F.; Meo, F.; Michelsen, P.L.; Michelsen, S.; Nielsen, S.K.; Tsakadze, E.L.; Westerhof, E.; Woskov, P.; Egedal, J.; Porte, L.; Eester, D.V., Fast ion collective Thomson scattering on TEXTOR and ASDEX upgrade. 12. International symposium on laser-aided plasma diagnostics, Snowbird, UT (US), 26-29 Sep 2005. Unpublished.

Block, D.; Teliban, I.; Piel, A.; Naulin, V., Superresolution algorithm for turbulence investigations. 47. Annual meeting of the Division of Plasma Physics, American Physical Society, Denver, CO (US), 24-28 Oct 2005. Unpublished. Abstract available

Borba, D.; Sips, G.; Buttery, R.; Loarer, T.; Litaudon, X.; Challis, C.; Chrisanti, F.; Murari, A.; Luna, H. de la; Brzozowski, J.; Pitts, R.; Fundamenski, W.; Philipps, V.; Onegena, J.; Mailloux, J.; Pinches, S.; Koslowski, R.; Mantica, P.; Naulin, V.; Tala, T., Preparation of ITER operating scenarios. STAC ad hoc group meeting, Culham (GB), 8 Feb 2005. Unpublished.

Garcia, O.E.; Kendl, A.; Naulin, V.; Nielsen, A.H.; Juul Rasmussen, J., Differential rotation in electromagnetic plasma edge turbulence. Task Force Transport (TF-T) workshop, Abingdon (GB), 24-27 Jan 2005. Unpublished.

Garcia, O.E.; Naulin, V.; Nielsen, A.H.; Juul Rasmussen, J., Turbulence and intermittent transport in the edge/SOL of a toroidal plasma (Invited paper). 2. IAEA technical meeting on the theory of plasma instabilities: Transport, stability and their interaction, Trieste (IT), 5-30 Sep 2005. Unpublished. Abstract available

Garcia, O.E.; Naulin, V.; Nielsen, A.H.; Juul Rasmussen, J.; Rypdal, K., Interchange motions, coherent structures, and intermittent transport in magnetized plasmas. 8th International workshop on the interrelationship between plasma experiments in laboratory and space (IPELS 2005), Tromsø (NO), 4-8 Jul 2005. Unpublished. Paper available

Garcia, O.E.; Naulin, V.; Nielsen, A.H.; Juul Rasmussen, J., Radial advection of isolated structures by non-linear interchange motions. Seminar at École Polytechnique Fédérale de Lausanne, Centre de Recherches en Physique des Plasmas, Lausanne (CH), 12 Sep 2005. Unpublished.

Garcia, O.E.; Naulin, V.; Nielsen, A.H.; Juul Rasmussen, J., Intermittent transport in scrape-off layer plasmas. General Task Force E meeting, École Polytechnique Fédérale de Lausanne, Centre de Recherches en Physique des Plasmas, Lausanne (CH), 19-21 Jan 2005. Unpublished.

Juul Rasmussen, J.; Garcia, O.E.; Gavnholt, J.; Naulin, V.; Nielsen, A.H., Transport and impurities in the edge/SOL region of Tokamak plasmas. Task Force Transport (TF-T) workshop, Abingdon (GB), 24-27 Jan 2005. Unpublished.

Juul Rasmussen, J.; Garcia, O.E.; Naulin, V.; Nielsen, A.H.; Stenum, B., Generation and dynamics of large scale flows in magnetized plasmas and rotating fluids (Invited paper). Autumn college on plasma physics, International Center for Theoretical Physics (ICTP), Trieste (IT), 5-30 Sep 2005. Unpublished. Abstract available

Juul Rasmussen, J.; Bang, O.; Krolikowski, W.Z.; Wyller, J., Nonlinear wave dynamics in nonlocal media (Invited paper). Mini symposium on new trends in nonlinear physics, International Center for Theoretical Physics (ICTP), Trieste (IT), 17 Sep 2005. Unpublished. Abstract available

Juul Rasmussen, J.; Garcia, O.E.; Naulin, V.; Nielsen, A.H.; Priego, M., Particle diffusion and mixing of passive fields in plasma turbulence. Seminar at Institute for Ion Physics, University of Innsbruck, Innsbruck (AT), 11 Apr 2005. Unpublished.

Korsholm, S.B.; Bindslev, H.; Meo, F.; Michelsen, S.; Michelsen, P.K.; Nielsen, S.K.; Tsakadze, E.L.; Egedal, J.; Woskov, P.; Hoekzema, J.; Leuterer, F.; Westerhof, E., Preliminary results of the new fast ion CTS systems at TEXTOR and ASDEX upgrade. 47. Annual meeting of the Division of Plasma Physics, American Physical Society, Denver, CO (US), 24-28 Oct 2005. Unpublished. Abstract available

Müller, S.H.; Fasoli, A.; Labit, B.; McGrath, M.; Plyushev, G.; Podesta, M.; Poli, F.M.; Naulin, V., Investigations of turbulent structures in the TORPEX device. 47. Annual meeting of the Division of Plasma Physics, American Physical Society, Denver, CO (US), 24-28 Oct 2005. Unpublished. Abstract available

Naulin, V., Transport of impurities: Theory. EFDA-JET TF-T workshop, Culham (GB), 24-28 Jan 2005. Unpublished.

Naulin, V., Introduction to turbulence. EFDA-JET TF-E workshop, Lausanne (CH), 19-21 Jan 2005. Unpublished.

Naulin, V., Materialien mit negativem Brechungsindex. Habilitationskolloquium Heinrich-Heine Universität, Düsseldorf (DE), 20 Jan 2005. Unpublished.

Naulin, V., Impurity up gradient transport in plasma edge turbulence. In: Kurzfassungen der Vorträge. 69. Jahrestagung der Deutschen Physikalischen Gesellschaft, Berlin (DE), 4-9 Mar 2005. (Deutsche Physikalische Gesellschaft, Berlin, 2005) (Verhandlungen der Deutschen Physikalischen Gesellschaft, Reihe VI, Band 40, No. 3) p. 120

Naulin, V., Turbulenz und Transport am Rand von Fusionsplasmen. Kolloquium, University of Innsbruck, Innsbruck (AT), 13 Apr 2005. Unpublished.

Naulin, V., Turbulence, transport and consistency. Kolloquium, MPI Institute for Plasma Physics, Greifswald (DE), 6 Jun 2005. Unpublished.

Naulin, V., Shear flow generation and energetics in electromagnetic turbulence. 11. European fusion theory conference, Aix-en-Provence (FR), 26-28 Sep 2005. Unpublished.

Naulin, V.; Garcia, O.E.; Nielsen, A.H.; Juul Rasmussen, J., Some physics of shear flows. Festival de theorie 2005: Turbulence overshoot and resonant structures in fusion and astrophysical plasmas, Aix-en-Provence (FR), 4-22 Jul 2005. Unpublished. PowerPoint presentation available

Naulin, V.; Garcia, O.E.; Nielsen, A.H.; Juul Rasmussen, J., Turbulence and intermittent transport in the edge/SOL of a toroidal plasma. Seminar at University of Innsbruck, Institute for Theoretical Physics, Innsbruck (AT), 12 Apr 2005. Unpublished.

Naulin, V.; Juul Rasmussen, J., Turbulence and transport at the edge. Colloquium, University of Stuttgart, Institute for Plasma Research, Stuttgart (DE), 17 Apr 2005. Unpublished.

Nielsen, A.H.; Fundamenski, W.; Garcia, O.-E.; Naulin, V.; Juul Rasmussen, J.; Grulke, O., Transport modeling in edge and SOL region of a toroidal plasmas. Task Force Transport (TF-T) workshop, Abingdon (GB), 24-27 Jan 2005. Unpublished.

Rypdal, K.; Garcia, O.E., Routes to interchange mode turbulence and chaos in plasmas confined by a helical magnetic field. 8th International workshop on the interrelationship between plasma experiments in laboratory and space (IPELS 2005), Tromsø (NO), 4-8 Jul 2005. Unpublished. Paper available

Rypdal, O.E.; Garcia, O.E., Profile robustness and routes to turbulence in the helimak configuration (poster). 32. European Physical Society conference on plasma physics, Tarragona (ES), 27 Jun - 1 Jul 2005. Unpublished.

Woskov, P.P.; Korsholm, S.B.; Meo, F.; Tsakadze, E.L.; Oosterbeek, H.; Jakubowska, K.; Scholten, J.; Tito, C., Frequency measurements of the 110 GHz gyrotron used for fast ion CTS diagnostics at TEXTOR. 47. Annual meeting of the Division of Plasma Physics, American Physical Society, Denver, CO (US), 24-28 Oct 2005. Unpublished. Abstract available

Wyller, J.; Krolikowski, W.Z.; Bang, O.; Petersen, D.E.; Juul Rasmussen, J., Modulational instability in the nonlocal chi2- model (poster). 16. National congress, Australian Institute of Physics, Canberra (AU), 31 Jan - 4 Feb 2005. Unpublished.

3 Fusion Technology

3.1 Introduction

The work reported in this section has been carried out in the Materials Research Department. The overall objective of the research activities in this area is to determine the impact of neutron irradiation on physical and mechanical properties of metals and alloys, so that appropriate materials can be chosen for their application in irradiation environment (e.g. in fusion reactor). Various experimental techniques are employed to study different aspects of the micro-structural evolution during irradiation and the resulting consequences of the post-irradiation physical and mechanical properties of metals and alloys. Calculations and computer simulations are performed to understand the evolution of surviving defects and their clusters in collision cascades. The kinetics of defect accumulation during irradiation and the influence of irradiation-induced defects and their clusters on the deformation behaviour of irradiated metals and alloys are studies theoretically. In the following, the main results of these activities are highlighted.

3.2 Next step technology

3.2.1 In-reactor creep-fatigue cyclic testing of CuCrZr alloy[1]

B.N. Singh, S. Tähtinem, P. Moilanen* (*VTT Industrial Systems (Association EURATOM-TEKES), Espoo, Finland)), P. Jacquet** and J. Dekeyser** (**Reactor Experiment Department, SCK.CEN, Mol, Belgium)*

At present it seems almost certain that the precipitation hardened CuCrZr alloy will be used both in the first wall and divertor components of ITER. In the reactor vessel, this alloy will be exposed to a relatively high flux of 14 MeV neutrons and will experience thermo-mechanical cyclic loading as a result of the cyclic nature of the plasma burn operations of the system. Because of the "plasma-on" and "plasma-off" mode of operation, the deformation behaviour of the alloy is likely to be modified. This kind of cyclic loading would induce not only fatigue damage but also make the material creep during the operation. Not much is known at present about the impact of this complicated mode of deformation on the mechanical performance of metals and alloys particularly in the environment of intense neutron irradiation. The limited amount of experimental results on creep-fatigue experiments carried out on the unirradiated CuCrZr alloy (and in the absence of neutron irradiation) have shown, on the other hand, that hold-times are damaging and shorten the number of cycles to failure.

The materials employed in the first wall and the divertor components of ITER will experience thermo-mechanical stresses and displacement damage concurrently. This may modify the creep-fatigue deformation response of the material significantly. In order to make a realistic evaluation of the response of materials under these conditions, an experimental programme was initiated with the objective of carrying out creep-fatigue experiments directly in the environment of neutrons in the BR-2 reactor at Mol (Belgium). In order to carry out such tests**,** new fatigue specimens and test modules were designed and fabricated. The size and geometry of the new specimen of CuCrZr HT1 (overaged at 600°C for 1 hour) are shown in Figure 1.

1 TW3 – TVM - COFAT

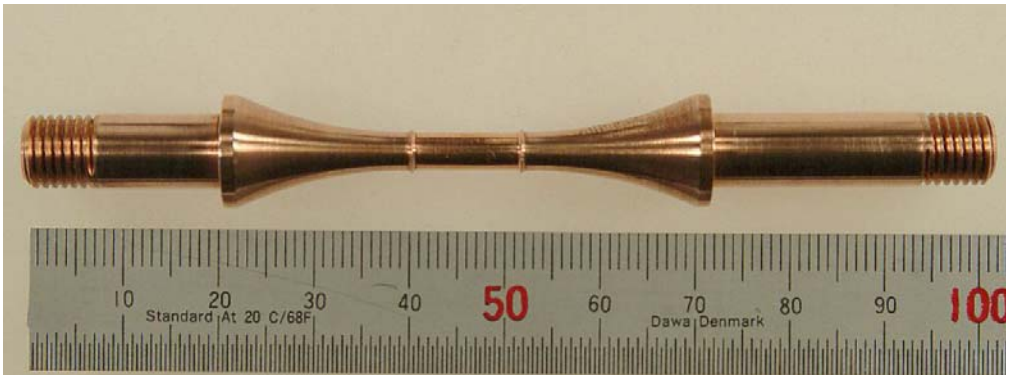

Figure 1. Size and geometry of CuCrZr specimen specially designed for the in-reactor creep-fatigue test.

The test facility consists of a pneumatic fatigue test module and a servo-controlled pressure-adjusting loop. The pressure-adjusting loop operates on a continuous flow of helium gas. The basic principle of the creep-fatigue test module is based on the use of two pneumatic bellows to introduce stress/strain and a linear variable differential transformer (LVDT) sensor to measure the resulting extension of the gauge length of the creep-fatigue specimen. The strain measured by the LVDT has been calibrated against the strain measured by strain gauges. The strain measured in the gauge length is used to control the pre-determined constant strain amplitude throughout the whole test. It should be pointed out that one bellows is used to induce tension whereas the other bellows induces compression.

Two such test modules were loaded into an instrumented rig. Assembly of the two test modules with specimens, bellows and LVDTs is shown in Figure 2. The temperature of specimens was measured by thermocouples placed immediately above the specimens. Thermocouples were also placed just above the bellows and LVDTs. Thus, each test module had three thermocouples so that its temperature during irradiations could be monitored at different positions in the irradiation rig. To avoid overheating of the specimens, water was circulated (600 litres per hour) from the top of the test assembly in the irradiation rig with the test module 2 forming the top and the test module 1 the bottom of the test assembly. This means that the cold water flowing in the rig first cools the test module 2 and somewhat warmer water flowing further down the rig cools the test module 1. Consequently, the test module 2 will be expected to remain at somewhat lower temperature than the test module 1.

The irradiation rig containing the assembly of specimens, $LVDT_s$, cooling system and thermocouples was lowered in the reactor core, when the local neutron flux near the rig had reached a steady state level after the reactor start. It took about 10 minutes to reach a stable temperature in the test module 1 and test module 2 of 90 and 70ºC, respectively. As expected, the temperature in the test module 2 always remained about 20ºC higher than that in the test module 1. The neutron flux and the damage rate in the test module 1 were 6.5×10^{17} n/m^{2}s (E>0.1 MeV) and 6.1×10^{-8} dpa/s, respectively. In the Test module 2 the neutron flux and the damage rate were 7.4×10^{17}n/m^{2}s (E>0.1 MeV) and 7.2×10^{-8} dpa/s, respectively. The specimens in the test modules 1 and 2 received a displacement dose of 3.7×10^{-5} and 5.6×10^{-5} dpa, respectively, before they were mechanically loaded. Both Test No. 1 and 2 were carried out with a strain amplitude of 0.5%.Time taken to reach from push to pull (i.e. compression to tension) was 50 s both in Test No. 1 and 2

giving a strain rate of $2x10^{-4}s^{-1}$ during the loading period. In the case of the Test No. 1, a hold time of 10 s was implemented both in the compression and the tension sides of the fatigue cycles. A holdtime of 100 s was used in the Test No. 2. Thus, the total time spent in each creep-fatigue cycle was 120 s in the case of Test No.1 and 300 s in the case of Test No. 2. In other words, the displacement dose accumulated per creep-fatigue cycle is $7.32x10^{-6}$ dpa in the Test No. 1 and $2.16x10^{-5}$ dpa in the Test No. 2.

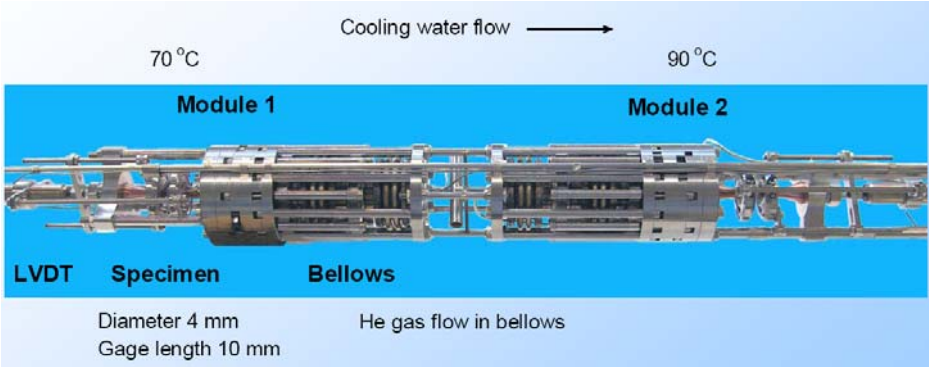

Figure 2**.** Assembly of two creep-fatigue test modules each containing specimen, LVDT and bellows prior to loading in the irradiation rig. Each test module has three thermocouples positioned just above the LVDT, specimen and the bellows. Each test module is operated independently so that two different tests can be carried out in simultaneously the same assembly in one irradiation rig.

During in-reactor creep-fatigue tests the evolution of the stress and strain was continuously recorded during the cyclic loading. The cyclic deformation behaviour of CuCrZr specimen during the in-reactor creep-fatigue Test No. 1 and Test No. 2 is shown in Figures 3 and 4, respectively, in the form of hysteresis loops for different cycles during the test. The symmetry and the stability of the loops demonstrate the validity of the in-reactor creep-fatigue tests. The average value of the maximum stress reached in the tension and the compression sides of a deformation cycle is plotted in Figure 5 as a function of numbers of cycles during Test No. 1 and 2. For comparison the results of a reference test carried out at 20ºC with a strain amplitude of 0.5% and with a holdtime of 100 s are also shown in Figure 5. All tests were carried out until the end of life of the specimens (i.e. until a stress level of 77 MPa was reached both in the Test No. 1 and 2). The number of cycles to failure, N_f, (i.e. when the test was stopped at a stress level of 77 MPa) in the Test No. 1 and 2 were 2270 and 2500, respectively. The fractured parts of the specimens used in the Test No. 1 and 2 are shown in Figure 6. Neither of the specimens showed any sign of necking prior to failure.

In summary, the feasibility of carrying out a properly controlled and accurate in-reactor creep-fatigue test has been successfully demonstrated. Preliminary results indicate that the cyclic hardening and softening behaviour of CuCrZr alloy during in-reactor and out-of-reactor tests are similar. The magnitude of hardening during in-reactor tests, however, appears to be somewhat higher than that in the out-of-reactor test.

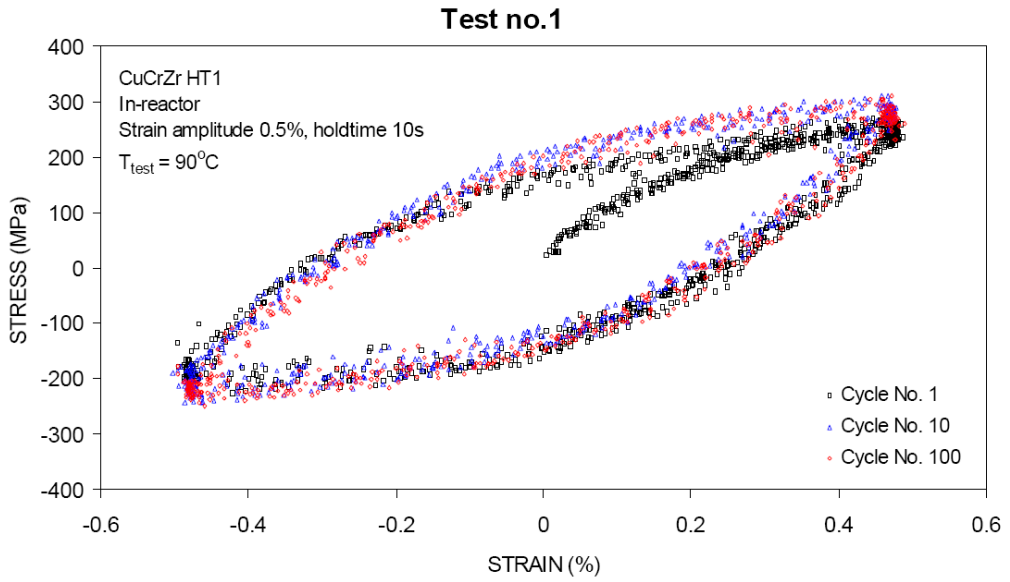

Figure 3**.** Cyclic deformation behaviour in the form of hysteresis loops for CuCrZr HT 1 alloy obtained for different cycles during the in-reactor creep-fatigue test (Module 1.) performed at 90ºC with a constant strain amplitude of 0.5 % and a holdtime of 10s both in the tension and compression sides of the cycle.

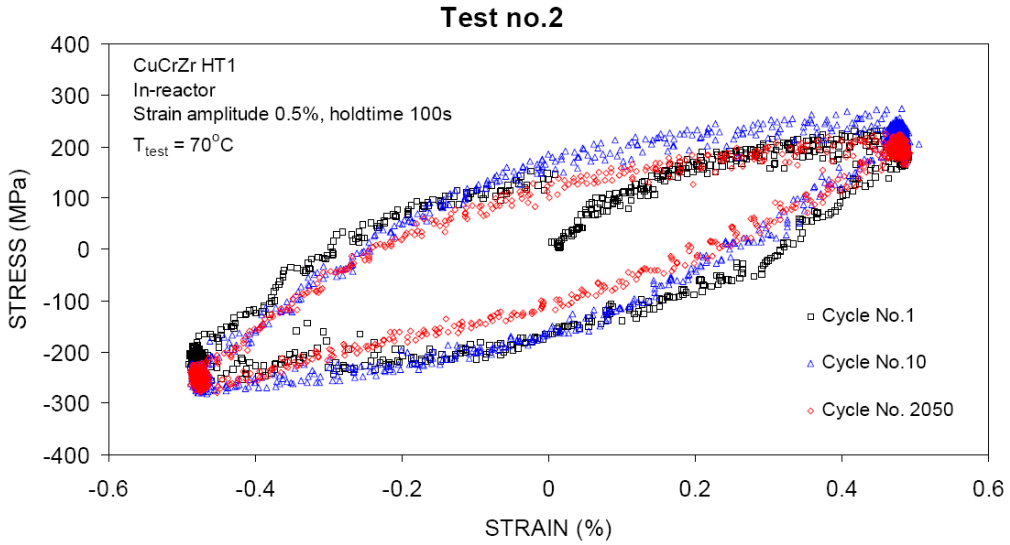

Figure 4**.** The same as in Figure 3 but test carried out in the Module 2 (Test No. 2) at 70ºC and with a holdtime of 100s.

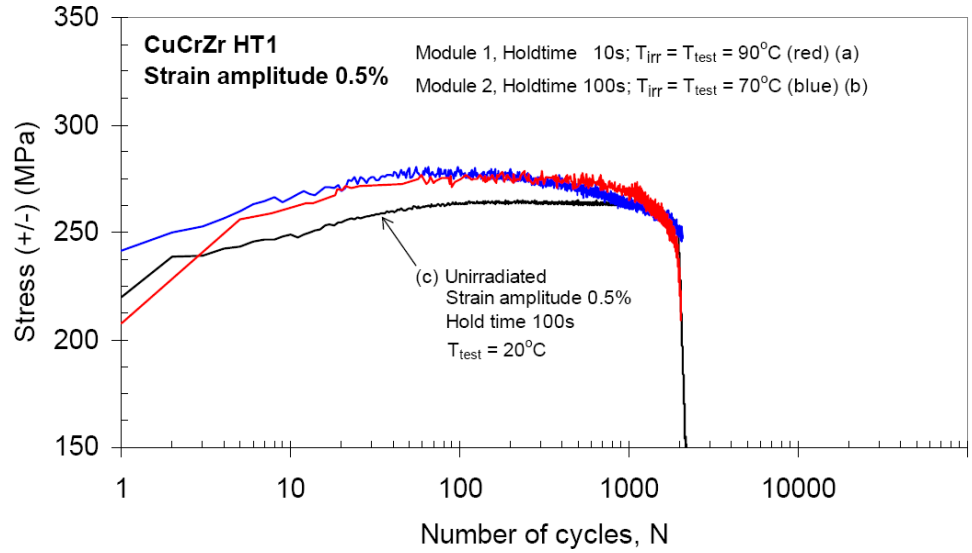

Figure 5. The variation of the average of the maximum stress reached in the tension (+) and the compression-sides of a creep-fatigue cycle in the in–reactor test with the number of cycles during Test No.1 (Module 1) and the Test No.2 (Module 2). Note the difference in the test temperature between Test No. 1 and 2. Note also that the displacement dose accumulated in one full creep-fatigue cycle is considerably lower in the Test No. 1 (~7.32×10^{-6} dpa/cycle) than that in the Test No. 2 (~2.16×10^{-5}dpa/cycle). The dose levels reached at the end of Test No. 1 and 2 are 0.0166 dpa and 0.054 dpa, respectively.

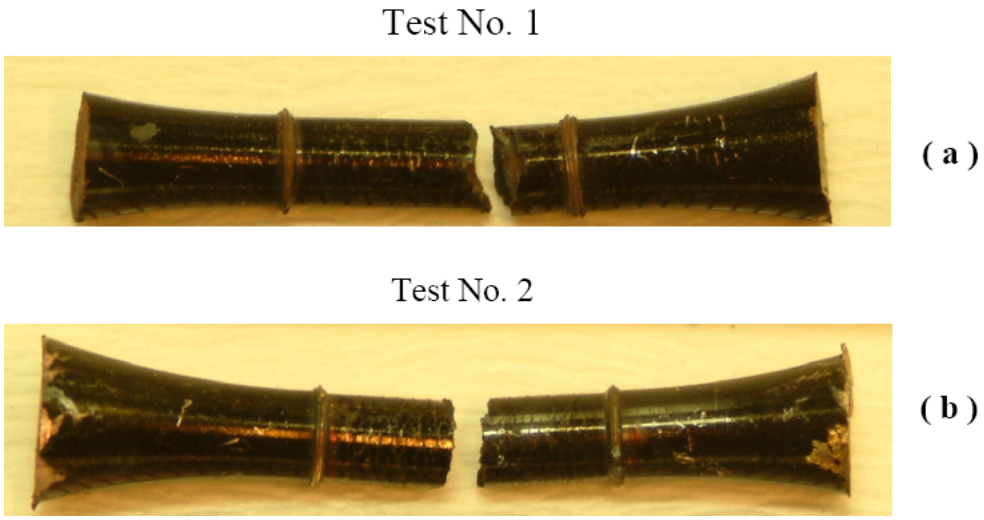

Figure 6. Photographs of the broken parts of the specimens used in (a) Test No. 1 and (b) Test No. 2. None of the broken parts showed any evidence of necking of specimens prior to fracture.

3.2.2 Cyclic hardening and softening behaviour during creep-fatigue loading of OFHC-copper and CuCrZr alloy[2]

B. N. Singh, M. Li. (*Metals and Ceramics Division, Oak Ridge National Laboratory. Oak Ridge, U.S.A., J.F. Stubbins** (**Department of Nuclear, Plasma and Radiological Engineering, University of Illinois, Urbana, Illinois, USA) and B. S. Johansen*

As indicated in the previous section (3.2.1), the problem of creep-fatigue interaction and its possible impact on mechanical performance of materials used in the first wall and divertor components of ITER is a matter of concern. We have investigated various aspects of this issue for a CuCrZr alloy which is ITER relevant material. The results obtained so far have indicated that although the effect of holdtime on creep-fatigue life is not very significant yet the application of holdtime practically always reduces the number of cycles to failure. The effect of holdtime appears to be very complicated in nature and seems to depend on a number of parameters such as stress/strain amplitude, the mode of cyclic loading, the yield strength of materials, etc. The fact that the reduction in creep-fatigue lifetime increases with decreasing stress/strain amplitude still remains unexplained.

In an effort to obtain some additional information on the deformation behaviour of these materials which may help rationalize the creep-fatigue performance, hardening and softening characteristics were determined as a function of number of cycle during creep-fatigue experiments. These experiments were performed on unirradiated pure copper and CuCrZr alloy with different ageing treatments (i.e. prime aged (PA) and overaged at 600ºC for 1 hour (HT1) and 4 hours (HT2)). All experiments were performed at 20ºC in strain controlled mode without any holdtime and with a holdtime of 10 seconds. The hardening behaviour during these experiments was determined as a function of number of cycles. The main purpose of these experiments was to obtain information on the hardening behaviour during cyclic loading at different levels of strain amplitudes for materials with significantly different yield stress and the role of extrinsic obstacles (i.e. precipitates) to dislocation motion on the hardening and softening features.

The maximum tensile stresses as a function of number of cycles are shown in Figure 7 for (a) OFHC-copper, (b) CuCrZr alloy in the prime aged (PA) condition, (c) CuCrZr alloy in the overaged HT1 condition and (d) CuCrZr alloy in the overaged HT2 condition. It can be easily seen in Figure 7(a) that OFHC-copper first hardens with increasing number of cycles and then reaches a stable stress level and remains at that level until the end of life. This behaviour is observed for all strain amplitudes and in specimens with and without holdtime. It should be noted, however, that the rate of increase in the maximum stress as well as the maximum level of stress reached increase with increasing strain amplitude. The hardening behaviour in the prime aged CuCrZr alloy (Figure ((7b)) and the overaged alloy CuCrZr HT1 (Figure 7c) follows the trends very similar to that observed in the case of OFHC-copper although the rates of hardening with the number cycles (at a given strain amplitude) are lower in the case of CuCrZr alloy. The CuCrZr HT2 alloy Figure 7(d) overaged at 600ºC for 4 hours generally softens with the number of cycles throughout cyclic life with a plateau in the maximum stress towards the end of life.

2 TW2-TVM-CUCFA and TW3-TVM-CUCFA2

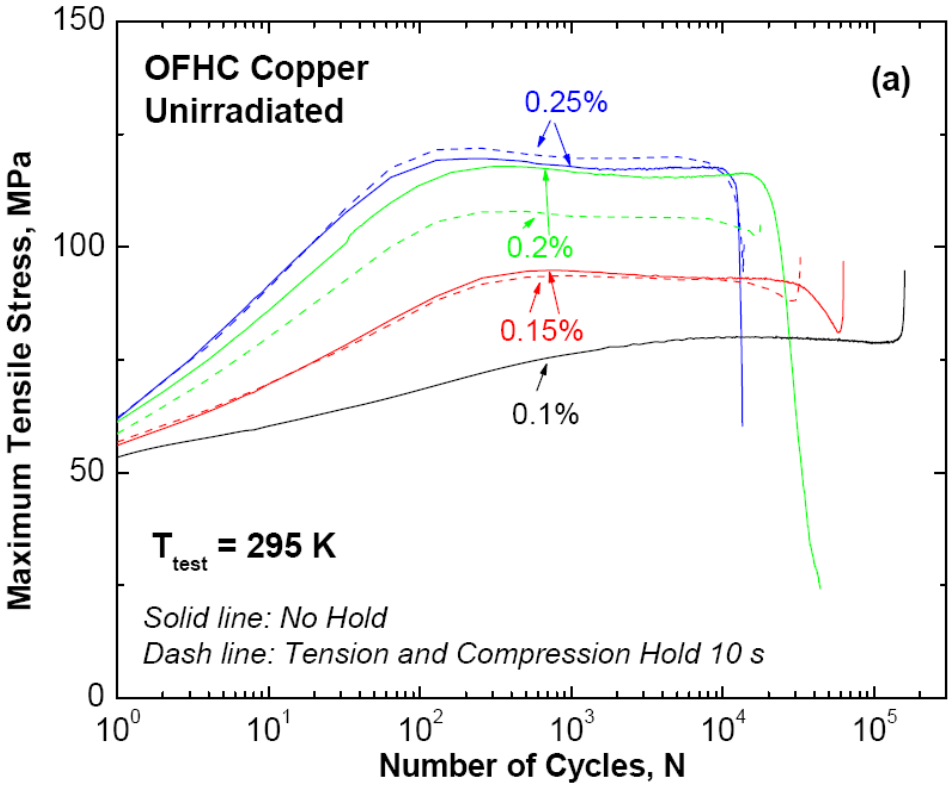
OFHC Copper
Unirradiated
(a)
0.25%
0.2%
0.15%
0.1%
T test = 295 K
Solid line: No Hold
Dash line: Tension and Compression Hold 10 s
Maximum Tensile Stress, MPa
Number of Cycles, N
150
100
50
0
10^0
10^1
10^2
10^3
10^4
10^5

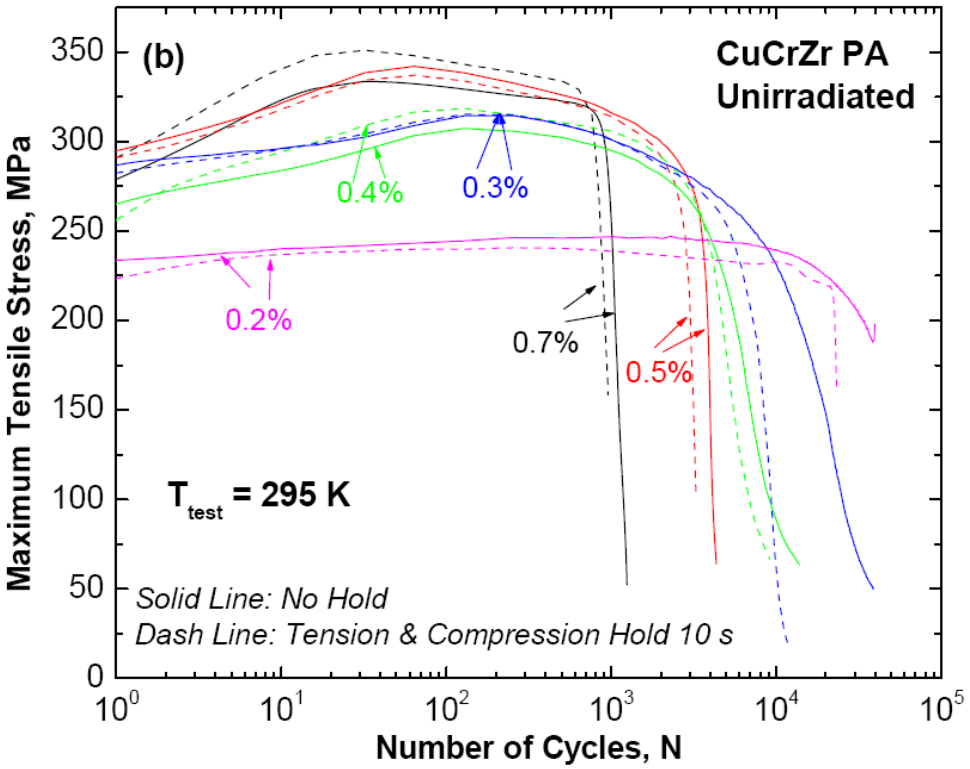
(b)
CuCrZr PA
Unirradiated
0.4%
0.3%
0.2%
0.7%
0.5%
T test = 295 K
Solid Line: No Hold
Dash Line: Tension & Compression Hold 10 s
Maximum Tensile Stress, MPa
Number of Cycles, N
350
300
250
200
150
100
50
0
10^0
10^1
10^2
10^3
10^4
10^5

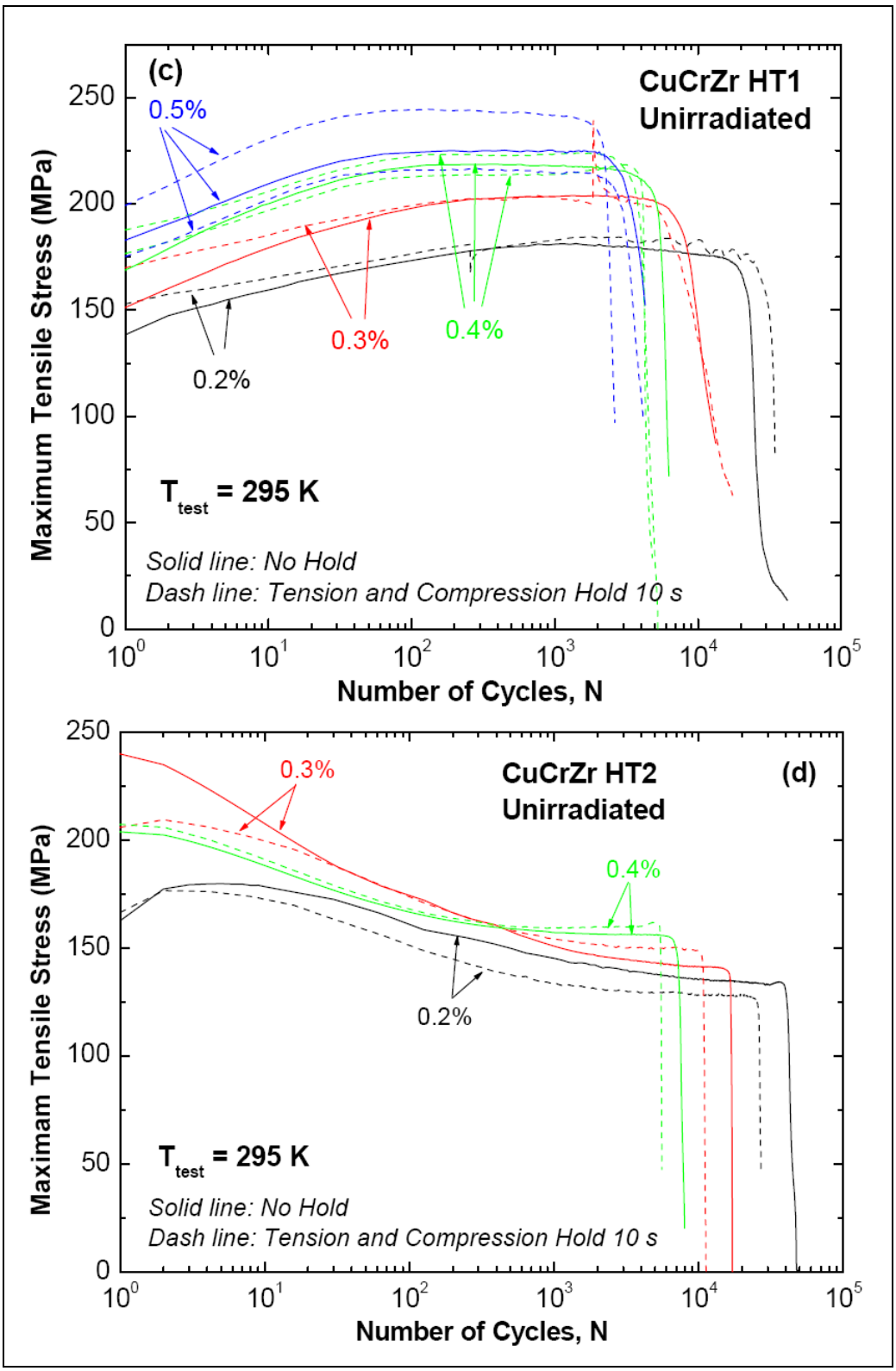

Figure 7. Maximum tensile stress as a function of number of cycles determined during strain controlled creep-fatigue tests carried out at 22ºC without holdtime and with a holdtime of 10 seconds at different levels of strain amplitude for (a) OFHC-copper and CuCrZr alloy in (b) PA, (c) HT1 and (d) HT2 conditions. Note that the hardening behaviour of OFHC-Cu is substantially different from that exhibited by the CuCrZr alloy with different heat treatments. The CuCrZr specimens with heat treatment HT2 generally show softening instead of hardening.

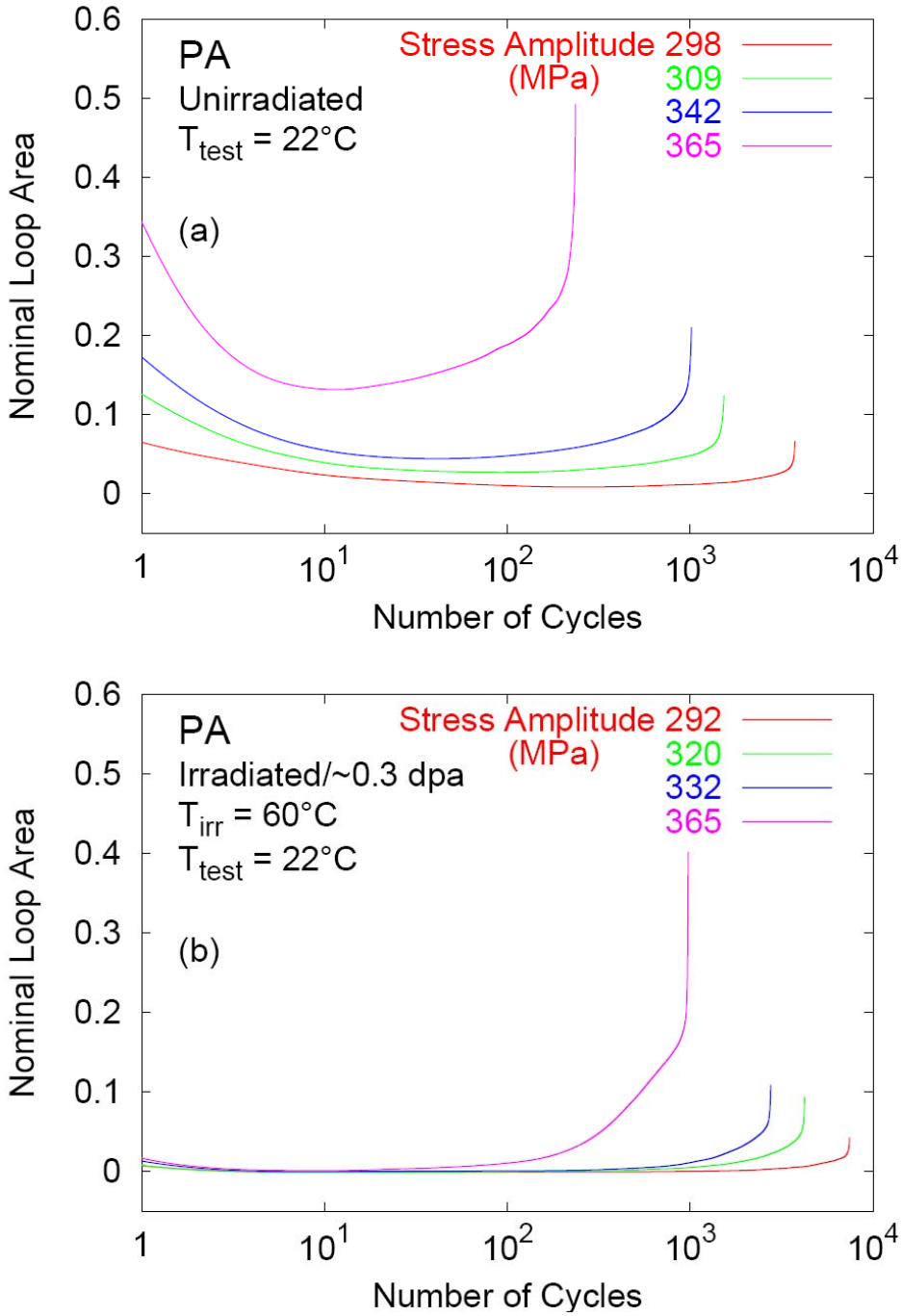

Figure 8. Nominal fatigue loop area as a function of number of cycles determined during load controlled creep-fatigue tests carried out at 22ºC with different stress amplitude on CuCrZr specimens in the prime aged (PA) condition (a) before the irradiation and (b) after irradiation at 333 K to ~0.3 dpa. Note that the decrease in the loop area represents hardening. It is interesting that the irradiated specimens do not show any indication of hardening during the test.

This tendency of cyclic hardening or softening has also been observed in the load controlled tests where the nominal area of the fatigue loops has been monitored during the fatigue cycling period. Results have been obtained for the prime aged (PA) and the overaged CuCrZr HT1 alloy tested at 20 and 300ºC in irradiated and unirradiated conditions. Figure 8 shows examples of the variation of the nominal loop area with the

number of creep-fatigue cycles for the unirradiated (Figure 8a) and the irradiated (Figure 8b) CuCrZr PA alloy tested at 20ºC. Irradiation was performed at 60ºC to a dose level of 0.3 dpa. The results for different stress amplitudes are shown. In the unirradiated specimens (Figure 8a), the loop size first decreases with the number of cycles and then reaches a stable loop size for most of the life and finally a loop broadening (which is an indication of severe plastic deformation) occurs at the end of life. Note that the decrease in the loop area represents hardening. The irradiated CuCrZr PA alloy (Figure 8b) tested at room temperature shows initially very small loop size indicating that the material is being loaded below its yield strength. However, as cyclic deformation continues, the material gradually softens to produce larger loop areas. This is presumably due to the removal of irraddiation induced defect clusters by mobile dislocations during cyclic deformation.

3.2.3 Effect of irradiation on low cycle fatigue behaviour of titanium alloys[3]

B.N. Singh and B.S. Johansen

Based on an attractive combination of thermophysical, mechanical and radioactive decay properties, titanium alloys have been identified as relevant materials for different structural components in fusion reactors. Two classical and industrially available alloys, Ti5Al2.5Sn (single phase α) and Ti6Al4V ($\alpha+\beta$), are being considered as candidate materials for flexible mechanical connectors between the blanket modules and the pressure vessel in ITER. Since not much is known about the effect of neutron irradiation on the phase stability and mechanical properties of these alloys, a limited number of screening experiments were carried out to determine the response of these alloys to neutron irradiation at 50 and 350ºC to a dose level of 0.3 dpa. The results of these irradiations have been reported earlier4. Later, it was decided to carry out some additional irradiations and testing at an intermediate temperature of 150ºC which is a more relevant temperature for ITER application. For these experiments only Ti 6A1 4V ($\alpha+\beta$) alloy was chosen.

A number of tensile and fatigue specimens of Ti6Al4V ($\alpha+\beta$) alloy were irradiated at 150ºC with a neutron flux of $3.5x10^{17}n/m^2s$ (E>1 MeV) corresponding to a displacement damage rate of $5x10^{-8}$dpa (NRT) /s. Irradiations were performed in the atmosphere of helium in a fission reactor at KFKI/AEKI Budapest (Hungary) to a fluence level of $3.1x10^{24}$ n/m^2(E>1 MeV) corresponding to a displacement dose level of 0.3 dpa (NRT). Both unirradiated and irradiated tensile specimens were tested at 150ºC in vacuum at a strain rate of $1.3x10^{-3}$ s^{-1}. The low cycle fatigue tests were carried out at 150ºC in vacuum with a loading frequency of 0.5 Hz. The loading cycles were always fully reversed (i.e. R= -1) so that the maximum tension load was the same as the maximum compression load. Tests were conducted in a load control mode in a servo-electrical mechanical test stand. Figure 9 shows the stress-strain curves for theTi6Al4V ($\alpha+\beta$) alloy tensile tested at 150ºC in the unirradiated and irradiated conditions. It can be clearly seen that the irradiation to 0.3 dpa causes a significant increase in the yield strength and a corresponding decrease in the uniform elongation. Note that the irradiated specimen does not show any sign of work hardening and instead shows the sign of plastic instability.

3 TW3-TVM-TICRFA

4 S.Tähtinen, P. Moilanen, B. N. Singh and D.J. Edwards, J. Nud. Mater. 307-311 (2002) 416.

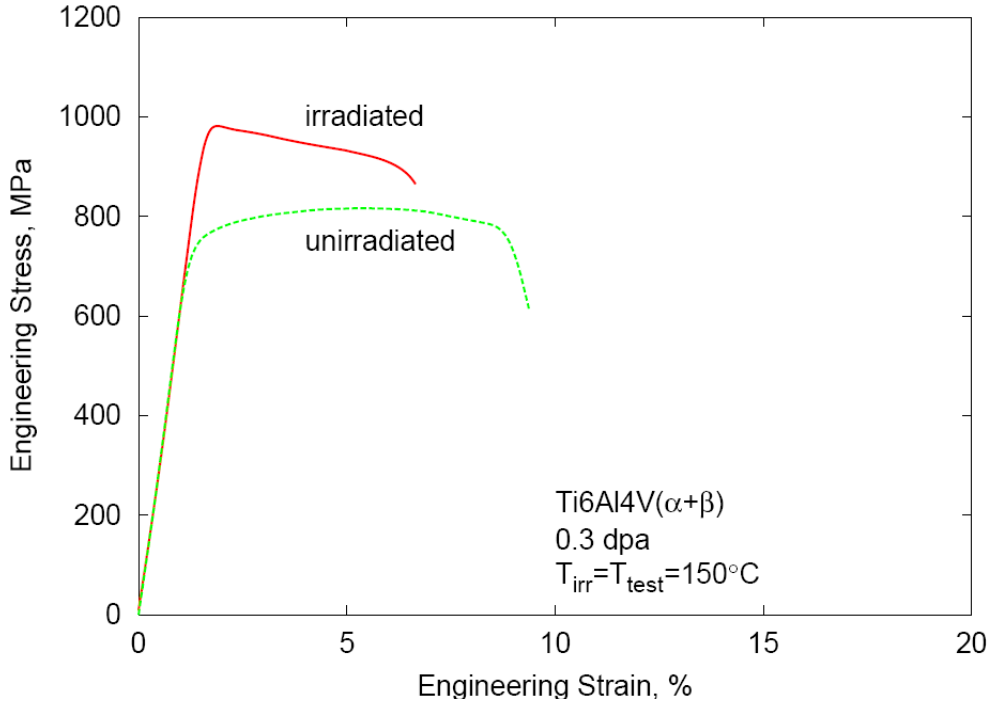

Figure 9. Stress-strain curves for Ti 6Al 4V (α+β) titanium alloy tensile tested at 150ºC in the unirradiated and irradiated (0.3 dpa) conditions. Note that the irradiated specimen does not seem to work harden during the test.

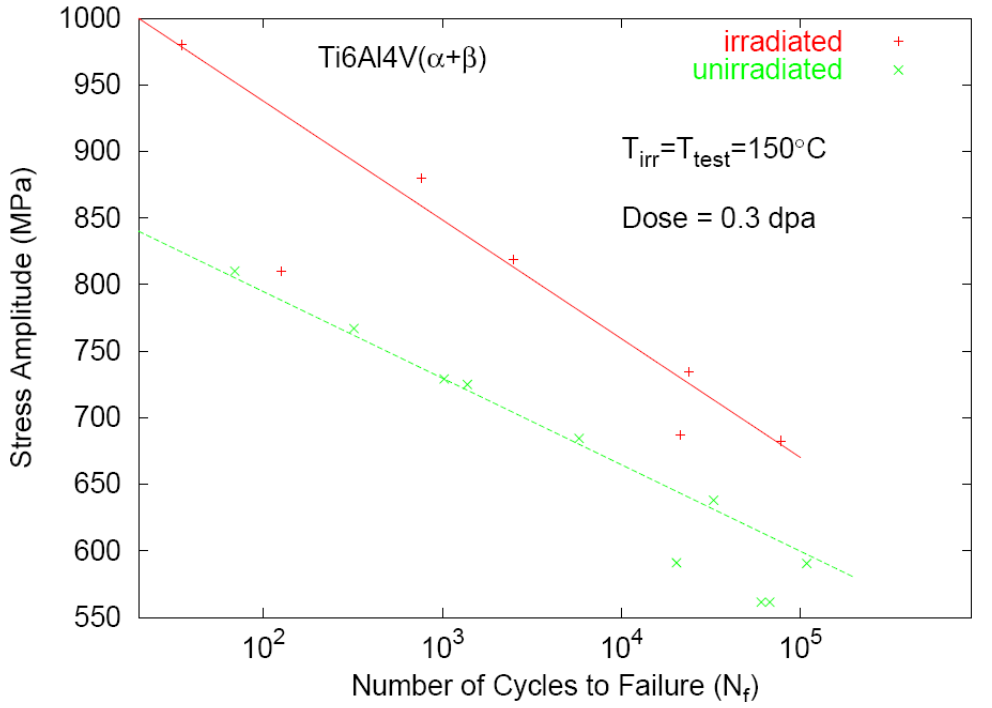

Figure 10. Number of cycles to failure (N_f) as a function of stress amplitude in fatigue tests performed on Ti6Al 4V (α+β) alloy at 150ºC in the unirradiated as well as irradiated (0.3 dpa at 150ºC) conditions. The tests were carried out in stress controlled mode. Irradiation at 150ºC to a dose level of 0.3 dpa seems to increase the fatigue life (at a given stress amplitude level) during the post-irradiation fatigue test at 150ºC. This improvement seems to arise due to an increase in the yield strength due to irradiation.

The result of low cycle fatigue tests are shown in Figure 10 illustrating the dependence of fatigue life in terms of the number cycles to failure on the stress amplitudes for both the unirradiated and irradiated Ti6Al4V(α+β alloy tested at 150ºC. Clearly, the irradiation at 150ºC to a dose level of 0.3 dpa leads to an increase in the fatigue life and this increase seems to be more pronounced at higher stress amplitudes.

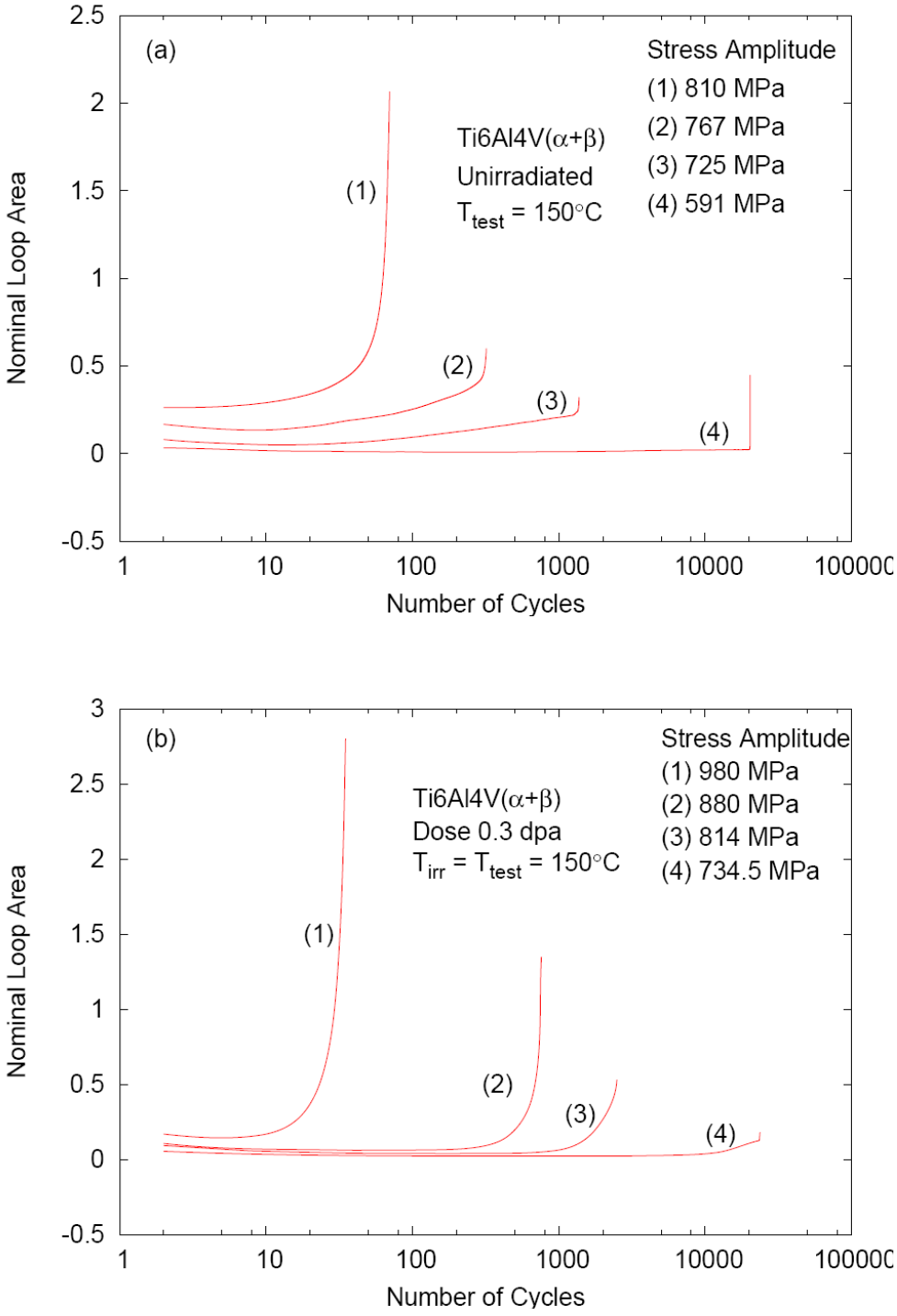

Figure 11. Nominal fatigue loop area as a function of number of cycles determined during the load controlled fatigue tests at 150ºC on Ti 6Al 4V (α+β) alloy in the (a) unirradiated and (b) irradiated conditions. Irradiation was carried out at 150ºC to a dose level of 0.3 dpa.

In order to illustrate the cyclic hardening or softening behaviour during the fatigue test, the nominal loop area was monitored as a function of number of cycles for different stress amplitudes. The results for both unirradiated and irradiated Ti6A14V ($\alpha+\beta$) alloy tested at 150ºC are shown in Figure 11. Note that the decrease in the loop area represents hardening and the increase represents softening. The rapid increase in the loop areas is an indication of severe plastic deformation towards the end of life of the specimens. These results suggest that while there is some indication of cyclic softening with increasing numbers of cycles in the case of unirradiated specimens (Figure 11a), the irradiated material does not show any sign of softening. The results further suggest that the increase in lifetime due to irradiation in all probability arises from the increase in the yield strength due to irradiation.

3.3 Long-term technology

3.3.1 Effect of helium implantation and neutron irradiation on cavity formation in iron and Eurofer-97[5]

M. Eldrup, B. N. Singh and P. Jung(*Forschungszentrum Jülich, Association EURATOM-FZJ, Germany)*

As part of the investigations of neutron irradiation effects in low activation steels, Positron Annihilation Spectroscopy (PAS) investigations have been carried out of the effect of helium implantation and neutron irradiation (mainly carried out at SCK.CEN, Mol, Belgium) on cavity formation in pure iron and Eurofer-97. The He implantations were carried out at the Jülich Compact Cyclotron and the neutron irradiations mainly at SCK.CEN, Mol, Belgium. The emphasis has been on helium implantations of pure Fe and Eurofer-97 with low implantation rates, i.e. 0.0006 and 0.0018 appm He/s at 50°C, and 0.0012 and 0.0036 appm He/s at 350°C. Previously, we have used implantation rates of 0.006 appm He/s at 50°C and 0.012 appm He/s at 350°C. The ambition has been to obtain information about the effect of implantation rate on He bubble sizes and densities. Figure 12 shows a few characteristic positron lifetime spectra for iron for different He implantation doses at the two different implantation temperatures. The spectra show clear effects of both He dose and implantation temperature.

Unfortunately, it has turned out that up till now the combined experimental uncertainties (arising from implantation, sample handling and PAS measurements) are so large that they prevent a clear definition of He dose rate effects. On the other hand, the effect of He and neutron displacement dose is clear. This is illustrated by the variation of the mean positron lifetime for iron as function of total displacement dose in Figure 13 (for each dose, the plotted lifetime is an average of all measurements at that dose). Both n-irradiation and He implantation lead to the formation of cavities of nanometer size both at 50°C and at 350°C as evidenced by the increase of the positron mean lifetime with displacement dose. At 50°C the presence of He does not seem to enhance the cavity nucleation compared to neutron irradiation to the same displacement level, while a clear effect is observed at 350°C, in qualitative agreement with the TEM observations. More detailed quantitative analysis of the positron lifetime data to obtain cavity sizes and densities is possible, if the distributions of sizes and He-to-vacancy ratios are not too wide. Theoretical estimates (Section 3.3.2) suggest that this condition is fulfilled for He implantation at 350°C. Quantitative analyses of data for 350°C He implanted specimens do indeed lead to He bubble sizes and densities in fairly good agreement with the

5 TW3-TTMS-007 and TW4-TTMS-007

theoretical calculations (Section 3.3.2). On the other hand, the data for specimens that were He implanted at 50°C qualitatively show the presence of a high density of sub-nm sized cavities. However, a detailed, quantitative analysis of these data is presently found to be difficult. Work on this problem is in progress.

A collaborative project with the Institute for Materials Research, Tohoku University, Japan has been established on some aspects of the present project. Annealing of specimens that were He implanted at 50°C has been carried out up to a temperature of 900°C and PAS measurements (positron lifetime and coincidence Doppler broadening) have been carried out. In parallel with the experimental work, theoretical calculations of the electronic structure and positron behaviour have been performed to support the interpretation of the experiments. Clear effects are observed on the positron lifetime on annealing to about 300°C and above, which suggest that nano-voids disappear at this temperature (in agreement with the annealing behaviour of room-temperature-neutron-irradiated Fe), leaving a population of He bubbles that coarsen at higher annealing temperatures. This work is still in progress.

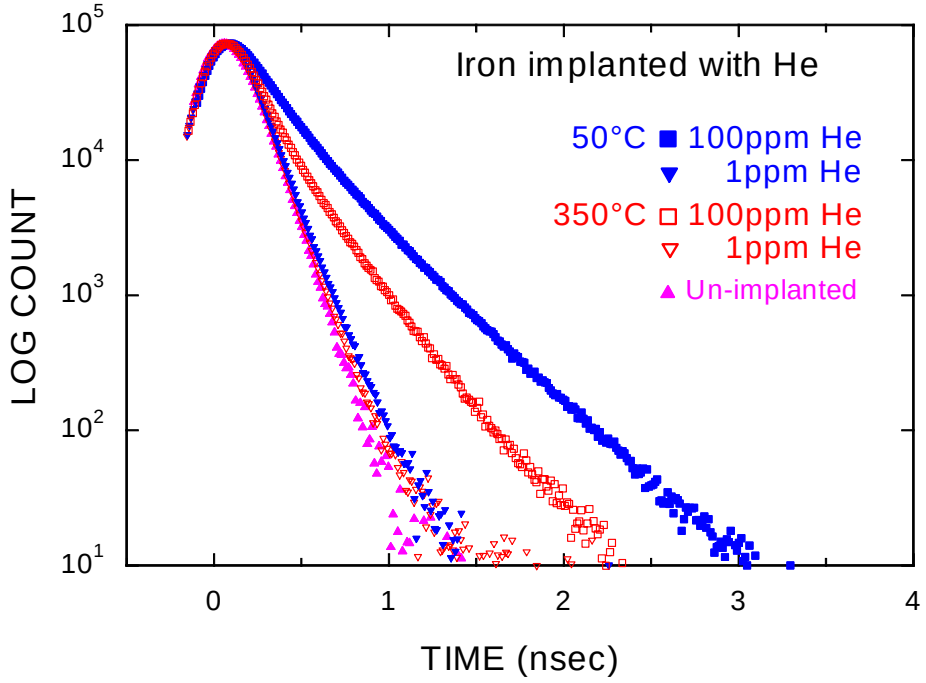

Figure 12. Positron lifetime spectra for iron that has been He implanted at two different temperatures (50°C or 350°C) and to two different He levels (1 appm or 100 appm). The clear differences between the spectra reflect the differences in cavity (He bubble) sizes and densities.

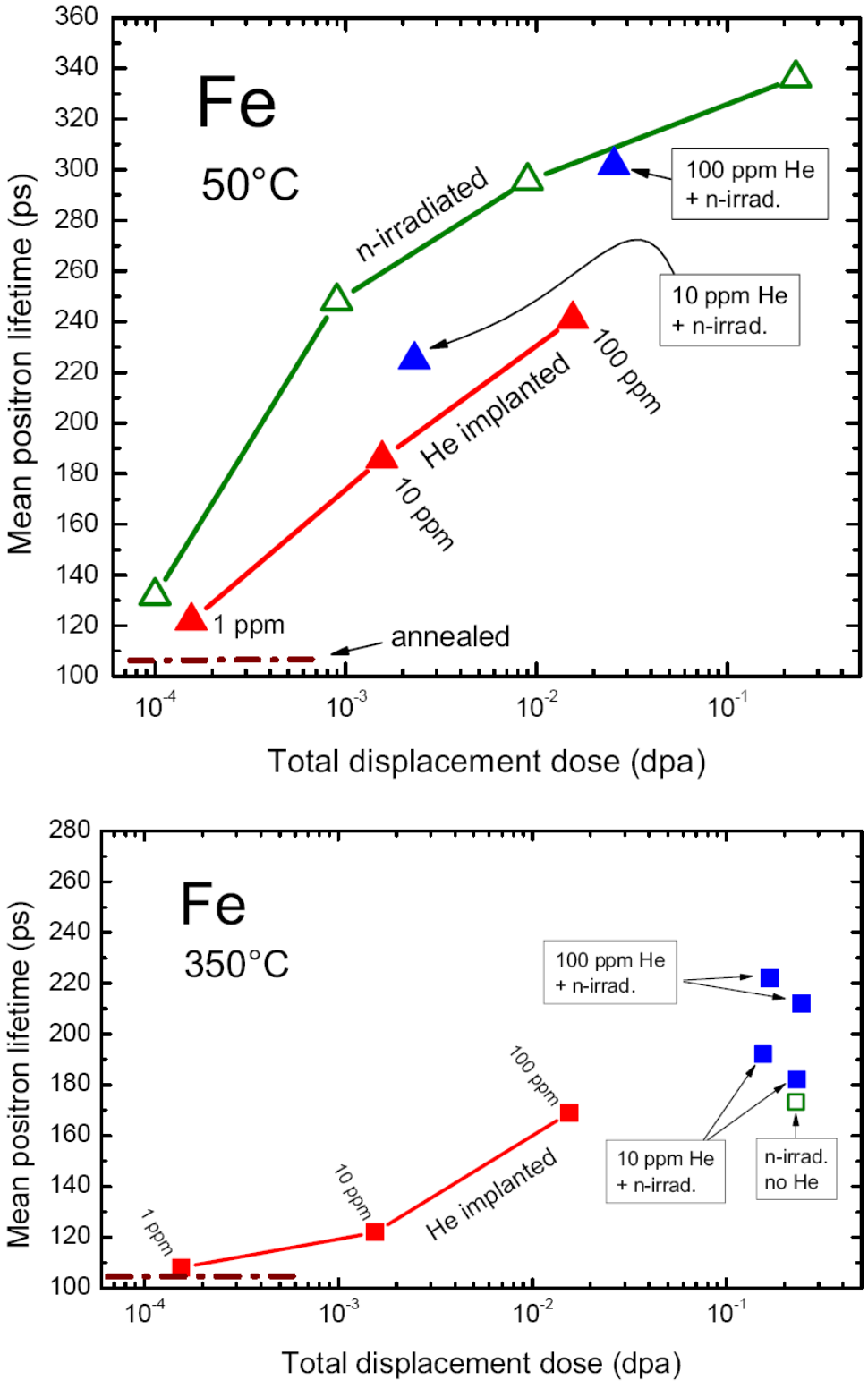

Figure 13. Positron mean lifetimes for He implanted, for neutron irradiated and for He implanted plus neutron irradiated iron as functions of total displacement dose. $T_{impl.} = T_{n\text{-}irr.} = 50°C$ or 350°C.

3.3.2 Cavity evolution in bcc iron during neutron irradiation with and without helium implantation[6]

S. I. Golubov (*Oak Ridge National Laboratory, Oak Ridge, USA),*
B. N. Singh and M. Eldrup

It is well known that the interaction of 14 MeV neutrons (produced during the D-T fusion reactions) with the materials surrounding the plasma will generate helium atoms in these materials via nuclear reactions at a relatively high rate. This is a matter of serious concern for the performance and lifetime of the structural components such as first wall and divertor in a fusion reactor since the accumulation of helium and vacancies produced during irradiation may cause excessive amount of volumetric swelling and grain boundary embrittlement. Over the years a considerable amount of effort has been made to rationalize and understand the processes responsible for causing these effects. Unfortunately, at least to our knowledge, there exists no theoretical framework as yet within which the details of cavity nucleation and growth (i.e. void swelling), for instance, can be treated adequately accurately for the condition of concurrent generation of cascades and helium atoms. It is well known, however, that the creation of an excess of vacancies during irradiation and the concentration of the available gas atoms are the two most potent parameters that control the scale of cavity nucleation at a given irradiation temperature.

The present work was initiated to perform detailed numerical calculations of temporal evolution of vacancy concentration and super-saturation and kinetics of cavity nucleation and growth under cascade damage conditions. The computer code developed earlier to treat the problem of void swelling within the framework of the production bias model (PBM) has been modified to include the treatment of concurrent generation of helium and displacement cascades. In order to investigate the effect of helium on the evolution of cavity microstructure under cascade damage condition, it was necessary to find the solution of two-dimensional kinetic equation for the size distribution function of helium-vacancy clusters in pure iron implanted with helium and irradiated with neutrons. In order to reduce the number of equations needed to be solved for describing the evolution of helium-vacancy complexes, a new grouping method has been employed to integrate the kinetic equations.

During helium implantation at very high implantation rate (~ $2x10^{-2}$ appm/s) used in the present experiments, a dense population of very small helium bubbles are expected to be produced even at the implantation temperature of 350ºC. During subsequent neutron irradiation at 350ºC these bubbles are likely to perform Brownian-like motion leading to coalescence of these closely spaced bubbles which would then result in a reduction in the final density of cavities. A separate subroutine has been formulated to calculate the influence of the Brownian-like motion on the final cavity density. This subroutine has been incorporated in the main PBM code. The Brownian-like motion is assumed to occur via the surface diffusion controlled mechanism. Under all these conditions, the evolution of vacancy supersaturation is calculated using the PBM.

6 TW3-TTMS-007

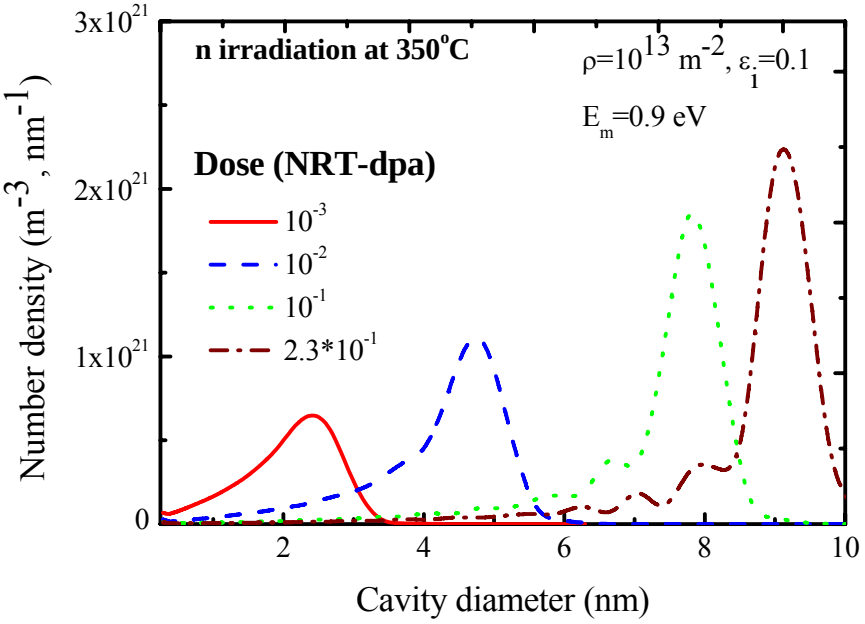

Figure 14. Calculated size distributions of cavities during neutron irradiation of iron at 350ºC as a function of displacement dose level. The evolution of the size distributions is calculated using the production bias model.

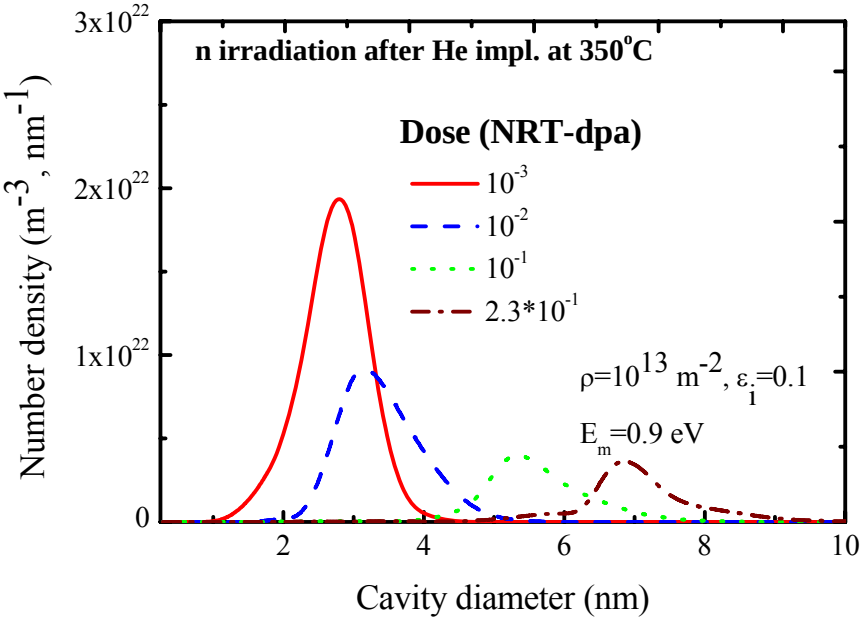

Figure 15. Calculated size distributions of cavities in pure iron during neutron irradiation at 350ºC; prior to neutron irradiation, 100 appm of helium was implanted at 350ºC.

Using the updated PBM code detailed numerical calculations have been carried out to investigate the evolution of the cavity size distribution as a function of displacement dose level during neutron irradiation of pure iron at 350ºC. The calculations have been carried out for the case of pure neutron irradiation (i.e. without any implanted helium) as well as for the case of irradiation of iron which was implanted with 100 appm of helium at 350ºC prior to neutron irradiation. The fundamental difference between these two cases is that in the case of pure neutron irradiation the cavities first nucleate and then grow with increasing displacement dose level. In the case where 100 appm of helium has been implanted at 350ºC prior to irradiation, the material contains a high density of small helium bubbles with a cavity size distribution already at the start of the neutron irradiation. This as-implanted size distribution will then deform during subsequent neutron irradiation. In other words, in the case of implanted helium, no further nucleation of cavities is likely to occur during neutron irradiation. The calculated evolution of distributions for the case of pure neutron irradiation and neutron irradiation after helium implantation are shown in Figures 14 and 15, respectively, for different displacement dose levels. It can be easily seen that in the former case (Figure 14) both the cavity density and size increase with increasing dose level whereas in the later case (Figure 15) although the cavities produced during implantation grow with increasing displacement dose level, their density decreases. The main reason for this decrease is the Brownian-like motion and coalescence of cavities during the neutron irradiation.

Figure 16 shows the dose dependence of cavity density and size during helium implantation at 350ºC. Note that displacement dose in this case refers to displacement damage caused by the energetic helium ions during implantation. For comparison, the results estimated from the lifetime analysis of measurements performed on as-implanted iron specimens using the position annihilation technique (PAS) are also shown in Figure 16. It should be pointed out that the cavity density estimated from the PAS measurements represents the lower bound values because the fraction of cavities containing a large number of helium atoms may not be detected by PAS technique.

The calculated number density and diameter of cavities for the case of pure neutron irradiation and that of the neutron irradiation after helium implantation at 350ºC are shown in Figure 17 as a function of displacement dose level due to neutron irradiation. While the cavity density increases with increasing dose level in the case of pure neutron irradiation and tends to saturate at high doses, the cavity density decreases with the displacement dose in the case of neutron irradiation of helium implanted specimen. For comparison, the results of TEM investigations of cavity density and sizes for these cases are also shown in Figure 17. Although the calculated densities are reasonably consistent with the TEM measurements, the calculated cavity sizes are somewhat larger. The reason for this discrepancy is being investigated.

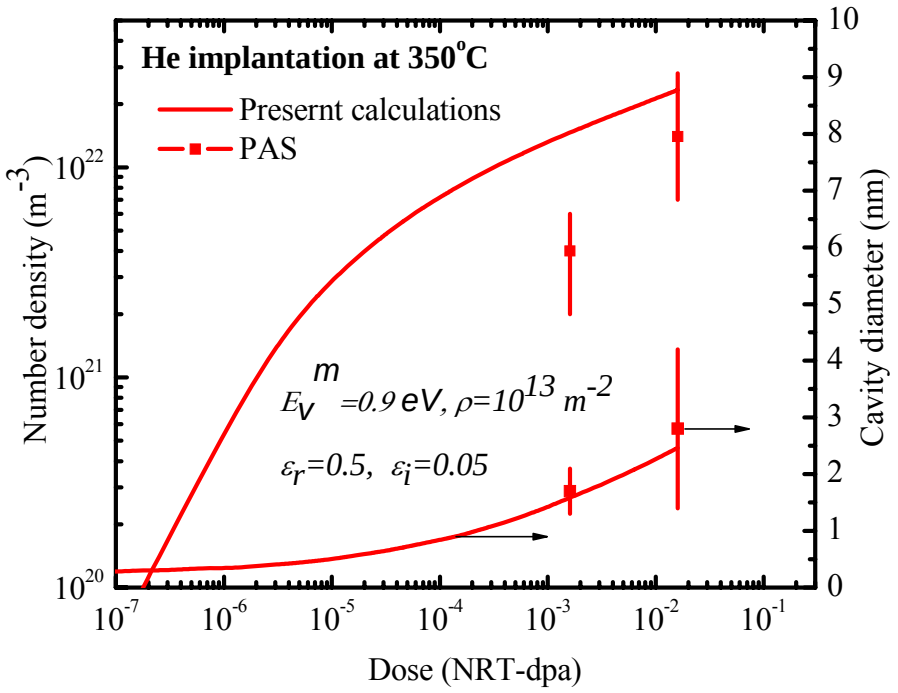

Figure 16. Dose dependence of cavity density and size in iron during helium implantation at 350ºC.

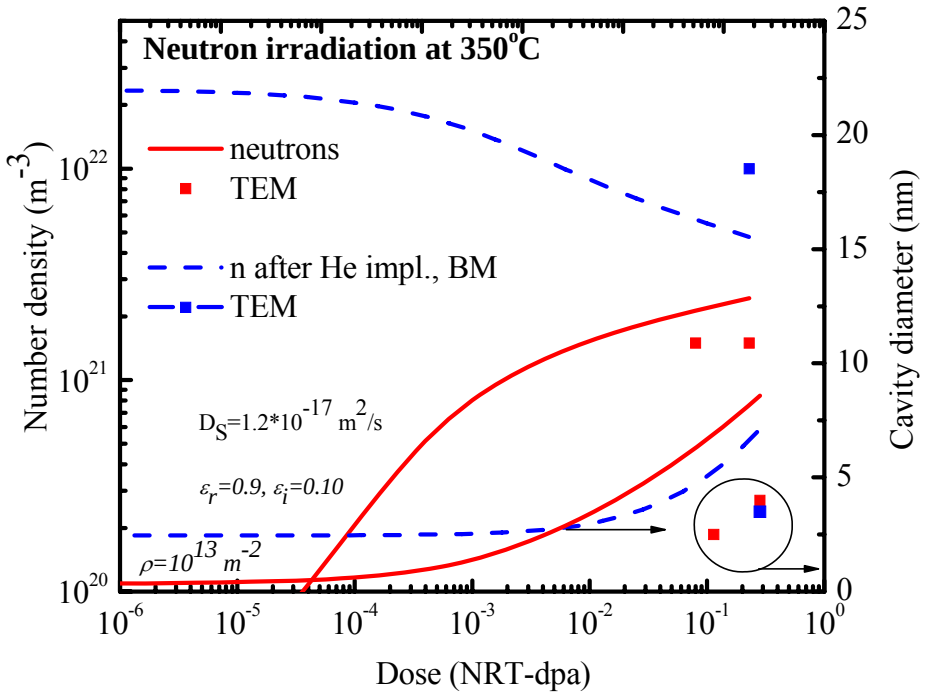

Figure 17. Dose dependence of cavity density and size in neutron irradiated iron at 350ºC without helium implantation and with helium implantation at 350ºC to a concentration level of 100 appm.

3.3.3 In-reactor uniaxial tensile deformation of pure iron and Fe-Cr alloy[7]

B. N. Singh, S. Tähtinan, P. Moilanen* (*VTT Industrial systems (Association EURATOM-TEKES), Espoo, Finland), P. Jacquet** and J. Dekeyser** (**Reactor Experiment Department, SCK. CEN, Mol, Belgium)*

It is well known that neutron irradiation of iron and ferritic-martensitic steels at temperatures below 0.3Tm (where Tm is the melting temperature in Kelvin) causes a decrease in the uniform elongation and leads to plastic flow localization. This is a matter of concern from the point of view of application of these materials in the structural components of a fusion reactor. It should be recognized, however, that this conclusion and the concern are based exclusively on the results of post-irradiation tests. Clearly, the microstructure as well as the test conditions during a post-irradiation mechanical test are fundamentally so different from those expected during deformation of materials in the reactor environment that the results of the post-irradiation tests may not be representative of in-reactor deformation behaviour. In fact, the in-reactor tensile tests performed recently on pure copper and a CuCrZr alloy have demonstrated that indeed the deformation behaviour observed in the in-reactor dynamic tests is significantly different from that in the case of a post-irradiation test*8*. However, since the dynamic behaviour of dislocations is likely to be different in bcc iron and steel from that in the fcc copper, it is of a particular interest to investigate the in-reactor deformation behaviour of bcc iron and steel. The results of these investigations would be valuable not only from technological points of view but may also be very useful for understanding and modelling the deformation behaviour of bcc materials under the condition of dynamic deformation in reactor environment. With these expectations, a task has been initiated to perform in-reactor tensile tests on pure iron and a single phase Fe-Cr alloy.

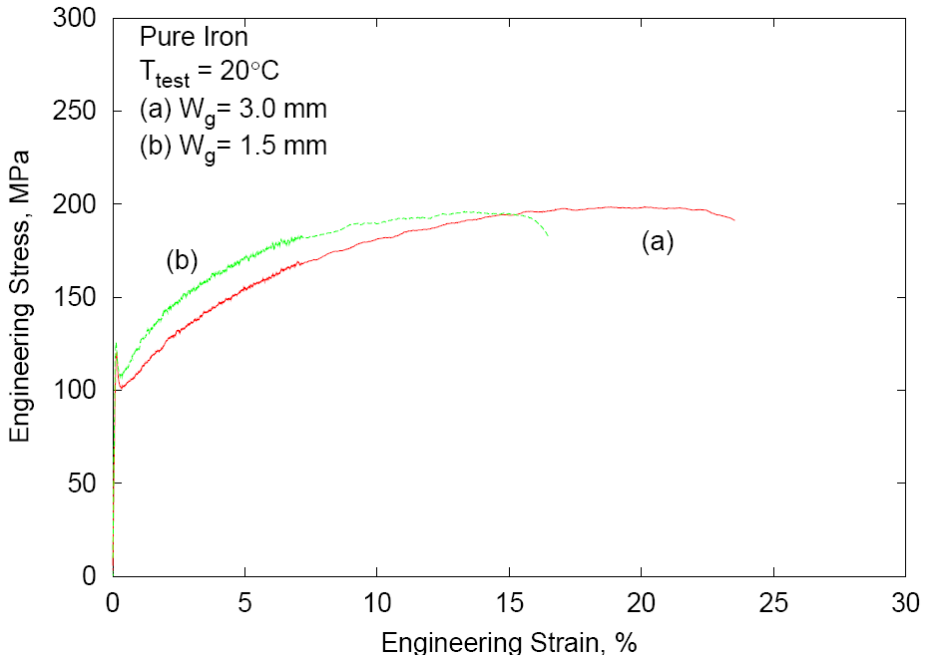

Figure 18. Stress-strain curves for pure and annealed (650ºC for 2 hours) iron tested at 20ºC width a strain rate of 1.3×10^{-3} s^{-1} with a gauge with (W_g) of 3.0mm and 1.5 mm.

7 TW5-TTMS-007

8 B. N. Singh, D. J. Edwards, S. Tähtinen, P. Moilanen, P. Jacquet and J. Dekeyser, Risø-R-1481 (EN) (1004) 47 p.

Preparations are in progress for carrying out these in-reactor tests. Preliminary out-of-reactor tensile tests have been carried out on pure iron using test modules similar to what was used for the in-reactor tensile tests of OFHC- copper. The results showed that during the test the specimen was sliding in the grips of the test module. To overcome this problem the grips have been redesigned. Furthermore, the specimen design has also been altered so that the stress level in the grips during the test would be only one half of the level used earlier. The specimens of both the old and the new design have been tensile tested to evaluate the effect of the change in specimen design on the deformation behaviour. The two relevant stress strain curves are shown in Figure 18, for (a) gauge width of 3.0 mm and (b) gauge with of 1.5 mm. Clearly the two curves are very similar indicating that the change in the gauge width of 1.5 mm from 3.0 mm does not alter the deformation behaviour in any significant way.

In order to avoid water corrosion of iron specimens during in-reactor tests it was decided to coat the specimens with a thin layer of gold or platinum. The gold coating was not very successful. However, coating with platinum turned out to be perfectly acceptable. A number of iron specimens were given a coating of 10 nm thickness. Coated specimens were examined in a scanning microscope to determine the quality of coating.

Figure 19(a) shows an example of the coated surface in the as-coated condition. The coated specimens were then tensile tested at 20ºC to a plastic strain of about 20% in a standard tensile machine at a strain rate of 1.3×10^{-3} s^{-1}. The surface of the tensile tested specimens was examined again in a scanning microscope to determine the integrity of the coated layer during the deformation. Figure 19(b) shows an example of the topography of the coating existing after the 20% of plastic deformation, illustrating that the coated layer survived during the tensile test very well and would be expected to provide protection to iron specimen during in-reactor tests. It should be added that the presence of the coated layer did not affect the mechanical behaviour during tensile tests. The stress-strain curves for the uncoated (a) and the coated (b) specimens are shown in Figure 20.

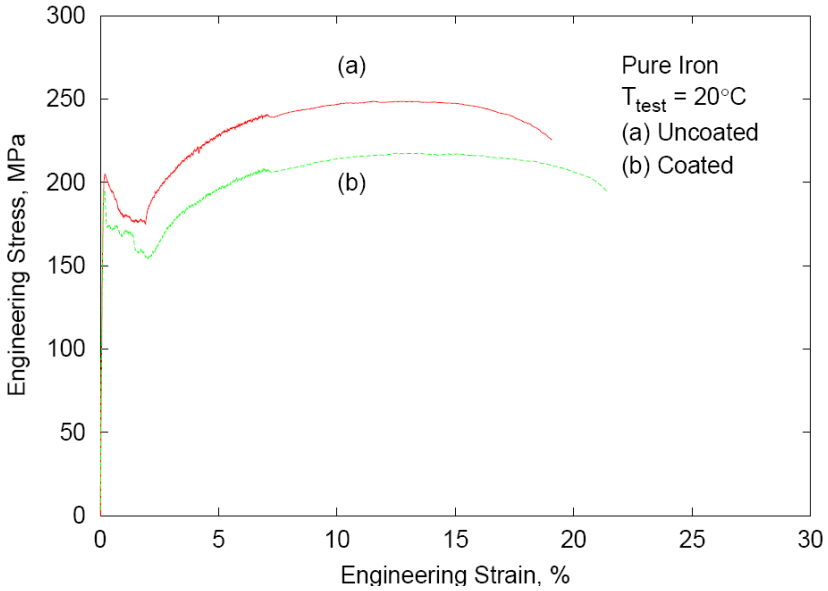

Figure 20. Stress-strain curves for pure and annealed (650ºC for 2 hours) iron tensile tested at 20ºC with a strain rate at 1.3×10^{-3} s^{-1} (a) without coating (b) with a coating of 10nm of platinum prior to deformation.

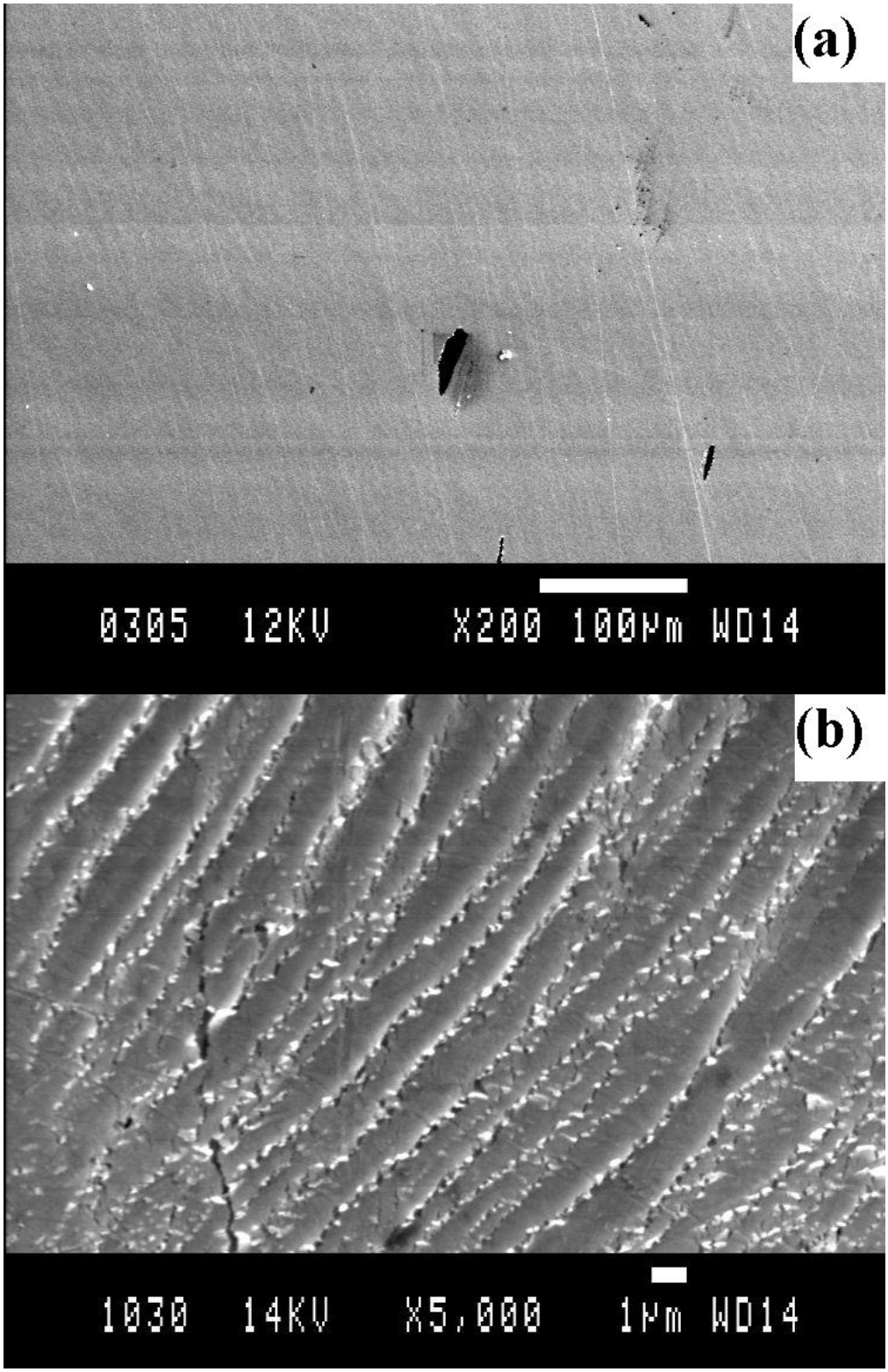

Figure 19. Surface topography of iron specimen coated with a thin (~10nm) layer of platinum in (a) as coated and (b) deformed (to 20% strain after coating) conditions.

3.4 Underlying technology

3.4.1 Atomic-scale dynamics of dislocation interactions with vacancy agglomerates in neutron irradiated bcc iron

Yu. N. Osetsky (*Oak Ridge National Laboratory, Oak Ridge, USA), D. J. Bacon** (**University of Liverpool, Liverpool, U.K.) and B. N. Singh*

It is well established that during neutron irradiation significant fractions of vacancies and self-interstitial atoms (SIA_s) produced in displacement cascades (induced by energetic neutrons) are in the form of clusters. In bcc iron practically all SIA clusters produced directly in the displacement cascades are glissile and perform 1-D diffusion with very low activation energy. These 1-D and fast diffusing SIA clusters have been shown to cause decoration of grown-in dislocations and formation of rafts of SIA loops. The population of vacancies generated in the neutron-induced displacement cascades in bcc iron form small loose clusters of vacancies and a high density of three-dimensional very small voids. The formation of vacancy clusters and nanovoids in pure iron irradiated with neutrons has been confirmed experimentally using positron annihilation spectroscope (PAS) technique. The presence of loose vacancy clusters and nanovoids is expected to cause resistance to moving dislocations which in turn would cause hardening of the material under consideration. Even though the magnitude of hardening caused by relatively large voids can be calculated in terms of linear elasticity theory, the level of hardening caused by the small nanovoids (≤ 1.0 nm. in diameters) and loose vacancy clusters cannot be obtained in any reliable fashion within the framework of the continuum elasticity.

In order to explore some of the details of the physical processes causing hardening as a result of interaction between moving dislocations and vacancy clusters and nanovoids, we have recently initiated molecular dynamics (MD) simulation studies. These studies are, in our view, directly relevant for rationalizing the hardening behaviour in the in-reactor deformation experiments during which the production of defect clusters and mobile dislocations occurs concurrently and continuously. Such experiments have already been carried out on pure copper and a precipitation hardened CuCrZr alloy and similar experiments are being prepared and will be soon carried out on pure iron and a single phase Fe-Cr alloy. The results of these simulation studies will be used as in-put parameters in the dislocation dynamic simulation studies and analytical description of the hardening behaviour during in-reactor tensile experiments.

In the present work atomistic simulations of interactions between a gliding edge dislocation and obstacles such as loose vacancy clusters and compact clusters of vacancies with three-dimensional configurations have been carried out. The hardening resulting from these interactions has been determined as a function of obstacle size and separation distance between the obstacles, crystal temperature and strain rate. Both molecular statics (MS) and MD techniques have been used. In both cases, a model based on a periodic array of dislocations has been employed. It has the advantage that either resolved stress or strain can be applied and monitored with high accuracy. It should be mentioned that the MS technique was used for simulations at 0K where dislocation glide was activated by applying increasing strain in increments of 10^{-4}. The crystal was then relaxed to minimize the potential energy at each step and the shear stress was calculated. This procedure made it possible to determine the stress-strain curve and the critical stress for glide at 0K. For temperatures above 0K, constant stress was applied and the position of the dislocation and obstacles monitored during the MD simulations. In MD

simulations at temperature above 0K, different strain rates in the range of (0.5-100) x 10^6 s^{-1} were used. The size of loose vacancy cluster was varied between 1 and 3nm ($N_v \cong 30$-100) with a local vacancy concentration of 15-30 at. %. The size of voids used in the present simulations varied between 0.5 to 5 nm ($N_v \cong 29$-1000).

Some of the preliminary results obtained recently on the effect of vacancy clusters and voids on the hardening behaviour of pure iron are presented in the following. Figure 21, for example, illustrates the effect of void size on the hardening behaviour of pure iron tested at 0K in molecular static mode with a constant strain incremental step of 10^{-4}. The calculation is performed for a given length of dislocation segment, L, (L=62 nm) between two obstacles. The measured shear stress refers to the stress necessary for the dislocation segment to overcome the obstacles. It can be seen (Figure 21) that this stress increases with increasing obstacle size and seems to be approaching a maximum value at the obstacle size of 5 nm. The hardening behaviour due to voids and loose clusters has been calculated for different temperatures for voids containing 59 vacancies and loose clusters containing 60 vacancies; the results are compared in Figure 22. The dislocation segment length between the obstacles is the same (62 nm) in both cases. Note that the hardening at temperatures above 0K is calculated using molecular dynamics code with a strain rate of $5x10^6$ s^{-1}. In both cases the stress necessary to overcome obstacles decreases with increasing temperature. The result suggests that the loose clusters of vacancies are stronger obstacles than the voids when compared in terms of increase in strength per vacancy.

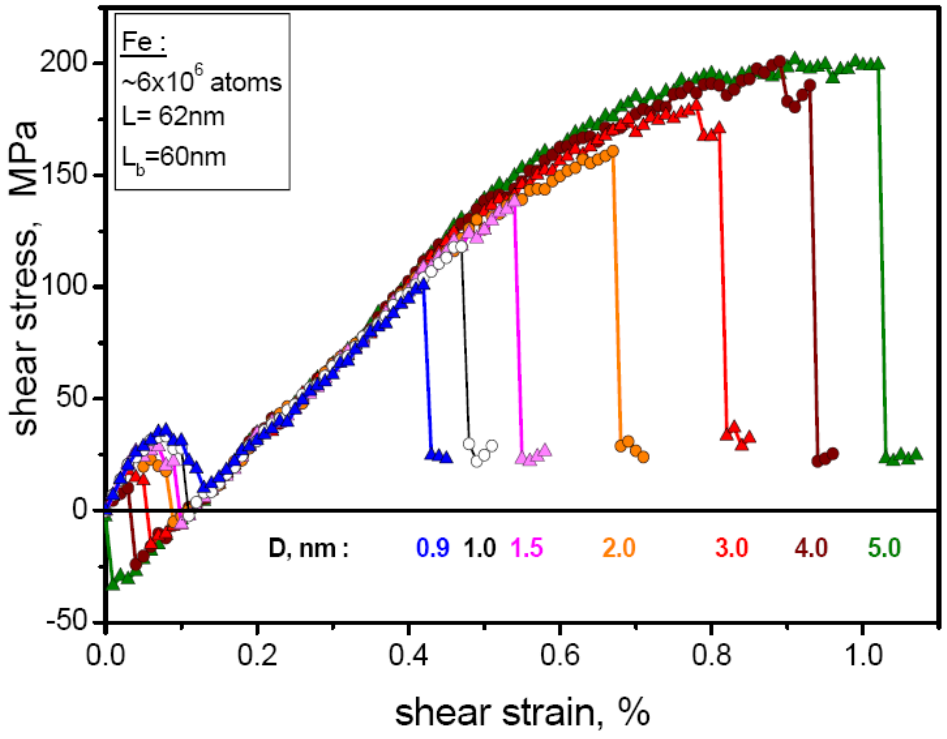

Figure 21. Stress-strain response for a gliding edge dislocation in a bcc iron crystal containing voids of different sizes. The test was carried out at 0K and in the molecular static mode and with a constant strain incremental step of 10^{-4}. Note that the shear stress increases with increasing void size.

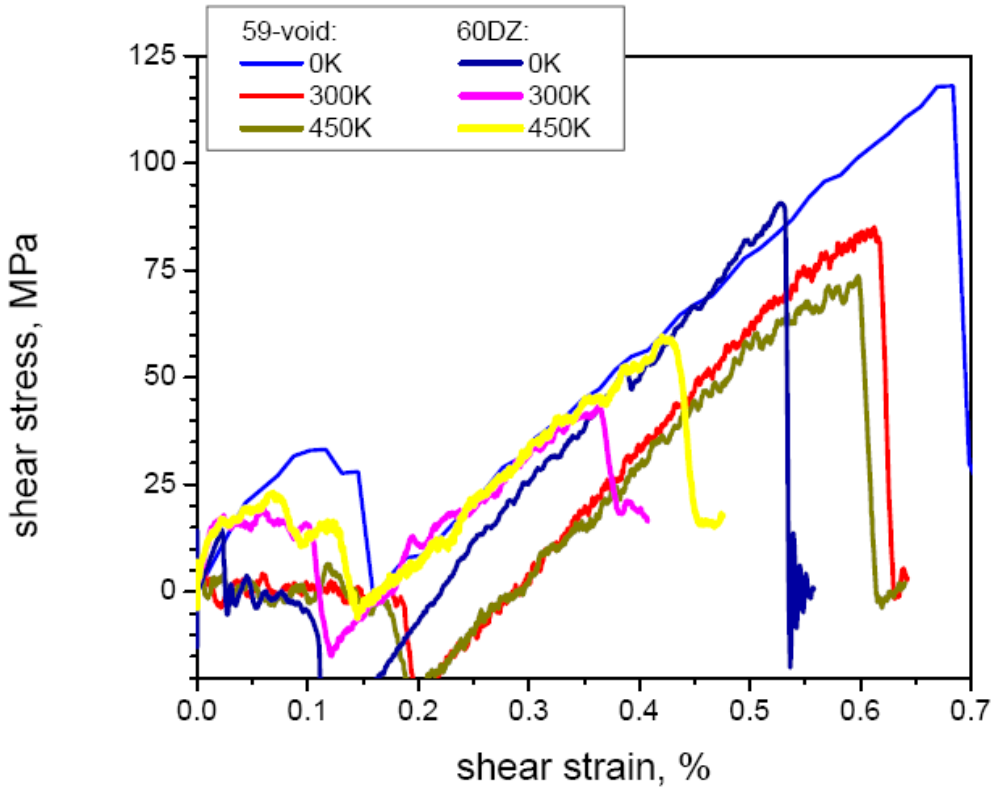

Figure 22. Stress-strain curves for pure iron with a dispersion of either voids or loose vacancy clusters containing 59 or 60 vacancies, respectively, tested using MD code at a strain rate of $5x10^6$ s^{-1} and at different temperatures between 0 and 450 K. The distance between the voids or loose vacancy clusters in the glide plane was 62nm.

It should be mentioned that as dislocations glide and interact with vacancy clusters and voids under the influence of applied stress, they absorb a certain number of vacancies from these obstacles. It is interesting in this context that the moving edge dislocation absorbs more vacancies from the clusters than from the voids. Furthermore, the absorption effect is found to depend on strain rate more strongly in the case of vacancy clusters than that in the case of voids. These effects may have significant influence on the microstructureral evolution and hardening behaviour during in-reactor deformation experiments.

3.4.2 Analytical treatment of defect accumulation and plastic during in-reactor tensile tests

H. Trinkaus (*Forschungszentrum Jülich, Jülich, Germany) and B.N. Singh*

Recent in-reactor tensile tests (IRT) on pure Cu and CuCrZr alloy have revealed a deformation behaviour which is significantly different from that observed in conventional post-irradiation tensile tests (PITs). In IRTs, (1) the material deforms uniformly and homogeneously without yield drop and plastic instability and (2) an increase in the pre-yielding dose results in an increase in the hardening rate as well as the level of maximum hardening and a decrease in the uniform elongation. This deformation behaviour in IRTs suggests that the materials must "remember" over the whole test period the impact of the damage level reached before yielding.

The deformation behaviour observed in PITs has been previously modelled in terms of "source hardening"[9] resulting from the trapping of cascade induced one-dimensionally diffusing glissile self-interstitial (SIA) clusters of dislocation loop type in the strain field of grown-in dislocations during irradiation[10]. The degree of decoration reached at typical dose levels around or above about 10^{-2} dpa has been shown to be so high that decorated dislocations are completely locked by their cluster clouds and new dislocations are generated only locally at heterogeneities of the lattice where the stress is substantially intensified which initiates localized and inhomogeneous deformation associated with a sudden yield drop and formation of cleared channels.

In IRTs, dislocation decoration is more moderate as long as the pre-yield dose is kept below 10^{-2} dpa. Under such conditions, dislocations can drag the loops decorating them and multiply homogeneously. In the thus defined continuous "decoration hardening", the resistance of dislocations against motion and the stress required to move them at given strain rate depends on the degree of decoration evolving during plastic deformation. The three main effects controlling the evolution of decoration are:(1) The interaction of a moving decorated dislocation with the clusters located on its track will result in the incorporation of loops with Burgers vector parallel to that of the dislocation, (2) the interaction of such loops with loops of different Burgers vector may result in alignment of the latter or, alternatively, mutual immobilisation and excretion of the corresponding complex from the moving loop cloud, depending on the degree of decoration reached during pre-yield irradiation, (3) the increase of the dislocation line length during dislocation multiplication will result in a thinning of the accompanying cluster clouds. The degree of decoration evolving by these mechanisms will determine the instantaneous flow stress.

According to this physical description of the processes occurring during an IRT, a quantitative model to predict the material response requires detailed consideration of:

(1) The kinetics of the trapping of cascade-induced one-dimensionally diffusing glissile SIA clusters by static grown-in dislocations during pre-yield irradiation which determines the initial condition for the degree of decoration under deformation,
(2) The kinetics of "dynamic decoration" of dislocation moving under deformation, including the sweeping of loops with parallel Burgers vector and their loss due to their immobilisation by loops of different Burgers vectors, as well as the thinning of decoration by the increase of the dislocation line length,
(3) The evolution of decorated dislocations during deformation, and
(4) The dynamic interaction of the moving dislocations with their loop clouds to correlate the degree of decoration with the instantaneous flow stress.

We are presently developing kinetic equations for pre- and post-yield dislocation decoration with dislocation loops and estimates for correlating the calculated dislocation decoration with the flow stress. Preliminary results are shown in Figure 23 where the evolution of decoration, before and after yielding, represented by the number of SIAs per unit dislocation length, is plotted as a function of pre-yield dose and post-yield dose/plastic strain, respectively. For the post-yielding evolution, two extreme cases assumed for low and high pre-yield irradiation, are plotted. Realistic evolutions may be expected to be between these two extreme cases.

9 B.N. Singh, A.J.E. Foreman, H. Trinkaus, J. Nucl. Mater. 249 (1997) 103.

10 H. Trinkaus, B.N. Singh, A.J.E. Foreman, J. Nucl. Mater. 249 (1997) 91; 251 (1997) 172.

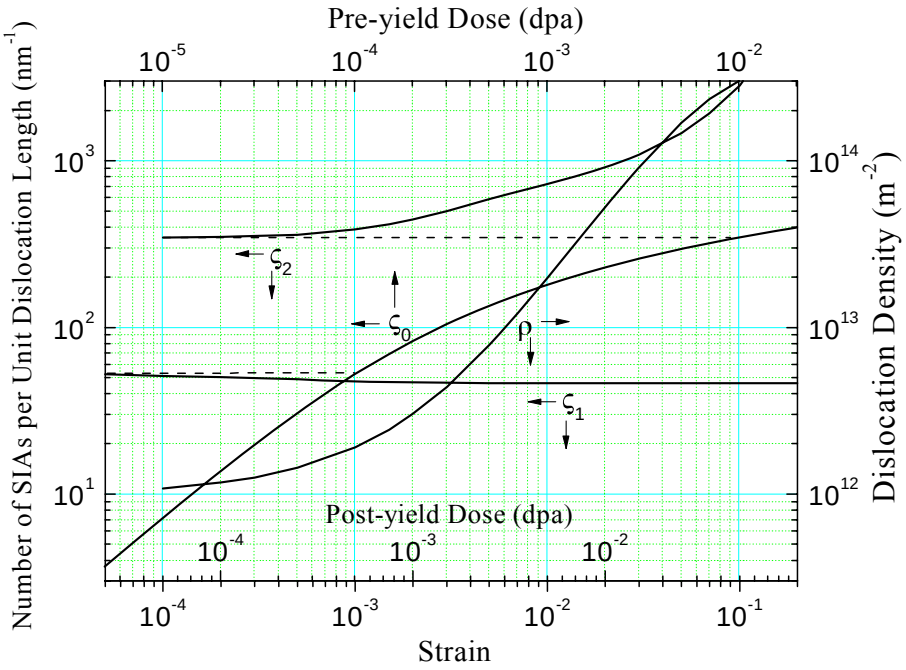

Figure 23. Evolution of the number of SIAs per unit dislocation length before and after yielding, ς_0 and $\varsigma_{1/2}$, with $\varsigma_{1/2}(\varepsilon=0) = \varsigma_0(D_y=10^{-4}/10^{-2}\text{dpa})$, as a function of pre-yield dose, $D_{pre} \leq D_y$, and post-yield dose/plastic strain, $D_{post} \geq D_y/\varepsilon$, respectively. The evolution of the dislocation density with strain is also shown. For the "weak" and "strong" post-yield decoration following "weak" and "strong" pre-yield irradiation, ς_1 and ς_2, alignment of loops with non-parallel Burgers vectors is assumed to be negligible and complete, respectively. The "weak" and "strong" pre-yield irradiation would result in a weak constant "decoration hardening" and a strong "decoration source hardening", respectively.

3.4.3 Positron annihilation spectroscopy investigations of neutron irradiated CuCrZr alloy with different heat treatments.

Peter Domonkos(*Department of Nuclear Physics and Technology, Slovak University of Technology, Bratislava, Slovak Republic), Morten Eldrup and B.N. Singh*

The present work is a continuation of positron annihilation spectroscopy (PAS) studies of the effect of heat treatments of un-irradiated Outokumpu CuCrZr alloy specimens (Annual Progress Report 2004). The heat treatments were: Solution annealing (SA), Prime ageing (PA) and PA followed by ageing at successively higher temperatures (HT1 - HT5). Several of these specimens were neutron irradiated to different dose levels at temperatures in the range from 50°C to 350°C and subsequently investigated by PAS.

For the un-irradiated alloy, there were two main features of the PAS results as a function of heat treatment. One was that the positron "defect lifetime" ($\tau_2 \sim 175$ ps) changed only little, while a strong variation of its intensity I_2 was observed which could be correlated with a variation of precipitate size and density as observed by TEM. These results suggest that PAS detects vacancy-sized defects at the precipitate matrix interface.

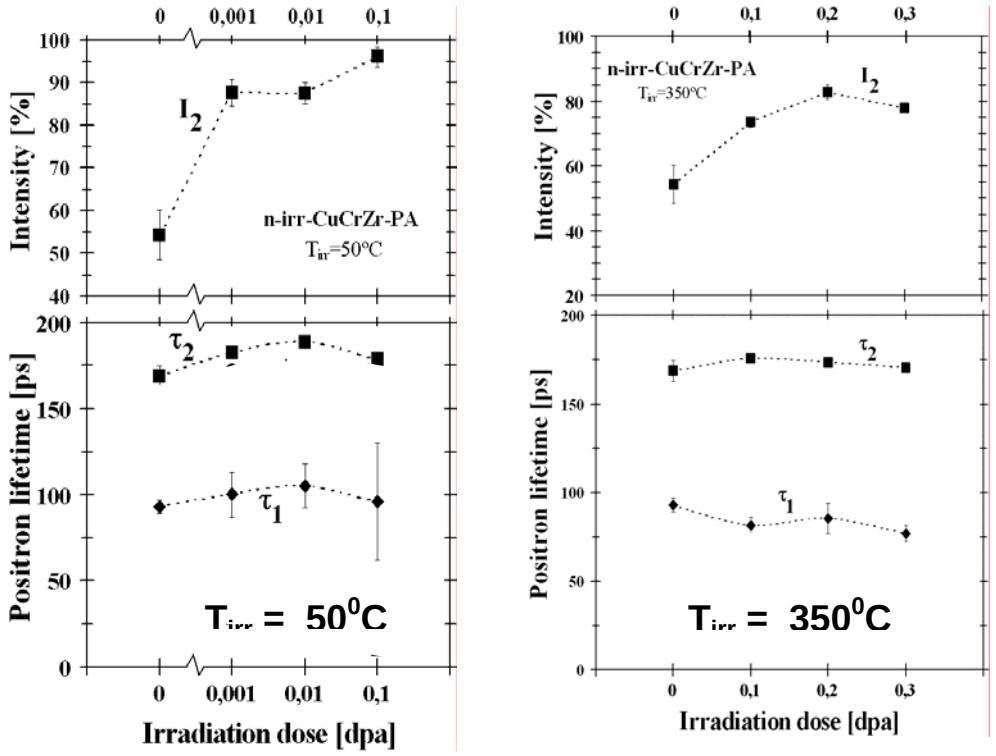

Figure 24. PAS results for Prime Aged and neutron irradiated CuCrZr alloy (Outokumpu) as functions of displacement damage dose for irradiation temperatures of 50°C and at 350°C. The longer lifetime, τ_2 ~ 175 ps, is associated with defects at the precipitate matrix interface and radiation created defects. The intensity I_2 of this defect component is a measure of the defect density and increases strongly with dose.

Some of the results for neutron irradiated specimens are shown in Figure 24. The figure shows the effect of irradiation dose for neutron irradiation at 50°C and at 350°C for the PA alloy. Similar to the effect of heat treatment of un-irradiated alloys, only small variations in the positron "defect lifetime" τ2 are observed as a function of irradiation dose while the intensity I2 of the defect component increases strongly with dose.

This behaviour is ascribed to additional positron trapping in radiation created defects, maybe defects associated with stacking fault tetrahedra, which are known from pure copper also to give rise to positron lifetimes of about 180 ps. The densities of SFTs in pure Cu after n-irradiation to dose levels of 0.2 – 0.3 dpa have been found to be about 5×1023 m-3 (at ~ 50°C) and ~ 1022 m-3 (at 350°C). This is the same order of magnitude as the precipitate densities after PA and should therefore be expected to influence the positron trapping by about the same magnitude as the prime ageing does. This is in agreement with the results in Figure 24.

3.5 Publications and conference contributions

International publications

Edwards, D.J.; Singh, B.N.; Bilde-Sørensen, J.B., Initiation and propagation of cleared channels in neutron-irradiated pure copper and a precipitation hardened CuCrZr alloy. J. Nucl. Mater. (2005) v. 342 p. 164-178

Osetsky, Y.N.; Bacon, D.J.; Rong, Z.; Singh, B.N., Dynamic properties of edge dislocations decorated by interstitial loops in alpha-iron and copper. Phil. Mag. Lett. (2004) v. 84 p. 745-754

Wen, M.; Ghoniem, N.M.; Singh, B.N., Dislocation decoration and raft formation in irradiated materials. Phil. Mag. (2004) v. 85 p. 2561-2580

Danish reports

Bindslev, H.; Singh, B.N (eds.), Association Euratom - Risø National Laboratory annual progress report 2004. Risø-R-1520(EN) (2005) 62 p.

Singh, B.N; Eldrup, M.; Golubov, D.J.; Edwards, D.J.; Jung, P., Final report on neutron irradiation at low temperature to investigate plastic instability and at high temperature to study caviation. Risø-R-1496(EN) (2005) 38 p.

Singh, B.N.; Li, M.; Stubbins, J.F.; Johansen, B.S., Creep-fatigue deformation behaviour of OFHC-copper and CuCrZr alloy with different heat treatments and with and without neutron irradiation. Risø-R-1528(EN) (2005) 55 p.

International reports

Tähtinen, S.; Singh, B.N., Effects of neutron irradiation on mechanical properties of titanium alloys. VTT Research Report BTU073-051386 (2005) 18 p.

Unpublished international conference contributions

Domonkos, P.; Eldrup, M.; Singh, B.N., Investigation of CuCrZr alloys with different heat treatments using positron annihilation spectroscopy. 12. International conference on fusion reactor materials (ICFRM-12), Santa Barbara (US), 4-9 Dec 2005. Unpublished.

Edwards, D.J.; Singh, B.N.; Tähtinen, S., Effect pf jeat treatments on precipitate microstructure and mechanical properties of CuCrZr alloy. 12. International conference on fusion reactor materials (ICFRM-12), Santa Barbara (US), 4-9 Dec 2005. Unpublished.

Eldrup, M.; Singh, B.N.; Jung, P.; Johnson, E.; Edwards, D., Cavity formation in ion and Eurofer-97 due to He implantation and neutron irradiation (poster). 12. International conference on fusion reactor materials (ICFRM-12), Santa Barbara (US), 4-9 Dec 2005. Unpublished.

Eldrup, M.; Singh, B.N., Helium bubble formation and growth during helium implantation and subsequent neutron irradiation in iron and Eurofer steel. Workshop on fundamental aspects of radiation damage, Risø (DK), 14-16 Jul 2005. Unpublished.

Golubov, S.I.; Singh, B.N., Kinetics of damage accumulation in alpha-iron and copper during neutron irradiation at temperatures below the recovery stage V. Workshop on fundamental aspects of radiation damage, Risø (DK), 14-16 Jul 2005. Unpublished.

Golubov, S.I.; Singh, B.N.; Trinkaus, H.; Zinkle, S.J.; Stoller, R.E., The evolution of stacking fault tetrahendra and damage accumulation in fcc metals under cascade damage conditions. 12. International conference on fusion reactor materials (ICFRM-12), Santa Barbara (US), 4-9 Dec 2005. Unpublished.

Golubov, S.I.; Singh, B.N.; Trinkaus, H.; Ovcharenko, A.M.; Stoller, R.E.; Zinkle, S.J., Investigations of helium effects on cavity evolution in metals under cascade damage conditions. 12. International conference on fusion reactor materials (ICFRM-12), Santa Barbara (US), 4-9 Dec 2005. Unpublished.

Heinisch, H.L.; Singh, B.N.; Trinkaus, H., Kinetic Monte Carlo studies of the reaction kinetics of crystal defects that diffuse one-dimensionally with occasional transverse migration. 12. International conference on fusion reactor materials (ICFRM-12), Santa Barbara (US), 4-9 Dec 2005. Unpublished.

Moilanen, P.; Tähtinen, S.; Singh, B.N.; Jacquet, P.; Dekeyser, J., In-reactor creep-fatigue tests of a CuCrZr alloy at about 333K. 12. International conference on fusion reactor materials (ICFRM-12), Santa Barbara (US), 4-9 Dec 2005. Unpublished.

Osetsky, Yu.N.; Bacon, D.J.; Singh, B.N., Atomic-scale dynamics of dislocation interaction with vacancy agglomerates in neutron irradiated bcc iron. 12. International conference on fusion reactor materials (ICFRM-12), Santa Barbara (US), 4-9 Dec 2005. Unpublished.

Osetsky, Yu.N.; Stoller, R.E.; Zinkle, S.J.; Singh, B.N., Dislocation channeling in irradiated fcc metals: atomic scale mechanisms. Workshop on fundamental aspects of radiation damage, Risø (DK), 14-16 Jul 2005. Unpublished.

Osetsky, Yu.N.; Stoller, R.E.; Zinkle, S.J.; Singh, B.N., Atomic-scale mechanisms of cleared channel formation in neutron-irradiated low stacking fault energy fcc metals. 12. International conference on fusion reactor materials (ICFRM-12), Santa Barbara (US), 4-9 Dec 2005. Unpublished.

Singh, B.N., In-reactor deformation experiments: results and implications. Workshop on fundamental aspects of radiation damage, Risø (DK), 14-16 Jul 2005. Unpublished.

Singh, B.N.; Tähtinen, S.; Moilanen, P.; Jacquet, P.; Dekeyser, J.; Edwards, D.J., In-reactor deformation behaviour of copper and CuCrZr alloy: Experiments, results and implications. 12. International conference on fusion reactor materials (ICFRM-12), Santa Barbara (US), 4-9 Dec 2005. Unpublished.

Stubbins, J.F.; Wu, X.; Pan, X.; Li, M.; Singh, B.N., Hold-time effects on the fatigue life of copper and copper alloys for fusion applications. 12. International conference on fusion reactor materials (ICFRM-12), Santa Barbara (US), 4-9 Dec 2005. Unpublished.

Tähtinen, S.; Moilanen, P.; Singh, B.N., Qualification of CuCrZr alloy to stainless steel joints. 12. International conference on fusion reactor materials (ICFRM-12), Santa Barbara (US), 4-9 Dec 2005. Unpublished.

Tähtinen, S.; Moilanen, P.; Singh, B.N., Effect of neutron dose and temperature on tensile and fracture toughness properties of titanium alloys. 12. International conference on fusion reactor materials (ICFRM-12), Santa Barbara (US), 4-9 Dec 2005. Unpublished.

Wen, M.; Wang, Z.; Ghoniem, N.M.; Singh, B.N., The effects of irradiation on the deformation of Cu: A comparison between dislocation dynamics modeling and experiments. 12. International conference on fusion reactor materials (ICFRM-12), Santa Barbara (US), 4-9 Dec 2005. Unpublished.

Zinkle, S.J.; Singh, B.N., Effect of test temperature and strain rate on radiation hardening. 12. International conference on fusion reactor materials (ICFRM-12), Santa Barbara (US), 4-9 Dec 2005. Unpublished.

4 ITER and Danish industry activities

S. B. Korsholm and H. Bindslev
soeren.korsholm@risoe.dk

Risø has over a longer period sought to interest companies and the Confederation of Danish Industries in industrial tasks in ITER and the wider fusion programme. This effort was met with modest interest until the ITER site decision on June 28th 2005. Hereafter interest has been growing. To develop the Danish interest in the industrial aspects of ITER, Risø, The Confederation of Danish Industries, The Trade Council of Denmark and the Ministry of Research organised and a conference on industrial opportunities in the ITER project. Sixty managers, executives, engineers and others from a broad range of Danish industries participated in this conference which was held at the Confederation of Danish Industries in Copenhagen. The programme (www.risoe.dk/iter/Arrangementer/konference-kbhvn.htm), which was chaired by Ambassador Anne Steffensen, included presentations from fusion research managers and from industries with experience from participation in the fusion programme. As a special honor, the Danish Minister of Science addressed the audience.

Another important effort has been the building of a website for the Danish industry and other companies: www.risoe.dk/iter. The website contains information on the coming tasks at ITER, background information, news and announcements, links to relevant international websites, description of experiences of other companies, and, following the Copenhagen ITER conference, the website includes an online database, where companies can present their fusion relevant competences and their interests in ITER tasks.

Apart from the fully public ITER and industry website, a site with restricted access is maintained. Companies may request a password to access the site that contains tender action material such as the EFDA and JET calls for expression of interest.

In parallel to these efforts, a mailing list have been maintained and extended. This is an important way of distributing news and advertising tender actions. Currently, 50 companies are on the mailing list and about 20 companies have registered in the database (http://www.risoe.dk/iter/Database/Competences-Danish-companies.pdf). A very important aspect of the activities has been the formation of a series of networks of interested industries and public research organisations grouped around particular topics (http://www.risoe.dk/iter/DKnetvaerk/DKindustrinetvaerk.htm).

Risø's research is aimed at solving concrete problems in the society.

Research targets are set through continuous dialogue with business, the political system and researchers.

The effects of our research are sustainable energy supply and new technology for the health sector.